

DR. MATHIAS MUELLER (Orcid ID : 0000-0002-8879-1534)

DR. CARL JACQUEMYN (Orcid ID : 0000-0002-8627-7144)

DR. CHELSEA LYNN PEDERSON (Orcid ID : 0000-0002-0480-4597)

Article type : Original Article

## **Constraints on the preservation of proxy data in carbonate archives – lessons from a marine limestone to marble transect, Latemar, Italy**

MATHIAS MUELLER\*, CARL JACQUEMYN<sup>†</sup>, BENJAMIN F. WALTER<sup>‡</sup>, CHELSEA L. PEDERSON\*, SIMON L. SCHURR<sup>¶</sup>, ONYEDIKA A. IGBOKWE\*<sup>§</sup>, NIELS JÖNS\*, SYLVIA RIECHELMANN\*, MARTIN DIETZEL\*\*, HARALD STRAUSS<sup>¶</sup> and ADRIAN IMMENHAUSER\*<sup>††</sup>

\*Ruhr-University Bochum, Institute of Geology, Mineralogy and Geophysics, Universitätsstraße 150, 44801 Bochum, Germany (E-mail: mathias.mueller-11y@rub.de)

<sup>†</sup>Imperial College London, Department of Earth Science and Engineering, Exhibition Road, SW7 2AZ London, United Kingdom

<sup>‡</sup>Karlsruhe Institute for Technology, AGW Institute for Applied Geoscience, Adenauering 20b, 76131 Karlsruhe, Campus South, Germany

<sup>¶</sup>Westfälische Wilhelms-Universität Münster, Institut für Geologie und Paläontologie, Corrensstr. 24, 48149 Münster, Germany

<sup>§</sup>Department of Geology, Alex Ekwueme Federal University Ndufu-Alike, Ikwo, P.M.B. 1010, Abakaliki, Ebonyi State, Nigeria

\*\*Institute of Applied Geosciences, Graz University of Technology, Rechbauerstraße 12, 8010 Graz, Austria

This article has been accepted for publication and undergone full peer review but has not been through the copyediting, typesetting, pagination and proofreading process, which may lead to differences between this version and the [Version of Record](#). Please cite this article as [doi: 10.1111/SED.12939](https://doi.org/10.1111/SED.12939)

This article is protected by copyright. All rights reserved

††Fraunhofer IEG (Institution for Energy Infrastructures and Geothermal Systems), Am Hochschulcampus 1, 44801 Bochum, Germany

**Associate Editor – Tracy Frank**

**Short Title – Constraints on preservation of proxy data in carbonate archives**

## ABSTRACT

This work evaluates an exceptionally complex natural laboratory, the Middle Triassic Latemar isolated platform in the northern Italian Dolomite Mountains and explores spatial and temporal gradients in processes and products related to contact metamorphism, dolomitization and dedolomitization of marine limestones. The relation between petrographic change and re-equilibration of geochemical proxy data is evaluated from the perspective of carbonate-archive research. Hydrothermal dolomitization of the limestone units is triggered by dykes and associated hydrothermal fluids radiating from the nearby Predazzo Intrusion. Detailed petrography, fluid inclusion analysis,  $\delta^{13}\text{C}$  and  $\delta^{18}\text{O}$  data and  $^{87}\text{Sr}/^{86}\text{Sr}$  isotope ratios shed light on the extreme textural and geochemical complexity. Metamorphic and diagenetic patterns include: (i) peak-metamorphic and retrograde-metamorphic phases including three dolomite marbles, two dedolomite marbles, brucite, magnesium silicates and late-stage meteoric/vadose cement at the contact aureole; (ii) four spatially defined episodes of dolomitization, authigenic quartz, low magnesium calcite and late-stage meteoric cement at the Latemar isolated platform; and (iii) kilometre-scale gradients in  $\delta^{13}\text{C}$  values from the contact aureole towards the platform interior. Results shown here are relevant for two reasons: first, the spatial analysis of alteration products ranging from high-grade metamorphic overprint of marbles at temperatures of  $700^\circ\text{C}$  in the contact aureole to moderately altered limestones in the platform interior at temperatures  $<100^\circ\text{C}$ , allows the observation of processes that commonly occur along vertical (prograde) gradients from shallow burial to metamorphism at depths  $>20$  km. Second, under rock-buffered conditions, and irrespective of metamorphic to diagenetic fluid-rock interactions, both marbles, and low-temperature hydrothermal dolomites have conservative marine  $\delta^{13}\text{C}$  and  $\delta^{18}\text{O}$  values. The fact that metamorphism and hydrothermal dolomitization of precursor limestones and early diagenetic dolostones did not *per se* reset environmental proxy data is of interest for those concerned with carbonate archive research in Earth's deep time.

**Keywords** Diagenesis, dedolomitization, dolomite, dolomitization, geochemistry, Latemar, metamorphism, petrography.

## INTRODUCTION

Carbonate archive data represent a snapshot of the evolution of Earth's surface environments, recording complex interactions of equilibrium and non-equilibrium processes. However, carbonate archives are susceptible to post-depositional alteration (e.g. Bathurst, 1975; Swart, 2015). The challenge is to separate a meaningful environmental signal from one that is modified by diagenetic or metamorphic alteration, and hence to reliably assess the integrity and robustness of the extracted data as indicators of past depositional environments. Dolomitization, i.e. calcite to dolomite neomorphism, is prominent among the complex array of diagenetic processes, and may result in partial to complete resetting of primary geochemical values (Geske *et al.*, 2015; Mueller *et al.*, 2020). Metamorphic alteration of archive data by regional or contact metamorphism is documented in numerous examples worldwide (Wada *et al.*, 1998; Bowman *et al.*, 2009; Boomeri *et al.*, 2010). These processes are of fundamental relevance in deep-time climate dynamics research, specifically concerning the Palaeoproterozoic and Archean, which are characterized by abundant, often overprinted dolomite archives (Veizer *et al.*, 1989; Brady *et al.*, 1998; Bau *et al.*, 1999; Franchi and Abebe, 2020).

Numerous and controversial conceptual models for dolomitization exist, but there is general consensus that many of the volumetrically important dolomite cements and replacement fabrics formed during prograde burial diagenesis (Machel, 2005, and references therein; Gregg *et al.*, 201). Furthermore, the concept of early-marine diagenetic dolomitization and the intricate topic of dolomite precursor minerals (amorphous carbonates, highest-Mg calcites and non-stoichiometric dolomites; Geske *et al.*, 2012; Petrash *et al.*, 2017) merits attention. Dolomitizing fluids, both in the shallow subsurface and the burial domain, are often (modified) seawater or Mg-rich basement brines (e.g. Dewit *et al.*, 2014; Gregg *et al.*, 2015; Hendry *et al.*, 2015; Navarro-Ciurana *et al.*, 2016; Yang *et al.*, 2020). Beyond fundamental carbonate research, dolostones are of great interest for economic geologists (hydrocarbon reservoirs: Qing & Mountjoy, 1994; Davies & Smith, 2006; or Mississippi Valley Type mineralization: Gregg *et al.*, 1993; Shelton *et al.*, 2020). Moreover, contact metamorphic dolomitization (Schutter, 2003; Nader *et al.*, 2004; Farooqui *et al.*, 2009; Dong *et al.*, 2013; Jacquemyn *et al.*, 2014; Hou *et al.*, 2016; Yang *et al.*, 2020) is predominantly studied by metamorphic petrologists and geochemists with focus on skarns (Baumgartner & Valley, 2001; Ferry *et al.*, 2002; Gallien *et al.*, 2007), necessitating a sedimentological approach to this type of alteration.

Here, it is argued that contact metamorphism is relevant, albeit underexplored, for those concerned with palaeoenvironmental data from dolomitized carbonate archives. The rationale is, that contact metamorphic aureoles of magmatic bodies in limestones offer unique and accessible windows into processes and features that otherwise take place along burial to metamorphic gradients from near-surface down to 20 km or more of burial depth.

The Anisian–Ladinian Latemar isolated platform and the neighbouring Predazzo magmatic intrusion in the northern Italian Dolomite Mountains, form an ideal case example in this sense. At Latemar, 74% of the calcitic mineralogy is preserved (Jacquemyn *et al.*, 2014), allowing for the investigation of a marine limestone to marble transect. The Latemar isolated platform is one of the most intensively studied carbonate edifices worldwide, with previous work focusing (among other topics) on bedding patterns, orbital forcing and cycle patterns, evidence for subaerial exposure, stratigraphy, platform geometry, reservoir analogue properties and dolomitization (see references in Christ *et al.*, 2012; Table 1). Work on the Predazzo Intrusion metamorphic aureole includes that of Ferry *et al.* (2002), dealing with the direction of fluid flow, and various petrological studies (Castellarin *et al.*, 1982; Sloman, 1989; Marrocchino *et al.*, 2002, 2009; Casetta *et al.*, 2018a,b). Jacquemyn *et al.* (2014, 2015) developed a paragenetic sequence and revealed the exceptionally complex spatial relation between platform carbonates and the Predazzo sub-volcanic intrusion (Castellarin *et al.*, 1982). The intrusion metamorphosed underlying strata and is genetically related to swarms of dykes that cross-cut the platform and formed transport and interaction pathways for dolomitizing fluids. Previous work includes a wide range of dolomitizing fluid temperatures. Based on fluid inclusion thermometry, Wilson *et al.* (1990) suggested 75 to 220°C, whereas Ferry *et al.* (2011) proposed temperatures from 40 to 80°C based on carbonate clumped isotope thermometry.

Research presented here combines new evidence based on petrographic (transmitted light and cathodoluminescence microscopy, electron microprobe, microthermometry) and geochemical ( $\delta^{18}\text{O}$ ,  $\delta^{13}\text{C}$ ,  $^{87}\text{Sr}/^{86}\text{Sr}$ ) analysis with published data from Jacquemyn (2013) and Jacquemyn *et al.* (2014, 2015). This paper has three aims: (i) to characterize a petrographic and geochemical transect across the complex metamorphic to low-temperature diagenetic reaction pathway of Triassic Latemar carbonates; (ii) to systematically place these data into spatial and temporal context ranging from contact metamorphic (de-)dolomite marbles (700°C; Ferry *et al.*, 2002) to marine limestones exposed to low-temperature diagenetic fluids (< 80°C; Ferry *et al.*, 2011); and

(iii) to establish tipping points and tools for their recognition along the alteration pathway of a marine carbonate archive exposed to increasing degrees of overprint.

Acknowledging the inherent complexity of carbonate archives and their proxy data, the authors do not claim that the Latemar case example represents a litmus test for any given outcrop throughout Earth's geological history. In contrast, this contribution aims to provide a framework against which existing and subsequent work can be placed to extract quantitative science, patterns and methods for the community.

## GEOLOGICAL BACKGROUND

Sedimentary rocks of the Latemar and the nearby Monte Agnello are remnants of Middle Triassic (Anisian–Ladinian) isolated platforms (Fig. 1; Marangon *et al.*, 2011). The pre-volcanic Late-Anisian to Ladinian Latemar is predominantly composed of the Sciliar (Schlern) Formation (Fig. 2A). Carbonate deposition began on a structural high under an extensional regime. Extensional synsedimentary tectonics has subsequently controlled the platform geometry and led to faulting. Based on sedimentological data, the Latemar has been interpreted as an isolated, flat-topped (microbial carbonate) platform with steep slopes shaped by faults (Marangon *et al.*, 2011; Preto *et al.*, 2019), and is subdivided into different lithozones (Fig. 2B; Goldhammer *et al.*, 1987; Egenhoff *et al.*, 1999).

Carbonate deposition ceased with the onset of the Predazzo Intrusion in the Late Ladinian (Bosellini, 1984). A Plinian/Vesuvian eruptive phase draped the Latemar with volcanic material and locally caused contact metamorphic overprinting of the carbonates (Fig. 2C). The subsequent emplacement of the Predazzo Intrusion took place in several phases from 238 to 232 Ma (Castellarin *et al.*, 1982; Laurenzi and Visonà, 1996; Mundil *et al.*, 1996, 2010). The Predazzo Intrusion is composed of approximately coeval intrusive bodies arranged in a circular arrangement, 2 km in diameter, and is controlled by faults that formed during caldera collapse (Laurenzi & Visonà, 1996). Three magmatic pulses are recorded: two shoshonitic (silica saturated; SiSa), silica undersaturated; SiUSa, and one granitic unit (GU; Fig. 2D to F; Casetta *et al.*, 2018a,b). The relative age of each pulse was determined by cross-cutting relationships (Marrocchino *et al.*, 2009). A contact metamorphic aureole ( $T \leq 700^{\circ}\text{C}$ ) composed of dedolomitized marbles formed around the Predazzo Intrusion (Fig. 2C), and locally contains up to

40 vol.% of brucite [Mg(OH)<sub>2</sub>] and a series of complex silicates (Jacquemyn *et al.*, 2014). This marble unit represents the high-temperature target lithology in this paper.

The intrusion was coupled with the emplacement of numerous north/north-west to south/south-east oriented dykes cross-cutting the Latemar isolated platform (Riva & Stefani, 2003). These dykes correspond to the three aforementioned magmatic pulses and bear a similar composition revealing their relative timing (Marrocchino *et al.*, 2009; Casetta *et al.*, 2018a,b). High-permeability brecciated zones along the dyke margins served as fluid pathways that caused partial (26%) and spatially localized dolomitization of the otherwise calcitic Latemar isolated platform (Fig. 3; Jacquemyn *et al.*, 2014). Replacement dolomitization started during, or shortly after, dyke emplacement. The stratigraphically lower portion (Lower Platform Facies) and lower parts of Middle Tepee Facies are mostly dolomitized, while the upper portions of the buildup escaped significant dolomitization. The most recent overview on dolomitization mechanism, dolostone distribution, contribution of dykes to the dolomitization process and amount of dolomitization of the Latemar isolated platform was by Jacquemyn (2013) and Jacquemyn *et al.* (2014, 2015). The most recent overview of the petrological evolution of the Predazzo Intrusion was by Casetta *et al.* (2018a,b).

## MATERIALS AND METHODS

### Fieldwork and sampling strategy

The following sampling strategy was applied to build a transect from most to least overprinted.

**1** The Canzoccoli quarry, located 3 to 4 km to the south-east of the Latemar at 1000 m above sea-level (a.s.l.), serves as a high-temperature ( $T \leq 700^\circ\text{C}$  *sensu* Ferry *et al.*, 2002) end member. This site provided access to ‘contact aureole’ samples recording the spatial petrographic and geochemical impact of metamorphism on (de)dolomitization patterns (metamorphosed Contrin Formation dolostone; array #1 in Fig. 2B; Figs 1, 3F and 3G).

**2** The steep, southward-facing slope of the Latemar Mountain, located 4 to 5 km north-west of the intrusion between 1800 and 2300 m a.s.l. (Valsorda; dolomitized Contrin Formation and Lower Platform Facies; array #2 in Fig. 2B; Fig. 3D and E), represents an intermediate setting between contact metamorphism and moderate hydrothermal alteration of ‘Latemar slope samples’.

**3** The Latemar mountain (platform interior) located 5 to 7 km north-west of the intrusion between 2400 and 2600 m a.s.l., exposes the highest occurrence of partially dolomitized Sciliar Formation, and access to the low-temperature ( $T < 100^{\circ}\text{C}$ ) end member. ‘Latemar interior’ samples represent low-temperature hydrothermal dolomitization (Middle Tepee Facies, Lower Cyclic Facies and Lower Tepee Facies; array #3 in Fig. 2B and Fig. 3A to C).

A complete (metamorphic) phase sequence at the contact metamorphic aureole was established along this transect and complemented the sequence from marine diagenetic limestones to dedolomites at the Latemar with calcsilicates in the context of a peak-metamorphic to retrograde diagenetic pathway. All visible rock types, vein types and cement types were sampled and characterized by thin section and geochemical analyses, enabling the assessment of temperature-related and fluid-related petrographic and geochemical differences within their spatial and petrographic context. Dolomite replacement fabrics and cement phases were documented in their relation to dykes. To identify time-equivalent facies between Latemar carbonates (Sciliar Formation) and the metamorphosed dolostones at the Predazzo Intrusion contact (Contrin Formation), the basal, early diagenetic dolostones of the Contrin and Werfen (shallow water marls) formations exposed at the Latemar slope were sampled. Note that arrays 2 and 3 are stratigraphically distinct as they cover different parts of the isolated platform. Refer to Appendix S1 for further information on sampling locations and measured sections (Fig. S1).

### **Petrographic and mineralogical analysis**

A total of 119 thin sections were analyzed using polarized ( $n = 119$ ), cathodoluminescence ( $n = 41$ ), and scanning electron microscopy ( $n = 4$ ). Polarized photomicrographs were taken with a Leica DM4500P microscope (Leica Microsystems GmbH, Wetzlar, Germany). The thin sections were sputter-coated with a 15 nm thick gold layer to avoid charging for both cathodoluminescence and scanning electron microscopy. Cathodoluminescence microscopy was performed using a hot cathode (HC1-LM) facility at the Ruhr-University Bochum (Neuser *et al.*, 1996) equipped with a DC73 video camera system (Olympus Corporation, Tokyo, Japan). The electron beam had an acceleration voltage of 14 kV, current density from 5 to 10  $\mu\text{A}/\text{mm}^2$ , and beam current between 0.1 and 0.2 mA. For scanning electron imaging, a high-resolution field emission scanning electron

microscope (HR-FESEM) type Merlin Gemini II (Carl Zeiss AG, Jena, Germany) using secondary electrons was used at the Ruhr-University Bochum.

To identify mineral phases, 105 samples were analyzed with a Philips X'Pert MPD Theta-Theta X-ray Diffractometer (Malvern PANalytical, Malvern, UK) using Cu K $\alpha$  radiation at 45 kV and 40 mA. The scanning range was 0 to 70°(2 $\theta$ ), with a step of 0.025° (2 $\theta$ ), and an acquisition time of 11 s per step. A graphite secondary monochromator was used to minimize background noise.

Electron microprobe analyses of six thin sections were performed using a SX5FE field emission electron microprobe (CAMECA, Paris, France) at Ruhr-University Bochum. Natural and synthetic minerals were used as reference materials (see Appendix S1 for details). Element distribution maps were acquired using an acceleration voltage of 15 kV, a probe current of about 75 nA, and a fully focused beam. The X-ray intensities of Mg K $\alpha$ , Sr L $\alpha$ , Si K $\alpha$ , Fe K $\alpha$  and Ca K $\alpha$  were measured using wavelength-dispersive spectrometers, whereas additional elements (Al, Mn) were recorded using energy-dispersive X-ray spectrometry with a silicon drift detector. The images were acquired in continuous stage scan mode. They have a resolution of 1367  $\times$  544 to 1863  $\times$  1040 pixels, with a dwell time of 40 ms per pixel.

Microthermometric analyses (n = 22) were carried out using a Linkam THMS600 heating-freezing stage (Linkam Scientific Instruments Limited, Tadworth, UK) at the Karlsruhe Institute for Technology (KIT) for internal standardization of the fluid inclusions. For the preparation of the fluid petrography, double-polished thick sections (100 to 150  $\mu$ m) were prepared. The petrographic relation of each fluid inclusion assemblage was carried out by optical and cathodoluminescence microscopy following Goldstein & Reynolds (1994). The documented fluid inclusion assemblages (FIA) were classified as primary inclusions, which are situated on growth zones (p), pseudo-secondary (ps), secondary (s) and isolated inclusions with no genetic relationship (iso; Walter *et al.*, 2015). For each analysis, three repeated heating and freezing cycles were performed to document the final dissolution temperature of ice ( $T_{m,ice}$ ) and hydrohalite ( $T_{m,hh}$ ), and the homogenization temperature ( $T_h$ ). For further genetic interpretations, only fluid inclusions which had a triplet measurement between <0.1°C for  $T_{m,ice}$  and  $T_{m,hh}$  and <1°C for  $T_h$  were considered. All inclusions and the corresponding data were evaluated for evidence of any post-entrapment modification.

## Geochemical analyses

A total of 248 subsample powders were extracted using a hand-held drill. Those with a mixture of calcite and dolomite [based on X-ray diffraction (XRD) and inductively coupled plasma – optical emission spectrometry (ICP-OES) data] were treated with 0.27 M Di-Na-EDTA to dissolve the calcitic phase (Geske *et al.*, 2015).

Carbon-isotope and oxygen-isotope values ( $\delta^{13}\text{C}$  and  $\delta^{18}\text{O}$ ) were measured by reacting  $0.1 \pm 0.01$  mg of sample powder with phosphoric acid at  $70^\circ\text{C}$ . Sample aliquots were measured on a Thermo Finnigan MAT 253 mass spectrometer equipped with a Gasbench II (Thermo Fisher Scientific, Waltham, MA, USA) and a GC PAL autosampler (CTC Analytics AG, Zwingen, Switzerland) at the Ruhr-University Bochum. The internal dolomite and calcite standards were calibrated against IAEA-603, CO-1, CO-8 and NBS 18 with a  $1\sigma$ -reproducibility (SD) of 0.04‰ and 0.07‰, respectively, for  $\delta^{13}\text{C}$ ; and 0.11‰ and 0.13‰, respectively, for  $\delta^{18}\text{O}$ . All values are reported in ‰ Vienna Pee Dee Formation belemnite (VPDB), and errors as  $1\sigma$  SD.

Strontium isotope ratios ( $^{87}\text{Sr}/^{86}\text{Sr}$ ) were analyzed for 53 samples using the method described in Mueller *et al.* (2020). Ratios were determined using a Thermal Ionization Mass Spectrometer (TIMS) TI-Box (formerly MAT 262; Spectromat, Bremen, Germany) at the Ruhr-University Bochum. Long-term reproducibility was determined using the reference materials NIST NBS 987 and USGS EN-1, and resulted in a  $^{87}\text{Sr}/^{86}\text{Sr}$  ratio of  $0.710242 \pm 0.000001$   $2\sigma$  SE and  $0.000031$   $2\sigma$  SD ( $n = 505$ ) for NIST NBS 987, and a  $^{87}\text{Sr}/^{86}\text{Sr}$  ratio of  $0.709159 \pm 0.000002$   $2\sigma$  SE and  $0.000032$   $2\sigma$  SD ( $n = 418$ ) for USGS EN-1. Errors are reported in  $2\sigma$  SE.

## RESULTS

### Petrography and succession of phases and cements

Input data for the phase sequence in the contact aureole include: (i) field observations (Fig. 3); (ii) thin section and cathodoluminescence evidence (Fig. 4 and Table 2); (iii) qualitative energy dispersive X-ray spectroscopy (EDX) analysis; (iv) microprobe element maps (Fig. 5); and (v) scanning electron microscope (SEM) imaging (Fig. 6). Based on previous work by Jacquemyn *et*

*al.* (2014), a significantly more complete paragenetic succession for the dolomitization pathways of the Latemar isolated platform was produced (Fig. 7 and Table 3). Here, the most essential features in the successions are presented. Refer to Appendix S1 for more details. Dolomite terminology is after Sibley & Gregg (1987).

### **Contact aureole**

The phase succession commences with medium-crystalline nonplanar dolomite marble 1 (Dol marble 1) that typically contains Mg-silicates {spinel ( $\text{MgAl}_2\text{O}_4$ ), forsterite [ $\text{Mg}_2(\text{SiO}_4)$ ] and clinohumite [ $(\text{Mg,Fe})_9(\text{SiO}_4)_4(\text{F,OH})_2$ ] } (Figs 4C, 4D and 6). The Mg-silicates bear high magnesium and silicon concentrations (Fig. 5B, C, F and G). Metamorphic dedolomitization and neomorphism resulted in two marble fabrics: (i) Dedol marble 1 consisting of a medium-crystalline to coarse-crystalline (up to 1 cm) calcitic marble, often containing up to 40 vol.% of dispersed brucite and minor amounts of Mg-silicates (Figs 4G, 4H; 5E to H; Fig. S2A and B) and (ii) Dedol marble 2 consisting of a medium crystalline, solid inclusion-rich calcite marble matrix with up to 60 vol.% of microcrystalline to macrocrystalline Mg-silicates (Fig. 4C to F; Fig. S2C to F). In places, neomorphosed or recrystallized dolomite marble with a larger mean crystal size is present. Dedol marble 2 differs from Dedol marble 1 by smaller average grain sizes, more elongated morphology of crystals, higher inclusion density and the presence of foliation. Millimetre-sized layers of non-luminescent Mg-serpentine [lizardite –  $\text{Mg}_6(\text{OH})_8\text{Si}_4\text{O}_{10}$ ] complement this succession (Fig. 4E and Fig. S3E to H).

The metamorphic carbonate and silicate succession is overgrown by centimetre-thick bands of undifferentiated phyllosilicates and cut by millimetre-thick up to centimetre-thick low magnesium calcite [low-Mg calcite 1 (LMC 1)] veins with orange luminescence. The succession ends with a third dolomite phase, Dol marble 3 (Figs 4E, 4F and 6D), which has a red luminescence similar to Dol marble 2 and is characterized by elongated crystal morphology. Submillimetre-sized to millimetre-sized low-Mg calcite 2 (LMC 2) veins cut LMC 1 veins and older metamorphic phases (Fig. 4C and D). The full metamorphic succession is overgrown by hydrothermal dolomite (Dol 1), meteoric dedolomite (Dedol 1), and aragonite needle cements (AC 1).

## Latemar slope and interior

The general cement-paragenetic succession of Latemar slope and interior begins with the deposition of calcitic and aragonitic precursor sediments that underwent early diagenetic, fabric-preserving dolomitization (Contrin Formation). Contrin dolostone consists of a medium-crystalline planar-s dolomite matrix (Cdol 1; Fig. 4A and B) with abundant recrystallized and poorly preserved *Dasycladacean* algae casts. Pore space is often occluded by medium-crystalline to coarse-crystalline, dull red luminescent, zoned Cdol2 cement. The overlying Latemar Sciliar Formation precursor limestones vary depending on the sub-facies (LPF to UTF in Fig. 2) and are generally characterized by a fine-crystalline to medium-crystalline, dominantly microbial calcite matrix (Harris, 1993; Blendinger, 1994; Emmerich *et al.*, 2005) including marine dog tooth and radial fibrous calcite (RFC) cement, which occludes pore space (Fig. 7G and H).

Based on the data presented here, hydrothermal dolostones consist of four dolomite cement phases. Dol 1 consists of inclusion-rich fine-crystalline (dominant at Latemar slope) to poorly zoned inclusion-rich coarse-crystalline (prevalent at Latemar interior) planar-s dolomite (Fig. 7A to D; Fig. S5C and D). Dol 1 and 2 are separated by a quartz phase (Qz 1), typically forming hypidiomorphic medium-crystalline to coarse-crystalline aggregates. Dol 2 is zoned, fine-crystalline to coarse-crystalline planar-e to nonplanar dolomite (Fig. 7A and B; Fig. S4A to G). Dol 3 is the volumetrically most significant, fine-crystalline to coarse-crystalline planar-s to nonplanar dolomite and was subdivided into inclusion-rich inner and inclusion-lean outer zones (Fig. 7E to H). Dol 4 is composed of coarse-crystalline nonplanar saddle dolomite (Fig. S5E and F). Most dolomite phases show slight features of dedolomitization and infill of iron oxides (Fe-oxides), best visible in individual Dol 2 zonations (Fig. 7B and D; Fig. S5C and D). Latest stage low Mg-calcite (LMC) cements consist of medium-crystalline to coarse-crystalline blocky calcite (LMC 1; Fig. 7E to H) and fibrous LMC 2 (Fig. S5G and H) typically observed in fissures and pore space in magmatic dykes. Meteoric cements HMC 1 and LMC 3 are volumetrically insignificant, pore-filling phases.

## Fluid inclusion thermometry

Detailed petrography by transmitted light microscopy and microthermometry of fluid inclusion assemblages (FIAs) enables classification according to relative age (Goldstein & Reynolds, 1994;

Walter *et al.*, 2015). Data are shown in Fig. 8, focusing on primary inclusions hosted in growth zones and pseudo secondary (*sensu* Walter *et al.*, 2015) inclusions (Table 4). Primary inclusions along crystal growth zones are typically smaller (<5 to 10  $\mu\text{m}$ ) than pseudo secondary assemblages (<5 to 20  $\mu\text{m}$ ), which are present in (partly) sealed fractures and cross-cut the primary structures of the host minerals.

Data from a dedolomitized marble sample (Dedol marble 2, CC4) taken at the contact aureole, a blocky calcite sample from the Latemar slope (LMC 1, VS10-7), a dolomite sample from the Latemar interior (Dol 2, S6.1), a dolomite (Dol 2, VS10-8), and a Contrin dolomite sample of the Latemar slope (Contrin) are documented in Fig. 8. These show a large variability in homogenization temperatures ( $T_h = 54\text{--}292^\circ\text{C}$ ) and a significant salinity range from 0.8 to 31.8 wt.% NaCl+CaCl<sub>2</sub>. Homogenization was always into the liquid phase. The volume fractions are constantly around 0.95 ( $L_{0.95}V_{0.05}$ ), indicating that no post-entrapment modifications occurred. No evidence for SO<sub>4</sub>, CO<sub>2</sub> or CH<sub>4</sub> was observed (Walter *et al.*, 2017). Homogenization temperatures (Fig. 8) include: 201 to 220°C at the contact aureole (n = 6), 191 to 282°C (n = 11) in Latemar slope phases and 54 to 72°C (n = 5) for the Latemar interior dolomite. See Appendix S1 for all data.

### **Carbon-isotope and oxygen-isotope data and radiogenic strontium ratios**

Geochemical data is shown in Tables 2 and 3, which include: (i) major-element and trace-element concentrations; (ii)  $\delta^{13}\text{C}$  and  $\delta^{18}\text{O}$  ranges; and (iii)  $^{87}\text{Sr}/^{86}\text{Sr}$  ratios in sample groups. See Appendix S1 for further data (Tables S1 to S4). Oxygen isotope values range from -13.4 (AC 1 and Dol 1 / Dedol 1 from the contact aureole) to -0.8‰ (Dol 1 from the Latemar slope), independent of sample mineralogy and age. The  $\delta^{13}\text{C}$  values range from -0.7 (Dedol marble 2) to +5.0‰ (dolomitized oolitic ironstone). The  $^{87}\text{Sr}/^{86}\text{Sr}$  ratios (n = 55, Table 2 and 3) range from 0.706666 (LMC 2 Latemar) to 0.710011 (LMC 1 CC). Marbles from the contact aureole show a general trend towards non-stratigraphic, more radiogenic  $^{87}\text{Sr}/^{86}\text{Sr}$  values from early dolomite and dedolomite marble to later phases with increasing Mg-silicate content. At the Latemar slope and interior, Triassic marine values are dominant, but outliers occur.

## INTERPRETATION AND DISCUSSION

Three data clusters are discussed below: (i) the metamorphic contact aureole, fringing the intrusion (elevation 1000 m a.s.l.); (ii) the Latemar slope, exposing carbonates 4 to 5 km to the north-west of the intrusion (1800 and 2300 m a.s.l.); and (iii) the Latemar interior, 5 to 7 km to the north-west of the intrusion (2400 and 2600 m a.s.l.). First discussed is the petrography from oldest to youngest phases, followed by the geochemistry and finally a brief synopsis.

### **Petrography and isotope geochemistry**

The history of these rocks commences with the deposition of Anisian–Ladinian Contrin and Sciliar precursor sediments in an isolated platform environment, which later (about 240 Myr) record (sub)recent meteoric diagenesis of the exhumed contact aureole and the Latemar carbonates (Fig. 9). The main events that affected the Contrin dolostones and Sciliar limestones are summarized in Figs 9, 10A and 10B.

#### *High-temperature contact metamorphism of early diagenetic dolostones*

##### *Contact aureole petrography.*

The Contrin Formation dolostones in the intrusive contact aureole preserve petrographic evidence of a peak-retrograde to retrograde-metamorphic cycle: (i) a peak-metamorphic mineral succession; (ii) neomorphosed minerals representing retrograde cooling; (iii) carbonate phases related to tectonic stress; and (iv) subrecent meteoric cements representing exhumation of the carbonates (Fig. 11).

The Predazzo subvolcanic body has metamorphosed early diagenetic Contrin dolostones into dolomite marble (Dol marble 1; Fig. 10A), which forms lenses with diameters of tens of metres (Figs 3F and 12A). The dominantly annealed microfabric (*sensu* Molli *et al.*, 2000) in Dol marble 1 (Fig. 4C) is indicative of a primary recrystallization stage at low to moderate metamorphic temperatures. Apart from locally preserved Dol marble 1, most Contrin marbles were dedolomitized under the influence of structurally-controlled fluids during peak-contact

metamorphism (Ferry *et al.*, 2002). The time-integrated fluid flux of about 300 mol fluid/cm<sup>2</sup> resulted in transformation of the dolomite marble to periclase-rich (MgO) calcite marbles (Dedol marble 1) at temperatures of 565 to 710°C (Ferry *et al.*, 2002). One possible factor inducing the transition from Dol marble 1 to dedolomite marble is the transition across the dolomite-to-calcite stability window at T = >500°C. At this stage, the Ca/Mg molar ratio is fairly constant, but the system temperature rises (Morrow, 1994, and references therein; Huang *et al.*, 2009). This process is also in agreement with the generation of supercritical aqueous fluids with a greatly reduced kinematic viscosity at pressures >22 MPa (MegaPascals). Peak-metamorphic micro-crystalline spinel and forsterite are present as the finely dispersed phase. The Predazzo Intrusion consists of three distinct intrusive pulses, with the oldest pulse composed of a silica saturated shoshonitic melt (Fig. 2D; Casetta *et al.*, 2018a) and thus probably silica-containing fluids during the first stage of dedolomitization [ $\text{CaMg}(\text{CO}_3)_2 = \text{MgO} + \text{CaCO}_3 + \text{CO}_2$ ]. Spatial variations in peak-metamorphic mineral content were used to determine a vertical direction of fluid flow during peak-metamorphic dedolomitization. With regard to the present mineral content, two dedolomitization reactions are possible: (i)  $\text{CaMgSi}_2\text{O}_6 + \text{CaMg}(\text{CO}_3)_2 = \text{Mg}_2(\text{SiO}_4) + \text{CaCO}_3$  (assuming  $X_{\text{CO}_2} > 0.7$ ); or (ii)  $\text{CaMg}(\text{CO}_3)_2 = \text{MgO} + \text{CaCO}_3$  (assuming  $X_{\text{CO}_2} > 0.05$ ).

Brucite [ $\text{Mg}(\text{OH})_2$ ; Bocchi & Morandi, 1971] evidences infiltration of aqueous fluids at about 560°C and is the first petrographic expression of retrograde metamorphism [ $\text{MgO} + \text{H}_2\text{O} = \text{Mg}(\text{OH})_2$ ]. Periclase (MgO) exclusively occurs as a remnant in micrometre-sized inclusions in calcite marbles (Figs 10A and 11; Ferry & Rumble, 1997; Ferry *et al.*, 2002). Subsequent fluid circulation during retrogression locally broke down brucite in favour of newly formed dolomite and lizardite. Serpentinization [ $3\text{CaMg}(\text{CO}_3)_2 + 2\text{Si}(\text{OH})_4 = (\text{Mg})_3\text{Si}_2\text{O}_5(\text{OH})_4 + 2\text{H}_2\text{O} + 3\text{CaCO}_3 + 3\text{CO}_2$ ] in a tectonically active regime is most common at the contact of preserved Dol marble 1 to the brucite-lean Dedol marble 1 zone. This is expressed by submillimetre-thick to decimetre-thick pseudo-bedding foliation of Dol marble 1, Dedol marble 2, Mg-silicates, lizardite and a suite of undifferentiated phyllosilicates (Figs 3G, 4D, 4E, 10A, 12A and 12D). A likely mechanism creating foliation-inducing strain during retrograde metamorphism could be emplacement of the subsequent granitic and shoshonitic intrusive pulses *sensu* Casetta *et al.* (2018a,b). Assuming this concept holds true, the above petrographic evolution should have occurred over less than 6 Myr (Laurenzi & Visona 1996; Mundil *et al.*, 1996; Visona, 1997).

Neomorphism of inclusion-poor Dol marble 2 is best assigned to the subsequent intrusive pulses and is exemplified by elongated dolomite crystals, which typically occur in the foliated Dedol marble 2 calcite matrix or direct contact to annealed Dol marble 1 fabrics. Dynamic, deformation-driven recrystallization, forming elongated crystals, is well known from other tectonically active metamorphic settings and is interpreted to represent temperatures of 350 to 400°C in deformed Carrara marbles (Molli *et al.*, 2000; Leiss & Molli, 2003). Petrographic and field evidence suggests that LMC 1 and neomorphosed, inclusion-lean Dol marble 3 mark the second stage of retrogression. These also form elongated crystals but are precipitated in a phase of tectonic activity, which is expressed by their occurrence in veins that pervasively cut older phases (Figs 3G, 4F and 10A). Clinohumite formed during the late stages of retrogression in rims around forsterite crystals.

Rare and isolated fluid inclusions represent the latest stage of retrogression in Dedol marble 2. Fluid inclusion homogenization temperatures from 200 to 220°C may represent the last stage of retrograde recrystallization (Walter *et al.*, 2018), which is also expressed by calcite twinning in Dedol marble 1. Predominantly thin-tabular to thick-tabular calcite twins are present (Fig. 4G and Fig. S2A); these may represent a comparable temperature range of about 170 to 200°C (Ferrill *et al.*, 2004). LMC 2 exclusively occurs in submillimetre-sized veins cutting all older phases (Figs 4F and 10A). This stage is followed by dolomite cement (Dol 1). Warped crystal faces in (saddle) Dol 1 indicate a hydrothermal origin (Fig. 9 and Fig. S2G and H). The moderate impact of Alpine Orogeny in this area of the Dolomite Mountains (Gaetani *et al.*, 1981; Jacquemyn *et al.*, 2014) induced some compressional stress-triggered circulation of hydrothermal fluids, wherein the precipitation of cementation related to hydrothermal fluids ceased. Latest stage meteoric dedolomite and aragonite cements (Dedol 1, AC 1) fill sub-recent fractures and karst-related porosity.

#### *Contact aureole isotope geochemistry.*

The meta-carbonates in the aureole display a wide range of geochemical signatures. Carbon-isotope, oxygen-isotope and strontium-isotope distributions range between a marine Triassic carbonate and a metamorphic endmember with numerous intermediate stages (Figs 14 and 15). A comparison between Dol marble 1 in the contact aureole with its recrystallized, early diagenetic

Contrin dolostone precursor at the base of the Latemar mountain (4 km to the north-west) reveals only moderate differences in  $\delta^{13}\text{C}$  (1.7 to 2.4‰ versus 3.1 to 3.3‰; Figs 14A and 15A) and  $\delta^{18}\text{O}$  values (-0.9 to -3.3‰ versus -2.9 to -3.1‰; Figs 14A and 15A). Both phases are outside the range of Anisian carbonate ( $\delta^{13}\text{C} = ca$  -0.5 to 1.7‰), but the oxygen-isotope signature of Dol marble 1 is weakly enriched in  $^{18}\text{O}$  (Anisian  $\delta^{18}\text{O} = -2.0$  to  $-6.5$ ‰). The  $^{87}\text{Sr}/^{86}\text{Sr}$  ratios of Dol marble 1 yield a wide range (0.707658-0.708929) from Triassic marine ratios to much more radiogenic values (Fig. 16). In contrast, Contrin dolostones have Triassic marine  $^{87}\text{Sr}/^{86}\text{Sr}$  ratios (0.707755). Previous work in the Latemar (Jacquemyn *et al.*, 2014) exclusively reported marine strontium-isotope data. The much wider isotopic range in the same metamorphic phase presented here, merits attention.

Counterintuitively, published bulk carbon-isotope and oxygen-isotope data of dolomite and dedolomite marbles suggests that these fall within the range of preserved Triassic marine carbonates (Ferry *et al.*, 2002; see dolomite and calcite data in Fig. 14). Differences in carbon-isotope composition between different calcite marbles (with and without brucite) have been assigned to Rayleigh-type processes during dedolomitization (Ferry *et al.*, 2002). The lack of pervasive geochemical re-equilibration during heating towards (high) metamorphic temperatures is of interest.

The observation of what seem only weakly overprinted (marine) isotope values in contact metamorphic marbles allows two basic interpretations.

**1** The recrystallization of precursor carbonates occurred in a diffusion-controlled system by fluid films at grain boundaries or along reaction fronts (Pingitore, 1982; Watson & Müller, 2009; Jonas *et al.*, 2017; Pederson *et al.*, 2019a). This type of rock-buffered metamorphism has previously been proposed for the Carrara marble and neighbouring dolomitic units, both geochemically indistinguishable from their non-metamorphic precursor lithologies (Cortecci & Lupi, 1994; Cortecci *et al.*, 1999).

**2** Recrystallization with larger fluid volumes, but still in a generally rock-buffered system (Greenwood, 1975). Baumgartner & Ferry (1991) suggested that if the time-integrated fluid flux is not extensive, reactants and products coexist along a significant portion of the flow path. This scenario was also insighted (Gallien *et al.*, 2007) explaining seemingly marine carbon-isotope and oxygen-isotope values in dolostones of the Monzoni Intrusive Complex aureole (about 10 km north-east of the Latemar platform). This preservation model depends on a suite of factors often

overlooked due to their complex nature: protolith composition, effects of volatilization, temperature of exchange, exchange kinetics, fluid isotope composition, fluid pressure and fluid flux/mixture (Baumgartner & Valley, 2001, and references therein; Duan *et al.*, 2021).

A closer look at the subsequent peak-metamorphic and retrograde phases reveals that Dedol marble 1, Dedol marble 2 and Dol marble 2 (in contrast to Dol marble 1) largely plot in the range of Anisian marine isotope and Ladinian contact metamorphic overprint values (Fig. 14A). A -3‰ shift of carbon isotope values starting with Dol marble 1, with the most  $^{13}\text{C}$ -depleted values in Dedol marble 2 and Dol marble 2. This observation contrasts previous work (Ferry *et al.*, 2002) proposing that differences in the bulk-carbon composition are related to differential volumes of brucite in a given sample. Note, Dedol marble 2 does not contain brucite. In the view of the authors, this prograding trend has not yet been documented. A driving mechanism for this subsequent trend could be the contribution of magmatic carbon from mantle-derived  $\text{CO}_2$ , which has  $\delta^{13}\text{C}_{\text{CO}_2}$  values between -5 and -8‰ (Kyser, 1986; Hoefs, 1997). When the isotopic fractionation of 2‰ between carbon in magma and gaseous  $\text{CO}_2$  at igneous temperatures is considered, a  $\delta^{13}\text{C}_{\text{CO}_2}$  range from -3 to -5‰ for  $\text{CO}_2$  from a magmatic origin results (Dietzel & Kirchhoff, 2002). Metamorphic phases at Predazzo Intrusion contact aureole were influenced by magmatic  $\text{CO}_2$ , with larger isotopic shifts dominantly inhibited by a large amount of (rock buffered) carbon from the carbonates.

Oxygen-isotope data indicate a shift of about -6‰ from Dol marble 1 to Dedol marble 1 and a reverse shift to  $^{18}\text{O}$ -enriched values of *ca* +4‰ from Dedol marble 1 to Dedol marble 2 (Fig. 14A). Figure 15 shows the  $\delta^{18}\text{O}$  values of the formation fluid calculated from the  $\delta^{18}\text{O}_{\text{VPDB}}$  values of marbles and the temperature (obtained from Ferry *et al.*, 2002) using the equations of Sheppard & Schwarcz (1970) and Friedman & O'Neil (1977) for dolomite and calcite, respectively, which considers isotopic equilibrium (Vho *et al.*, 2019). The oxygen isotope fractionation between the mineral (dolomite or calcite) and the fluid decreases at elevated temperature, resulting in an  $\delta^{18}\text{O}_{\text{carbonate-H}_2\text{O}}$  value of 300°C at about +6‰ and 600°C at about +1‰. Thus, at  $T \geq 600^\circ\text{C}$  the calculated fluid composition approaches the  $\delta^{18}\text{O}$  values of the marble (Figs 11 and 15; Ferry *et al.*, 2002). The calculated  $\delta^{18}\text{O}_{\text{SMOW}}$  of the fluid ranges from about -5‰ at 50°C up to about +30‰ at 650°C (Fig.15). A shift to  $\text{O}^{18}$ -enriched fluids may be explained by the admixture of hydrothermal fluid from altered silicates from the igneous intrusion and/or a so-called primary magmatic water (juvenile). However, corresponding  $\delta^{18}\text{O}_{\text{SMOW}}$  values are documented to be a

maximum of +10‰ (e.g. Giggenbach, 1992; Hoefs, 2009). Thus, the extremely O<sup>18</sup>-enriched calculated fluid values of about +30‰ (SMOW) cannot be solely explained by the leaching/exchange of oxygen of silicate minerals from the intrusions. During metamorphism, the oxygen isotope composition of marine Contrin dolostone ( $\delta^{18}\text{O}_{\text{VPDB}} = -2.0\text{‰} \pm 2$ ) is preserved (for example,  $\delta^{18}\text{O}_{\text{VPDB}}$  at 650°C: Dol marble 1) due to very low volumes of meteoric or magmatic fluids involved and the volatile character of H<sub>2</sub>O at such high temperatures. Accordingly, the  $\delta^{18}\text{O}$  distribution of high-temperature marble indicates closed-system conditions. The weak magmatic influence coincides with the observed  $\delta^{13}\text{C}$  shift in the marbles and the rock-buffered system for carbon as discussed above.

Dedolomitization during differential fluid flow may also control the carbonate strontium-isotope ratios. Strontium ratios plot between Triassic marine values in Dol marble 1 and Dedol marble 1 (0.707658 to 0.707942), to more common radiogenic values in all subsequent phases (up to 0.710011 in LMC 1). Although no clear phase-specific trend was observed, the most radiogenic ratios occur in carbonate phases rich in retrograde serpentinized silicates (lizardite, forsterite, clinohumite). If this holds true, the strontium source must be highly radiogenic as silicates are typically depleted in strontium compared to carbonates (Fig. 5D and H). In the absence of additional high-resolution data, it seems unclear how to accommodate the radiogenic strontium and its origin in the metamorphic sequence. Ferry *et al.* (2002) suggested an H<sub>2</sub>O-rich fluid from a portion of the intrusion cross-cutting the carbonate rocks at depth. Several studies reported strontium-isotope ratios for the different magmatic units of the Predazzo Intrusion below 0.706500 (Fig. 16, arrays 4 to 7). Other workers suggest albitization of basement granite by seawater formation fluids as process to contribute radiogenic strontium to hydrothermal fluids (Spencer, 1987). For the time being, it seems at least possible that deep-seated basement fluids may have contributed radiogenic strontium during metamorphism. Meteoric dedolomite and aragonite cements, typically occluding late-stage fractures or karst-related vuggy porosity, share similar carbon-isotope values with late marble phases, but are significantly depleted in their oxygen-isotope composition.

*Synopsis: Contact aureole.*

The peak-metamorphic and retrograde-metamorphic carbonate phases in the Predazzo aureole reveal: (i) complex petrographic and geochemical patterns driven by dedolomitization; (ii) carbonate neomorphism due to interactions with reactive fluids; and (iii) variable fluid–rock ratios. In contrast to a full metamorphic cycle, geochemical proxy data ( $\delta^{18}\text{O}$ ,  $\delta^{13}\text{C}$ ) of these rocks show uncommonly conservative (rock-buffered) behaviour and plot within the range of Middle Triassic marine-isotope values. Strontium-isotope ratios document fluid evolution during neomorphism of Mg-silicates and suggests mixing of fluids from different sources. Processes and products documented here may act as templates for metamorphic-related overprint patterns of carbonate archives commonly occurring over longer timescales and larger spatial extents.

*Metamorphism, early-marine diagenetic dolostones, and hydrothermal dolomitization at the Latemar slope*

*Latemar slope petrography.*

Despite the near-ideal conditions of the Latemar natural laboratory, the following limitations exist in establishing spatial patterns in cement paragenesis across a carbonate edifice of several kilometres in dimension: (i) inherited facies variability from the basal Contrin Formation (near the intrusion) to the uppermost dolomitized units of the Sciliar Formation (distance of 6 to 7 km; Middle Tepee Facies; Preto *et al.*, 2019); and (ii) differences in outcrop geometry ranging from dolostone bodies (tens to a few hundreds of metres in size) oriented near-vertical relative to slope bedding (Fig. 3D), to smaller (metres to tens of metres) often facies-bound and bedding-bound dolostone units in the Latemar interior (Fig. 3B and C; Jacquemyn *et al.*, 2015). The dimensions of dolostone bodies generally decrease with increasing distance from the intrusion.

The Contrin Formation in the Dolomite Mountains was previously described as fabric-preserving, early marine-diagenetic dolomite (Gaetani *et al.*, 1981; Sudiro, 2002). Ghost structures of *Dasycladacean* algae and the dolomitic nature of these rocks are considered evidence for syndepositional reflux dolomitization (Fig. 13A and Fig. S4A and B). These dolomites (or very high-Mg calcites) were probably calcian in nature and experienced further stabilization (Nordeng & Sibley, 1994).

At the base of the Latemar isolated platform, about 4 km north-west of the intrusion, later-stage dolomite recrystallization has obscured sedimentary features in the Contrin dolostone (Figs 4A, 4B and 13B) (Jacquemyn, 2013). The fabric is formed by zoned, euhedral, replacement dolomite (Fig. 4B). Fluid inclusion homogenization temperatures (185 to 200°C) suggest hydrothermal recrystallization of the early diagenetic Contrin dolostones (Fig. 8). During the deposition of the Sciliar precursor limestones, Contrin dolostones were affected by synsedimentary extensional tectonics induced by the overburden of the growing platform (Preto *et al.*, 2011). Domal uplift during emplacement of the intrusion caused north-west–south-south-east trending fractures which served as zones of weakness for subsequent dyke intrusion (Doglioni, 1983; Jacquemyn *et al.* 2014). During the cooling of dyke material, thermal contraction opened hydrothermal fluid pathways at the sediment–dyke interface.

The Sciliar Formation limestone precursor facies upsection of the Contrin Formation (Lower Platform Facies, 4 km north-west from Predazzo Intrusion) contains marine cements (radial fibrous calcite, dog tooth cement) and preserves a series of primary depositional features. With increasing distance from the intrusion, a series of features is observed that is best explained in context with decreasing fluid temperature and fluxes. Jacquemyn *et al.* (2014) described contact metamorphic to diagenetic, recrystallized metre-wide aureoles, in the vicinity of large dykes in outcrops of the Latemar slope (4 to 5 km from the aureole). With increasing distance to dykes, the dolomite cement paragenesis at the Latemar isolated platform is characterized by decreasing Fe-content from early-stage to late-stage dolomite (Jacquemyn *et al.*, 2014). Similarly, Blomme *et al.* (2017) documented that bulk Fe-content decreases within centimetres to a few metres from the dykes (Figs 9 and 10B). These authors hypothesized that seawater interaction with mafic minerals in dykes caused Fe-enrichment in the dolomitizing fluid.

In all thin sections, Fe-rich Dol 1 typically consists of patchy-luminescent, inclusion-rich, often corroded cores overgrown by zoned or non-zoned rims. Zonation indicates changes in fluid properties during the first phase of dolomitization. Similarly, the precipitation of Qz 1 in dyke-parallel veins and pore space between Dol 1 and Dol 2 suggests transient silica oversaturation at a specific stage between Dol 1 and Dol 2 precipitation. Qz 1 is only observed in the diagenetic halo of dykes, suggesting short-lived fluid pulses from the dykes. Zoned, in part patchy-luminescent, Dol 2 occurs as pore-filling cement. Dol 2 has curved crystal faces with sweeping extinction, typical of saddle dolomite (Radke & Mathis, 1980; Wallace & Hood, 2018) forming at fluid

temperatures of about 50 to 320°C (Davies & Smith, 2006; Liu *et al.*, 2014). The temperature range (260 to 290°C) of fluid inclusions in Dol 2 (4.5 km from the intrusion) is typically assigned to the deep burial-grade to the low-grade metamorphic realm. The volumetrically most significant Dol 3 phase consists of patchy-luminescent, non-corroded to partly corroded cores fringed by translucent rims, similar to Dol 1. The most prominent difference between these two phases is the higher Fe-content in Dol 1 (see Appendix S1). Where present as a pore-filling phase in limestones, the crystals show weakly-warped crystal faces with sweeping extinction similar to the Dol 2 saddle dolomites.

The dolomitizing sequence ends with Dol 4, a porosity-occluding saddle dolomite cement, characterized by a few millimetres to one centimetre-sized crystals with warped faces, sweeping extinction and low Fe-concentrations (Jacquemyn *et al.*, 2014). Dol 4 is volumetrically most significant in pores of boxwork dolostone. Boxwork/cell dolostone commonly occurs upsection of the contact between Contrin Formation dolostones and Lower Platform Facies dolostones at about 4 km from the intrusion. Zebra dolomite accompanied by dilational fracturing is present (Jacquemyn *et al.*, 2014). Boxwork dolomite does occur bed parallel or, in many cases, non-strata bound and rather chaotic (Fig. 3E). Boxwork dolomite may form as the result of previously fractured precursor limestones affected by pressure release during dolomitization and later dissolution of limestone clasts (Figs 3E, 12B and E; Dunsmore, 1973; Wallace & Hood, 2018). An alternative formation mode is dissolution in permeable limestone or dolostone beds (Morrow, 2014).

After a hiatus in the cement stratigraphy, fluids with lower Mg/Ca ratios, or an ephemeral temperature rise at fairly constant Mg/Ca ratios, led to precipitation of millimetre-sized to several centimetre-sized blocky LMC 1 in all dolomitized limestone samples. Fluid inclusion data from the Latemar slope (4.5 km from the intrusion) document elevated fluid temperatures (188 to 195°C). Blocky and fibrous LMC 2 filling fissures in dykes likely also precipitated during this stage or shortly thereafter. Some growth zones in several dolomite crystals show dedolomitization features (Fig. 7C and D). The resulting pore space is typically filled by Fe-oxides, which increase the bulk Fe-content of dolomite phases and limit the applicability of trace element data. The latest stage LMC 3 and HMC 1 cements are rare and represent a moderate petrographic meteoric/vadose overprint (Figs 9 and 10B).

### *Latemar slope isotope geochemistry.*

The ongoing controversy regarding the in part  $^{13}\text{C}$ -enriched marine signatures of the Latemar Sciliar limestones [see Jacquemyn (2013) and Jacquemyn *et al.* (2014) for a detailed discussion] is acknowledged. The argument is that Latemar limestones with  $^{13}\text{C}$ -enriched signatures, relative to coeval carbonate platforms in the Dolomite Mountains, might record early stages of hydrothermal  $\text{CO}_2$  exhalation at the seafloor predating the intrusion of igneous bodies. Based on bulk, and more recently, cement-specific analyses, Triassic marine values have been reported for carbon, oxygen and strontium isotopes (Wilson, 1989; Carmichael, 2006; Jacquemyn, 2014). Heavier carbon-isotope values, relative to Carnian seawater, were first reported by Carmichael *et al.* (2008). Jacquemyn *et al.* (2014) argued that most samples reflect the Carnian seawater isotope composition during Sciliar carbonate deposition. Phase-specific data presented here further support this interpretation. An alternative source of heavy  $^{13}\text{C}$  might be syndepositional methanogenesis of organic material in lagoon shoal-settings (Teal *et al.*, 2000).

Dolomitized Latemar slope oolitic ironstones yield the most positive  $\delta^{13}\text{C}$  values (up to +5‰; Fig. 17A), as do Dol 1 (Dol 1<sub>max.</sub> = +4.9‰; Fig. 17A) samples in the slope, 4 to 5 km from the intrusion. All of these samples were collected in close vicinity (i.e. within decimetres to metres) of dykes. This study observed a difference of +2.5‰ between the limestone precursor facies and Dol 1, and a difference of +1‰ between the limestone precursor and Dol 2. Later dolomite phases Dol 3 and Saddle Dol 4 lack this pattern, independent of the sampling location.

Werfen Formation marlstone bulk samples collected below the Contrin Formation in the direct vicinity of dykes (3.5 to 4 km north-west of Predazzo Intrusion) yield diagenetically altered  $\delta^{18}\text{O}$  values (-11.0 to -12.5‰). Generally, no significant burial-diagenetic or meteoric-diagenetic overprint of the  $\delta^{13}\text{C}_{\text{dolomite}}$  and  $\delta^{18}\text{O}_{\text{dolomite}}$  signatures was observed (Fig. 17A). Exceptions include a few samples (n = 5) of Dol 1 and later stage dolomites (Dol 3 and Dol 4). Diagenetic overprint of Sciliar  $\delta^{18}\text{O}_{\text{calcite}}$  signatures is reflected in late calcite cements occluding minute pores and vugs. This is best visible in LMC 1 cements with  $\delta^{18}\text{O}$  values as low as -12.3‰. Nearly all sampled phases, including early diagenetic Contrin dolomites from the base of Latemar slope, plot within the range of Triassic marine precipitates.

The concept of geochemical patterns in Dol 1 and Dol 2 precipitated from intrusion-derived fluids merits attention. Dolomitizing fluids may migrate at basin-scale, with fluid flow

driven by a range of processes (Braithwaite *et al.*, 2004). Still, the setting described here, i.e. metamorphic dedolomitization acting as a source of Mg in dolomitizing fluids, arguably represents a less-commonly described process. It seems likely that some of the Mg, released during peak-metamorphic dedolomitization, migrated with the dolomitizing fluid. This interpretation is strengthened by the observation that only some Mg at the contact aureole was sequestered within the neomorphosed Mg-silicates.

The strontium-isotope ratio of most Sciliar Formation phases, independent of their spatial position, plot in the range of biogenic and abiogenic marine calcite (Korte *et al.*, 2003; Fig. 16). The data reveal no difference between most precursor limestones and dolomite phases sampled in the Latemar slope. Generally, only two Latemar slope dolomite samples are less radiogenic compared to the global seawater curve. Similar patterns have been observed in the context of shoshonitic or granitic units of the Predazzo Intrusion (Jacquemyn *et al.*, 2014). Similarly, only three samples are more radiogenic than predicted Triassic marine calcites. The source of the more radiogenic strontium remains unclear at present. For the time being, the question if there is a relation between more radiogenic strontium ratios in samples collected in the contact aureole and samples from the Latemar isolated platform remains unresolved. If the radiogenic strontium was supplied by a deep-seated basement fluid rising through intrusion-related pathways, it would seem likely that both the contact aureole and the dolomitized strata of the Sciliar Formation at Latemar should be affected.

*Synopsis: Latemar slope.*

Metasomatizing fluids trigger the dolomitization of Sciliar Formation limestones now exposed at the slope of the Latemar (about 4 km from the intrusion). The volume and size of hydrothermal dolostone rock bodies embedded in limestones decrease systematically (from hundreds to a few metres) with increasing distance (kilometres) from the intrusion, arguably reflecting decreasing fluid–rock interaction. At the metre-scale, the dolomite cement paragenesis is characterized by decreasing Fe-content from early to late phases with increasing distance to dykes. At the sub-millimetre scale, fluid inclusion homogenization temperatures indicate a hydrothermal temperature regime between 180 and 290°C. The majority of paragenetic phases yield oxygen-isotope and strontium-isotope compositions typical of Triassic marine carbonates. This is remarkable,

particularly considering the carbonate oxygen-isotope system is prone to temperature-controlled fractionation. However, temperature-related fluid-carbonate fractionation of oxygen decreases at higher temperatures (Sheppard & Scharcz, 1970). A difference of  $\delta^{13}\text{C}$  values of +2.5‰ between limestone precursor and Dol 1, and +1‰ between limestone precursor and Dol 2 phase was observed. Dolomite phases Dol 3 and Saddle Dol 4 taken from the same specimen lack this trend.

### *Relation between contact metamorphism and dolomitization in the Latemar isolated platform interior*

#### *Latemar interior petrography.*

The isolated platform interior is spatially situated at 5 to 7 km lateral distance and 1.4 to 1.6 km in altitude from the intrusion and represents the low-temperature end member of the transect. The Sciliar Formation limestone precursor facies typically lacks the metre-wide aureoles fringing large dykes at sites closer to the intrusion. Sciliar limestones show limited-to-no evidence for petrographic alteration at the contact to intrusive dykes due to the comparably small volumes of low-temperature hydrothermal fluids involved. Alternative interpretations include higher crystallization rates due to a lower temperature gradient of the melt further from the source.

Replacive dolostones in Latemar's interior lack boxwork dolostone fabrics with saddle dolomite and later LMC 1. In the platform interior, limestone–dolostone transition zones are represented by vein swarms filled by euhedral dolomite, which cross-cut the precursor limestone in zones several decimetres wide (Figs 3C, 12C and 12F). Fluid-inclusion homogenization temperatures of 54 to 72°C in Dol 2 (at 6.5 km from the intrusion) are markedly cooler compared to those in Dol 2 (260 to 290°C), 2.5 km closer to the intrusion. This may indicate a time-equivalent temperature evolution with increasing distance from the fluid source for dolomitization. Interestingly, the range of 54 to 72°C is also in agreement with carbonate-clumped isotope data (Ferry *et al.*, 2011) from the Latemar interior. Further research to verify fluid inclusion data confidence and to detect a spatial temperature trend at Latemar is under way.

The directly comparable cement stratigraphy (Dol 1, 2 and 3) in outcrops at the Latemar slope and the platform interior supports the interpretation of contemporaneous dolomitization events. Differences are mainly related to: (i) the spatial distance between the sample and an

intrusive dyke; (ii) Fe-content; and potentially (iii) decreasing fluid inclusion homogenization temperatures towards the Latemar interior.

*Latemar interior isotope geochemistry.*

Metamorphic dedolomitization at the intrusive contact acted as a Mg source for dolomitizing fluids in the Latemar interior (Jacquemyn *et al.*, 2014, 2015). A spatially resolved carbon-isotope gradient is recognized when comparing outcrops of Latemar slope dolostones with those of the more distal Latemar interior. In agreement with petrographic evidence for decreasing fluid temperature, the metamorphic influence on  $\delta^{13}\text{C}_{\text{dolomite}}$  and  $\delta^{18}\text{O}_{\text{dolomite}}$  values become increasingly less important, with a difference of about +1‰ between all limestone and Dol 1 samples (Fig. 17B). All subsequent dolomite phases (Dol 2, Dol 3 and Dol 4) lack this pattern, suggesting  $\delta^{13}\text{C}$  values are rock-buffered. The weakly  $^{13}\text{C}$ -enriched data from the Latemar interior are likely related to increasing distance to the metasomatized fluid source. Remarkably, three subsamples of a partly recrystallized Sciliar limestone, from the direct vicinity (<1 cm) of a dyke (5 km from the intrusion), have a similarly positive  $\delta^{13}\text{C}_{\text{calcite}}$  signature (3.8 to 3.9‰; Fig. 17B). All of these patterns point to the complexity of the system, even when samples are placed in a temporal and spatial context.

Jacquemyn *et al.* (2014) argued that dedolomitization of the aureole dolomites alone is likely insufficient to provide the amount of Mg required to dolomitize significant volumes of limestone. These authors instead suggested that the characteristic Carnian seawater signatures in hydrothermal bulk replacement dolomite indicate a seawater contribution. If this holds true, two independent Mg sources best explain the early diagenetic dolomitization of the Latemar: (i) Mg from the contact metamorphic dedolomitization; and (ii) Mg from Carnian seawater.

When comparing the oxygen-isotope values of limestone precursors and dolomite phases, the most relevant factor is temperature-controlled fractionation (up to about 100°C), which adds to mineralogical fractionation between calcite and dolomite (up to 3‰; Swart, 2015). Care must be taken, however, as mineral-dependent fractionation is most significant at ambient seawater temperatures and decreases at higher fluid temperatures. Mineral-dependent fractionation is best documented in replacement dolomite Dol 3 exposed in the Latemar interior outcrops (Fig. 17B).

Similar to samples from the Latemar slope, the  $\delta^{18}\text{O}_{\text{dolomite}}$  values ( $n = 9$ ) of Dol 3 and Saddle Dol 4, are  $^{18}\text{O}$ -depleted compared to their limestone precursors (Fig. 17B).

Similar to Latemar slope samples, the strontium-isotope ratios of most Sciliar Formation phases, independent of their spatial position, plot in the range of marine calcite (Korte *et al.*, 2003; Fig. 16). Only a limited number ( $n = 2$ ) of late diagenetic LMC 2 samples are less radiogenic than predicted by the global seawater curve, implying that diagenesis and moderate hydrothermal dolomitization did not obscure the marine archive. Despite the fact that the Latemar slope and interior represent two distinct stratigraphic sections, it seems unlikely (but not impossible) that these trends in carbonate isotope values reflect spatial differences in seawater geochemistry.

*Synopsis: Latemar interior.*

The Latemar platform interior, located 5 to 7 km from the intrusion, lacks metre-wide recrystallized contact aureole fringing dykes. Dolomitizing fluid temperatures range from 50 to 70°C. A spatial carbon isotopic gradient between the Latemar slope and interior dolostones is observed. The influence of intrusion-related hydrothermal fluids in the  $\delta^{13}\text{C}_{\text{dolomite}}$  signatures of the Latemar interior is suppressed (+1‰ between limestone and Dol 1). The oxygen-isotope values of Sciliar limestones and hydrothermal dolomites are controlled by mineralogical and temperature-dependent fractionation, relevant in a temperature range from 40 to 80°C.

### **Significance for deep-time carbonate archive research**

The data and interpretations documented here are relevant for carbonate archive research because of several reasons. The Phanerozoic Eonothem offers sufficient well-preserved biogenic and abiogenic carbonate archives and, hence, samples with evidence for secondary alteration are discarded. Nevertheless, Swart (2015) and others argued that many of the proxy records from ancient carbonate archives may not represent the depositional environment, but are rather (early) diagenetic signals. Even in some sub-recent foraminifera tests and other carbonate archives, subtle yet significant diagenetic effects were found (Perrin & Smith, 2007; Bernard *et al.*, 2017; Lange *et al.*, 2018; Pederson *et al.*, 2019b). Although there is no correlation between the geological age of a given carbonate archive and its degree of preservation, these issues become increasingly

significant when dealing with the 'deep-time' rock record. Specifically, meta-carbonate rocks that have undergone pervasive recrystallization at greater depth and under fluid temperatures of  $>300^{\circ}\text{C}$  represent the frontier in this regard. In many natural systems, advective or diffusive transport creates fluid-buffered conditions. A common perspective is that 'wet' metamorphism eradicates any useful environmental signal. The issue is particularly relevant for the low-grade to high-grade Proterozoic and Archean carbonate archives. Examples include Archean stromatolitic carbonates in greenstone belts (Condie, 1981; Klein, 2005) and the 3.8 Ga Isua metacarbonates, heated to temperatures of 460 to  $600^{\circ}\text{C}$ , that contain debated evidence for the earliest life on Earth (Nutman *et al.*, 2016; van Zuilen *et al.*, 2002). Archean metacarbonate archives have often undergone multiple episodes of metamorphism with barely distinguishable episodes of regional and contact metamorphism (Hayashi *et al.*, 2000; Nutman *et al.*, 2010; Sizova *et al.*, 2018).

The present study in the Latemar offers important insights into metamorphic to diagenetic fluid-rock interaction gradients between some tens of degrees Celsius and  $700^{\circ}\text{C}$  in a low-temperature to contact metamorphic hydrothermal regime. Both strongly recrystallized marbles in the contact aureole and limestones affected by warm hydrothermal fluids in the platform interior display  $\delta^{13}\text{C}$  and  $\delta^{18}\text{O}$  values similar to (or overlapping with) Triassic seawater. Textbook interpretations in the sense of '*petrographic alteration of a given carbonate is accompanied by its geochemical re-equilibration*' are not applicable here. Following arguments brought forward by others (Ferry *et al.*, 2002; Jacquemyn *et al.*, 2014), this study finds evidence for decoupled (in both time and space) petrographic and geochemical alteration fronts in the Latemar rocks. It is emphasized, however, that they are fully aware of the differences in terms of pressure regimes and heat transfer rates between contact and regional metamorphism. Thus, care must be taken to avoid overly simplistic interpretations based on the data shown here (see also discussion in Baumgartner & Valley, 2001; Ferry *et al.*, 2010, 2014). Acknowledging all of these issues, it is argued that the alteration gradients at the Latemar offer fundamental insights into processes and products that have relevance for deep-time carbonate archive research.

## CONCLUSIONS

This study documents a complex suite of processes ranging from contact metamorphic to hydrothermal dolomitization of precursor limestones in the natural laboratory of the Triassic

Latemar isolated platform and the nearby subvolcanic Predazzo Intrusion (northern Italy). A transect from the contact metamorphic aureole towards the low-temperature hydrothermal endmember characterizes carbonates based on their petrographic, paragenetic and geochemical criteria. Spatially restricted dolostone bodies are embedded in marine precursor limestones and allow a direct comparison of processes and products.

At the contact metamorphic aureole, three dolomite marbles, two dedolomite marbles, several magnesium hydroxides, silicates and a series of hydrothermal to late-stage meteoric cements are observed. In strong contrast with petrographic and mineralogical evidence for a full metamorphic cycle, carbon-isotope and oxygen-isotope values seem to reflect preserved Triassic 'marine' values. Strontium-isotope ratios suggest multiple fluid sources. Partial dolomitization of carbonates occurred between 4 km and 7 km from the intrusive heat source and was driven by hydrothermal fluids circulating through north-west to south-east trending dykes radiating from the Predazzo Intrusion into the Latemar isolated platform. Four hydrothermal dolomite phases formed. These features are considered evidence for decreasing fluid temperature, fluid flow and Mg and Fe concentrations with increasing distance from the metamorphic heat source.

Oxygen-isotope values of Latemar Sciliar limestones and dolostones, as well as early diagenetic Contrin dolomites at its base, plot in the range of Triassic marine precipitates. A difference of up to 2.5‰ in  $\delta^{13}\text{C}$  values is observed between limestone precursors and early-stage hydrothermal dolomite phases. This shift is less pronounced in the Latemar interior, which has a difference of 1‰ between limestones and dolostones. The moderately  $^{13}\text{C}$ -enriched values of Latemar interior carbonates are best explained by decreasing fluid temperature with increasing distance to the metasomatizing fluid source. Late-stage dolomite phases overlap with precursor limestones in terms of their isotope geochemistry. This pattern arguably reflects coeval metamorphic dedolomitization releasing Mg into the dolomitizing fluids. The oxygen-isotope composition of Sciliar limestones and later hydrothermal dolomites is predominantly controlled by mineralogical fractionation from calcite to dolomite and temperature-dependent fractionation. The strontium-isotope ratios of most Sciliar Formation phases plot in the biogenic and abiogenic marine calcite range, independent of their spatial position.

This study is relevant as it documents that even significant petrographic alteration of carbonate archives does not *per se* invoke geochemical re-equilibration. The processes and products documented are best explained through rock-buffered metamorphic and diagenetic

alteration. Data provided offer a framework against which existing and subsequent work can be placed to extract quantitative results, patterns and methods for the community.

#### **ACKNOWLEDGEMENTS**

This study was performed in the context of the collaborative research initiative CHARON Phase II (DFG Forschergruppe 1644). The authors are grateful to the Gabrielli Family, the owners of the Rifugio Torre di Pisa, for the logistic help on the Latemar. Thanks go to B. Gehnen and K. Krimmler from the isotope geochemistry laboratory for isotope analysis, M. Born, A. Schulz, and T. Seemann from the thin section preparation department, S. Weisel from the Scanning Electron Microscopy Laboratory and H. Mammen for X-ray diffraction analysis at Ruhr-University Bochum. Thanks go to J. Parr for assistance in weighing samples for geochemical analyses and drawing of figures. Additional thanks go to L. Krone for assistance during fieldwork. Special thanks go to M. Trogisch from the thin section preparation department at Westfälische Wilhelms-Universität Münster for help with the preparation of additional thin sections. The authors express their gratitude to Sedimentology editors Dr. P. Pufahl and Dr. T. Frank, as well as to the reviewers Dr. B. Jones and Dr. D. Morrow.

## REFERENCES

- Bathurst, R.G.C.** (1975) Carbonate sediments and their diagenesis. *Elsevier Publ*, New York.
- Bau, M., Romer, R.L., Lüders, V. and Beukes, N.J.** (1999) Pb, O, and C isotopes in silicified Mooiaraai dolomite (Transvaal Supergroup, South Africa): implications for the composition of Paleoproterozoic seawater and ‘dating’ the increase of oxygen in the Precambrian atmosphere. *Earth and Planetary Science Letters*, **174**, 43-57.
- Baumgartner, L.P. and Ferry, J.M.** (1991) A model for coupled fluid-flow and mixed-volatile mineral reactions with applications to regional metamorphism. *Contributions to Mineralogy and Petrology*, **106**, 273–285.
- Baumgartner, L.P. and Valley, J.W.** (2001) Stable isotope transport and contact metamorphic fluid flow. *Reviews in Mineralogy and Geochemistry*, **43**, 415-467.
- Bernard, S., Daval, D., Ackerer, P., Pont, S. and Meibom, A.** (2017) Burial-induced oxygen-isotope re-equilibration of fossil foraminifera explains ocean paleotemperature paradoxes. *Nature communications*, **8**, 1-10.
- Blendinger, W.** (1994) The carbonate factory of Middle Triassic buildups in the Dolomites, Italy: a quantitative analysis. *Sedimentology*, **41**, 1147-1159.
- Blendinger, W.** (1997) Dolomitization of the Dolomites (Triassic, Northern Italy): Pilot study. *Neues Jahrbuch für Geologie und Paläontologie-Abhandlungen*, **204**, 83-110.
- Blendinger, W., Bertini, A. and Meissner, E.** (2011) Pale di San Lucano: esempio di importanza mondiale per geometrie di piattaforma carbonatica e problema della dolomitizzazione. In: B. Aldighieri and B. Testa (Eds.) *L'armonia fra uomo e natura nelle Valli Dolomitiche*. Aracne, 147-186.
- Blomme, K., Fowler, S. J., Bachaud, P., Nader, F. H., Michel, A. and Swennen, R.** (2017) Ferroan dolomitization by seawater interaction with mafic igneous dikes and carbonate host rock at the Latemar Platform, Dolomites, Italy: numerical Modeling of Spatial, Temporal, and Temperature Data. *Geofluids*, **2017**.
- Bocchi, G. and Morandi, N.** (1971) Sulla distribuzione della brucite (stima quantitativa in DTA) nella “predazzite” di Canzoccoli (Predazzo, nord Italia). *Mineralogica et Petrographica Acta*, **17**, 135–148.

- Boomeri, M., Ishiyama, D., Mizuta, T., Matsubaya, O. and Lentz, D.R.** (2010) Carbon and oxygen isotopic systematics in calcite and dolomite from the Sangan Iron Skarn Deposit, Northeastern Iran. *Journal of Sciences, Islamic Republic of Iran*, **21**, 213-224.
- Bosellini, A.** (1984) Progradation geometries of carbonate platforms: Examples from the Triassic of the Dolomites, northern Italy. *Sedimentology*, **31**, 1-24.
- Bowman, J.R., Valley, J.W. and Kita, N.T.** (2009) Mechanisms of oxygen isotopic exchange and isotopic evolution of  $^{18}\text{O}/^{16}\text{O}$ -depleted periclase zone marbles in the Alta aureole, Utah: insights from ion microprobe analysis of calcite. *Contributions to Mineralogy and Petrology*, **157**, 77-93.
- Brady, J.B., Cheney, J.T., Rhodes, A.L., Vasquez, A., Green, C., Duvall, M., Kogut, A., Kaufman, L. and Kovaric, D.** (1998) Isotope geochemistry of Proterozoic talc occurrences in Archean marbles of the Ruby Mountains, southwest Montana, USA. *Geological Materials Research*, **1**, 1-41.
- Braithwaite, C.J., Rizzi, G. and Darke, G.** (2004) The geometry and petrogenesis of dolomite hydrocarbon reservoirs. Geological Society of London, *Special Publications*, **235**, 1-6.
- Carmichael, S.K.** (2006) Formation of replacement dolomite by infiltration of diffuse effluent: Latemar carbonate buildup, Dolomites, northern Italy. (Doctoral dissertation, Johns Hopkins University).
- Carmichael, S.K., Ferry, J.M. and McDonough, W.F.** (2008) Formation of replacement dolomite in the Latemar carbonate buildup, Dolomites, northern Italy: Part 1. Field relations, mineralogy, and geochemistry. *American Journal of Science*, **308**, 851-884.
- Casetta, F., Coltorti, M. and Marrocchino, E.** (2018a) Petrological evolution of the Middle Triassic Predazzo Intrusive Complex, Italian Alps. *International Geology Review*, **60**, 977-997.
- Casetta, F., Coltorti, M., Ickert, R.B., Bonadiman, C., Giacomoni, P.P. and Ntaflos, T.** (2018b) Intrusion of shoshonitic magmas at shallow crustal depth: T-P path,  $\text{H}_2\text{O}$  estimates, and AFC modeling of the Middle Triassic Predazzo Intrusive Complex (Southern Alps, Italy). *Contributions to Mineralogy and Petrology*, **173**, 57 pp.
- Castellarin, A., Lucchini, F., Rossi, P.L., Sartori, R., Simboli, G. and Somnavilla, E.** (1982) Note geologiche sulle intrusioni di Predazzo e dei M. Monzoni. In: A. Castellarin and G. B. Vai (Eds.) Guida alla geologia del Sudalpino centroorientale. *Società Geologica Italiana, Bologna.*, 211-219.

- Chatalov, A.** (2018) Origin of fabric-selective dolomitization recognizable in the field: two case studies from Anisian carbonate rocks in the western Balkanides. *Geologica Balcanica*, **47**, 43-60.
- Christ, N., Immenhauser, A., Amour, F., Mutti, M., Preston, R., Whitaker, F.F., Peterhänsel, A., Egenhoff, S.O., Dunn, P.A. and Agar, S.M.** (2012) Triassic Latemar cycle tops—subaerial exposure of platform carbonates under tropical arid climate. *Sedimentary Geology*, **265**, 1-29.
- Condie, K.C.** (1981) Archean greenstone belts. *Elsevier*.
- Cortecci, G., and Lupi, L.** (1994) Carbon, oxygen and strontium isotope geochemistry of carbonate rocks from the Tuscan Nappe, Italy. *Mineralogica et Petrographica Acta*, **37**, 63-80.
- Cortecci, G., Dinelli, E., Indrizzi, M.C., Susini, C. and Adorni Braccesi, A.** (1999) The Apuane Alps Metamorphic Complex, Northern Tuscany: Chemical and isotopic features of Grezzioni and Marmi Dolomitici. *Atti Soc. Tosc. Sci. Nat., Mem., Serie A*, **106**, 79-89.
- Davies, G.R. and Smith, L.B.** (2006) Structurally controlled hydrothermal dolomite reservoir facies: an overview. *American Association of Petroleum Geologists Bulletin*, **90**, 1641–1690.
- Dewit, J., Foubert, A., El Desouky, H.A., Muchez, P., Hunt, D., Vanhaecke, F. and Swennen, R.** (2014) Characteristics, genesis and parameters controlling the development of a large stratabound HTD body at Matienzo (Ramales Platform, Basque–Cantabrian Basin, northern Spain). *Marine and Petroleum Geology*, **55**, 6-25.
- Dietzel, M. and Kirchhoff, T.** (2002) Stable isotope ratios and the evolution of acidulous ground water. *Aquatic Geochemistry*, **8**, 229-254.
- Dogliani, C.** (1983) Duomo medio-triassico nelle Dolomiti. *Rendiconti della Società geologica italiana*, **6**, 13-16.
- Dogliani, C.** (1987) Tectonics of the Dolomites (southern Alps, northern Italy). *Journal of structural geology*, **9**, 181-193.
- Dong, S., Chen, D., Qing, H., Zhou, X., Wang, D., Guo, Z., Jiang, M. and Qian, Y.** (2013) Hydrothermal alteration of dolostones in the Lower Ordovician, Tarim Basin, NW China: multiple constraints from petrology, isotope geochemistry and fluid inclusion microthermometry. *Marine and Petroleum Geology*, **46**, 270-286.
- Duan, G., Brugger, J., Etschmann, B., Ram, R., Friedrich, A. and Micklethwaite, S.** (2021) Formation of Mg-carbonates and Mg-hydroxides via calcite replacement controlled by fluid pressure. *Contributions to Mineralogy and Petrology*, **176**, 1-14.

- Dunsmore, H.E.** (1973) Diagenetic processes of lead-zinc emplacement in carbonates. *Trans. Inst. Min. Metall. Sec. B*, **82**, 168–173
- Egenhoff, S., Peterhänsel, A., Bechstädt, T., Zühlke, R. and Grötsch, J.** (1999) Facies architecture of an isolated carbonate platform: tracing the cycles of the Latemar (Middle Triassic, northern Italy). *Sedimentology*, **49**, 893-912.
- Emmerich, A., Zamparelli, V., Bechstädt, T. and Zühlke, R.** (2005) The reefal margin and slope of a Middle Triassic carbonate platform: the Latemar (Dolomites, Italy). *Facies*, **50**, 573-614.
- Farooqui, M.Y., Hou, H., Li, G., Machin, N., Neville, T., Pal, A., Shrivastva, C., Wang, Y., Yang, F., Yin, C., Zhao, J., and Yang, Z.** (2009) Evaluating volcanic reservoirs. *Oilfield Review*, **21**, 36-47.
- Ferrill, D.A., Morris, A.P., Evans, M.A., Burkhard, M., Groshong Jr, R.H. and Onasch, C.M.** (2004) Calcite twin morphology: a low-temperature deformation geothermometer. *Journal of structural Geology*, **26**, 1521-1529.
- Ferry, J. M. and Rumble III, D.** (1997) Formation and destruction of periclase by fluid flow in two contact aureoles. *Contributions to Mineralogy and Petrology*, **128**, 313-334.
- Ferry, J.M., Kitajima, K., Strickland, A. and Valley, J.W.** (2014) Ion microprobe survey of the grain-scale oxygen isotope geochemistry of minerals in metamorphic rocks. *Geochimica et Cosmochimica Acta*, **144**, 403-433.
- Ferry, J.M., Passey, B.H., Vasconcelos, C. and Eiler, J.M.** (2011) Formation of dolomite at 40–80 °C in the Latemar carbonate buildup, Dolomites, Italy, from clumped isotope thermometry. *Geology*, **39**, 571-574.
- Ferry, J.M., Wing, B.A., Penniston-Dorland, S.C., and Rumble, D.** (2002) The direction of fluid flow during contact metamorphism of siliceous carbonate rocks: new data for the Monzoni and Predazzo aureoles, northern Italy, and a global review. *Contributions to Mineralogy and Petrology*, **142**, 679-699.
- Franchi, F. and Abebe, A.** (2020) Statistically learning Archean carbonate diagenesis. *Precambrian Research*, **348**, 105867.
- Friedman, I. and O'Neil, J.R.** (1977) *Compilation of stable isotope fractionation factors of geochemical interest*, **440**, US Government Printing Office.
- Gaetani, M., Fois, E., Jadoul, F. and Nicora, A.** (1981) Nature and evolution of Middle Triassic carbonate buildups in the Dolomites (Italy). *Marine Geology*, **44**, 25-57.

- Gallien, F., Abart, R. and Wyhlidal, S.** (2007) Contact metamorphism and selective metasomatism of the layered Bellerophon Formation in the eastern Monzoni contact aureole, northern Italy. *Mineralogy and Petrology*, **91**, 25-53.
- Gallien, F., Abart, R. and Wyhlidal, S.** (2007) Contact metamorphism and selective metasomatism of the layered Bellerophon Formation in the eastern Monzoni contact aureole, northern Italy. *Mineralogy and Petrology*, **91**, 25-53.
- Geske, A., Lokier, S., Dietzel, M., Richter, D.K., Buhl, D. and Immenhauser, A.** (2015) Magnesium isotope composition of sabkha porewater and related (Sub-)Recent stoichiometric dolomites, Abu Dhabi (UAE). *Chemical Geology*, **393**, 112–124.
- Geske, A., Zorlu, J., Richter, D.K., Buhl, D., Niedermayr, A. and Immenhauser, A.** (2012) Impact of diagenesis and low grade metamorphism on isotope ( $\delta^{26}\text{Mg}$ ,  $\delta^{13}\text{C}$ ,  $\delta^{18}\text{O}$  and  $^{87}\text{Sr}/^{86}\text{Sr}$ ) and elemental (Ca, Mg, Mn, Fe and Sr) signatures of Triassic sabkha dolomites. *Chemical Geology*, **332–333**, 45-64.
- Giggenbach, W.F.** (1992) Isotopic shifts in waters from geothermal and volcanic systems along convergent plate boundaries and their origin. *Earth and planetary science letters*, **113**, 495-510.
- Goldhammer, R.K.** (1987) Platform carbonate cycles, middle Triassic of northern Italy: the interplay of local tectonics and global eustasy. (unpublished Doctoral dissertation, The Johns Hopkins University, Baltimore), 468 p.
- Goldstein, R.H. and Reynolds, T.J.** (1994) Systematics of fluid inclusions in diagenetic minerals. Short Course 31, *Society of Economic Paleontologists and Mineralogists*, **31**, 199 pp.
- Greenwood, H.J.** (1975) Buffering of pore fluids by metamorphic reactions. *American Journal of Science*, **275**, 573–593.
- Gregg, J.M., Bish, D.L., Kaczmarek, S.E. and Machel, H.G.** (2015) Mineralogy, nucleation and growth of dolomite in the laboratory and sedimentary environment: a review. *Sedimentology*, **62**, 1749-1769.
- Gregg, J.M., Laudon, P.R., Woody, R.E. and Shelton, K.L.** (1993) Porosity evolution of the Cambrian Bonnetterre Dolomite, south-eastern Missouri, USA. *Sedimentology*, **40**, 1153-1169.
- Grossman, E.L.** (2012) Applying Oxygen Isotope Paleothermometry in Deep Time. *The Paleontological Society Papers*, **18**, 39-67.
- Hardebol, N.J., Maier, C., Nick, H., Geiger, S., Bertotti, G. and Boro, H.** (2015) Multiscale fracture network characterization and impact on flow: A case study on the Latemar carbonate platform. *Journal of Geophysical Research: Solid Earth*, **120**, 8197-8222.

- Harris, M.T.** (1993) Reef fabrics, biotic crusts and syndepositional cements of the Latemar reef margin (Middle Triassic), northern Italy. *Sedimentology*, **40**, 383-401.
- Hayashi, M., Komiya, T., Nakamura, Y. and Maruyama, S.** (2000) Archean regional metamorphism of the Isua supracrustal belt, southern West Greenland: implications for a driving force for Archean plate tectonics. *International Geology Review*, **42**, 1055-1115.
- Hendry, J.P., Gregg, J.M., Shelton, K.L., Somerville, I.D. and Crowley, S.F.** (2015) Origin, characteristics and distribution of fault-related and fracture-related dolomitization: Insights from Mississippian carbonates, Isle of Man. *Sedimentology*, **62**, 717–752.
- Hoefs J.** (1997) Stable Isotope Geochemistry. *Springer-Verlag*, Berlin Heidelberg, 201 pp.
- Hoefs, J.** (2009) Stable Isotope Geochemistry. *Springer-Verlag*, Berlin Heidelberg.
- Hou, Y., Azmy, K., Berra, F., Jadoul, F., Blamey, N.J.F., Gleeson, S.A. and Brand, U.** (2016) Origin of the Breno and Esino dolomites in the western Southern Alps (Italy): implications for a volcanic influence. *Mar. Petrol. Geol.*, **69**, 38–52.
- Huang, W., Liu, T. and Shen, P.** (2009) Ca-Mg inter-diffusion in synthetic polycrystalline dolomite-calcite aggregate at elevated temperatures and pressure. *Miner Petrol* **95**, 327-340.
- Jacquemyn, C.** (2013) Diagenesis and application of LIDAR in reservoir analogue studies: Karstification in the Cretaceous Apulia platform and dolomitization in the Triassic Latemar buildup. (Doctoral dissertation, KU Leuven, Science, Engineering & Technology).
- Jacquemyn, C., El Desouky, H., Hunt, D., Casini, G. and Swennen, R.** (2014) Dolomitization of the Latemar platform: Fluid flow and dolomite evolution. *Marine and Petroleum Geology*, **55**, 43–67.
- Jacquemyn, C., Huysmans, M., Hunt, D., Casini, G. and Swennen, R.** (2015) Multi-scale three-dimensional distribution of fracture-and igneous intrusion-controlled hydrothermal dolomite from digital outcrop model, Latemar platform, Dolomites, northern Italy. *American Association of Petroleum Geologists*, **99**, 957-984.
- Jonas, L., Müller, T., Dohmen, R., Immenhauser, A., and Pulitz, B.** (2017) Hydrothermal replacement of biogenic and abiogenic aragonite by Mg-carbonates - Relation between textural control on effective element fluxes and resulting carbonate phase. *Geochimica et Cosmochimica Acta*, **196**, 289-306.
- Klein, C.** (2005) Some Precambrian banded iron-formations (BIFs) from around the world: Their age, geologic setting, mineralogy, metamorphism, geochemistry, and origins. *American Mineralogist*, **90**, 1473-1499.

- Korte, C., Kozur, H.W. and Veizer, J.** (2005)  $\delta^{13}\text{C}$  and  $\delta^{18}\text{O}$  values of Triassic brachiopods and carbonate rocks as proxies for coeval seawater and palaeotemperature. *Palaeogeography, Palaeoclimatology, Palaeoecology*, **226**, 287-306.
- Korte, C., Kozur, H.W., Bruckschen, P. and Veizer, J.** (2003) Strontium isotope evolution of Late Permian and Triassic seawater. *Geochimica et Cosmochimica Acta*, **67**, 47–62.
- Kyser T.K.** (1986) Stable isotope variations in the mantle. In: Stable Isotopes in High-Temperature Geological Processes (eds. J. W. Valley et al.). *Min. Soc. Am., Reviews in Mineralogy* **16**, 141–164.
- Lange, S.M., Krause, S., Ritter, A.C., Fichtner, V., Immenhauser, A., Strauss, H. and Treude, T.** (2018) Anaerobic microbial activity affects earliest diagenetic pathways of bivalve shells. *Sedimentology*, **65**, 1390-1411.
- Laurenzi, M.A. and Visonà, D.** (1996)  $^{40}\text{Ar}/^{39}\text{Ar}$  Chronology of Predazzo magmatic complex (Southern Alps, Italy). 78 Riunione estiva Soc. Geol. It., Geologia delle Dolomiti. San Cassiano, 186 pp.
- Laurenzi, M.A. and Visonà, D.** (1996)  $^{40}\text{Ar}/^{39}\text{Ar}$  Chronology of Predazzo Magmatic Complex (Southern Alps, Italy), 78° Riunione estiva Soc. Geol. It.: Geologia delle Dolomiti. San Cassiano, 16–18.
- Leiss, B. and Molli, G.** (2003) ‘High-temperature’ texture in naturally deformed Carrara marble from the Alpi Apuane, Italy. *Journal of Structural Geology*, **25**, 649-658.
- Liu, S., Huang, W., Jansa, L. F., Wang, G., Song, G., Zhang, C., Sun, W. and Ma, W.** (2014) Hydrothermal dolomite in the upper Sinian (upper Proterozoic) Dengying formation, east Sichuan basin, China. *Acta Geologica Sinica-English Edition*, **88**, 1466-1487.
- Machel, H.G.** (2005) Sedimentary Rocks: Dolomites. *Encyclopedia of Geology*, **30**, 79–94.
- Marangon, A., Gattolin, G., della Porta, G. and Preto, N.** (2011) The Latemar: A flat-topped, steep fronted platform dominated by microbialites and synsedimentary cements. *Sedimentary Geology*, **240**, 97-114.
- Marrocchino, E., Beccaluva, L., Coltorti, M., Siena, F. and Thirlwall, M.** (2009) Tectono-magmatic significance of Predazzo Magmatic Complex (Italy). Alpine Ophiolites and Modern Analogues Conference, Parma.
- Marrocchino, E., Coltorti, M., Visonà, D. and Thirlwall, M.F.** (2002) Petrology of Predazzo magmatic complex (Trento, Italy). *Geochimica et Cosmochimica Acta*, **66**, p. A486.

- Molli, G., Conti, P., Giorgetti, G., Meccheri, M. and Oesterling, N.** (2000) Microfabric study on the deformational and thermal history of the Alpi Apuane marbles (Carrara marbles), Italy. *Journal of Structural Geology*, **22**, 1809-1825.
- Morrow, D.W., Gorham, B.L. and Wong, J.N.Y.** (1994) Dolomite-calcite equilibrium at 220 to 240 °C at saturation vapour pressure: Experimental data. *Geochimica et Cosmochimica Acta*, **58**, 169-177.
- Morrow, D.W.** (2014) Zebra and boxwork fabrics in hydrothermal dolomites of northern Canada: Indicators for dilational fracturing, dissolution or in situ replacement? *Sedimentology*, **61**, 915–951.
- Mueller, M., Igbokwe, O. A., Walter, B., Pederson, C. L., Riechelmann, S., Richter, D. K., Albert, R., Gerdes, A., Buhl, D., Neuser, R.D., Bertotti G. and Immenhauser, A.** (2020) Testing the preservation potential of early diagenetic dolomites as geochemical archives. *Sedimentology*, **67**, 849-881.
- Mundil, R., Brack, P., Meier, M., Rieber, H. and Oberli, F.** (1996) High resolution U-Pb dating of Middle Triassic volcanoclastics: Time-scale calibration and verification of tuning parameters for carbonate sedimentation. *Earth and Planetary Science Letters*, **141**, 137-151.
- Mundil, R., Pálffy, J., Renne, P. R. and Brack, P.** (2010) The Triassic timescale: new constraints and a review of geochronological data. *Geological Society, London, Special Publications*, **334**, 41-60.
- Nader, F.H., Swennen, R. and Ellam, R.** (2004) Reflux stratabound dolostone and hydrothermal volcanism-associated dolostone: a two-stage dolomitization model (Jurassic, Lebanon). *Sedimentology*, **51**, 339-360.
- Navarro-Ciurana, D., Corbella, M., Cardellach, E., Vindel, E., Gómez-Gras, D. and Griera, A.** (2016) Petrography and geochemistry of fault-controlled hydrothermal dolomites in the Riópar area (Prebetic Zone, SE Spain). *Marine and Petroleum Geology*, **71**, 310-328.
- Neuser, R.D., Bruhn, F., Götze, J., Habermann, D. and Richter, D.K.** (1996) Kathodolumineszenz: Methodik und Anwendung [Cathodoluminescence: method and application], *Zentralblatt für Geologie und Paläontologie, Teil 1*, 287-206.
- Nordeng, S.H. and Sibley, D.F.** (1994) Dolomite stoichiometry and Ostwald's Step Rule. *Geochimica et Cosmochimica Acta*, **58**, 191-196.

- Nutman, A.P., Bennett, V.C., Friend, C.R., Van Kranendonk, M.J. and Chivas, A.R.** (2016) Rapid emergence of life shown by discovery of 3,700-million-year-old microbial structures. *Nature*, **537**, 535-538.
- Nutman, A.P., Friend, C.R., Bennett, V.C., Wright, D. and Norman, M.D.** (2010)  $\geq 3700$  Ma pre-metamorphic dolomite formed by microbial mediation in the Isua supracrustal belt (W. Greenland): simple evidence for early life?. *Precambrian Research*, **183**, 725-737.
- Pederson, C., Mavromatis, V., Dietzel, M., Rollion-Bard, C., Nehrke, G., Jöns, N., Jochum, K.P. and Immenhauser, A.** (2019a) Diagenesis of mollusc aragonite and the role of fluid reservoirs. *Earth and Planetary Science Letters*, **514**, 130-142.
- Pederson, C.L., Klaus, J.S., Swart, P.K. and McNeill, D.F.** (2019b) Deposition and early diagenesis of microbial mud in the Florida Everglades. *Sedimentology*, **66**, 1989-2010.
- Perrin, C. and Smith, D.C.** (2007) Earliest steps of diagenesis in living scleractinian corals: evidence from ultrastructural pattern and Raman spectroscopy. *Journal of Sedimentary Research*, **77**, 495-507.
- Petrash, D.A., Bialik, O.M., Bontognali, T.R.R., Vasconcelos, C., Roberts, J.A., McKenzie, J.A. and Konhauser, K.O.** (2017) Microbially catalyzed dolomite formation: From near-surface to burial. *Earth-Science Reviews*, **171**, 558–582.
- Pingitore, N.E., Jr.** (1982) The role of diffusion during carbonate diagenesis. *Journal of Sedimentary Petrology*, **52**, 27-39.
- Preto, N., Franceschi, M., Gattolin, G., Massironi, M., Riva, A., Gramigna, P., Bertoldi, L. and Nardon, S.** (2011) The Latemar: A Middle Triassic polygonal fault-block platform controlled by synsedimentary tectonics. *Sedimentary Geology*, **234**, 1-18.
- Preto, N., Klügel, A., Himmler, T. and Franceschi, M.** (2019) Origin of facies zonation in microbial carbonate platform slopes: Clues from trace element and stable isotope geochemistry (Middle Triassic, Dolomites, Italy). *Sedimentology*, **66**, 81-101.
- Qing, H. and Mountjoy, E.W.** (1994) Formation of coarsely crystalline, hydrothermal dolomite reservoirs in the Presqu'île Barrier, Western Canada Sedimentary Basin. *American Association of Petroleum Geologists Bulletin*, **78**, 55-77.
- Radke, B.M. and Mathis, R.L.** (1980) On the Formation and Occurrence of Saddle Dolomite. *Journal of Sedimentary Research*, **50**, 1149-1168.
- Rieder, M., Wegner, W., Horschinegg, M., Klackl, S., Preto, N., Breda, A., Gier, S., Klötzli, U., Bernasconi, S.M., Arp, G. and Meister, P.** (2019) Precipitation of dolomite from seawater

on a Carnian coastal plain (Dolomites, northern Italy): evidence from carbonate petrography and Sr isotopes. *Solid Earth*, **10**, 1243-1267.

**Riva, A. and Stefani, M.** (2003) Synvolcanic deformation and intraplateform collapsing: the Latemar case history from the Middle Triassic of the Dolomites. *Memorie di Scienze Geologiche*, **54**, 139–142.

**Saltzman, M.R. and Thomas, E.** (2012) Carbon Isotope Stratigraphy. In: *The Geologic Time Scale* (Eds. F.M. Gradstein, J.G. Ogg, M.D. Schmitz and G.M. Ogg) 1st edn, pp. 207-232. Elsevier BV, Oxford.

**Schutter, S.R.** (2003) Hydrocarbon occurrence and exploration in and around igneous rocks. *Geological Society of London, Special Publications*, **214**, 7-33.

**Shelton, K.L., Cavender, B.D., Perry, L.E., Schiffbauer, J.D., Appold, M.S., Burstein, I. and Fike, D.A.** (2020) Stable isotope and fluid inclusion studies of early Zn-Cu-(Ni-Co)-rich ores, lower ore zone of Brushy Creek mine, Viburnum Trend MVT district, Missouri, USA: Products of multiple sulfur sources and metal-specific fluids. *Ore Geology Reviews*, **118**, 103358.

**Sheppard, S.M. and Schwarcz, H.P.** (1970) Fractionation of carbon and oxygen isotopes and magnesium between coexisting metamorphic calcite and dolomite. *Contributions to Mineralogy and Petrology*, **26**, 161-198.

**Sibley, D.F. and Gregg, J.M.** (1987) Classification of dolomite rock texture. *J. Sediment. Petrol.*, **57**, 967–975.

**Sizova, E., Gerya, T., Brown, M. and Stüwe, K.** (2018) What drives metamorphism in early Archean greenstone belts? Insights from numerical modeling. *Tectonophysics*, **746**, 587-601.

**Sloman, L.E.** (1989) Triassic shoshonites from the dolomites, northern Italy: Alkaline arc rocks in a strike-slip setting. *Journal of Geophysical Research: Solid Earth*, **94**, 4655-4666.

**Spencer, R.J.** (1987) Origin of Ca-Cl brines in Devonian formations, western Canada sedimentary basin. *Applied Geochemistry*, **2**, 373-384.

**Sudiro, P.** (2002) Carbonate slope deposits of the Contrin formation, Costabella area (Western dolomites, NE Italy). *Mem. della Soc. Geol. Ital*, **57**, 19-28.

**Swart, P.K.** (2015) The geochemistry of carbonate diagenesis: The past, present and future. *Sedimentology*, **62**, 1233–1304.

**Teal, C.S., Mazzulo, S.J. and Bischoff, W.D.** (2000) Dolomitization of Holocene shallow-marine deposits mediated by sulfate reduction and methanogenesis in normal-salinity seawater, Northern Belize. *Journal of Sedimentary Research*, **70**, 649-663.

- van Zuilen, M.A., Lepland, A. and Arrhenius, G.** (2002) Reassessing the evidence for the earliest traces of life. *Nature*, **418**, 627-630.
- Veizer, J. and Prokoph, A.** (2015) Temperatures and oxygen isotopic composition of Phanerozoic oceans. *Earth-Science Reviews*, **146**, 92–104.
- Veizer, J., Hoefs, J., Lowe, D.R. and Thurston, P.C.** (1989) Geochemistry of Precambrian carbonates: II. Archean greenstone belts and Archean sea water. *Geochimica et Cosmochimica Acta*, **53**, 859-871.
- Vho, A., Lanari, P. and Rubatto, D.** (2019) An internally-Consistent Database for Oxygen Isotope Fractionation Between Minerals. *Journal of Petrology*, **60**, 2101-2130.
- Visonà, D.** (1997) The Predazzo multipulse intrusive body (Western Dolomites, Italy). Field and mineralogical studies. *Memorie di Scienze Geologiche*, **49**, 117-125.
- Wada, H., Ando, T. and Suzuki, M.** (1998) The role of the grain boundary at chemical and isotopic fronts in marble during contact metamorphism. *Contributions to Mineralogy and Petrology*, **132**, 309-320.
- Wallace, M.W. and Hood, A.v.S.** (2018) Zebra textures in carbonate rocks: Fractures produced by the force of crystallization during mineral replacement. *Sedimentary Geology*, **368**, 58–67.
- Walter, B.F., Immenhauser, A., Geske, A. and Markl, G.** (2015) Exploration of hydrothermal carbonate magnesium isotope signatures as tracers for continental fluid aquifers, Schwarzwald mining district, SW Germany. *Chemical Geology*, **400**, 87–105.
- Walter, B.F., Kortenbruck, P., Scharrer, M., Zeitvogel, C., Wälle, M., Mertz-Kraus, R. and Markl, G.** (2019a) Chemical evolution of ore-forming brines–Basement leaching, metal provenance, and the redox link between barren and ore-bearing hydrothermal veins. A case study from the Schwarzwald mining district in SW-Germany. *Chemical Geology*, **506**, 126-148.
- Walter, B.F., Steele-MacInnis, M. and Markl, G.** (2017) Sulfate brines in fluid inclusions of hydrothermal veins: compositional determinations in the system H<sub>2</sub>O-Na-Ca-Cl-SO<sub>4</sub>. *Geochimica et Cosmochimica Acta*, **209**, 184–203.
- Watson, E.B., and Müller, T.** (2009) Non-equilibrium isotopic and elemental fractionation during diffusion-controlled crystal growth under static and dynamic conditions. *Chemical Geology*, **267**, 111-124.
- Wilson, E.N.** (1989) Dolomitization of the Triassic Latemar buildup Dolomites, Northern Italy (Doctoral dissertation, Johns Hopkins University).

**Wilson, E.N., Hardie, L.A. and Phillips, O.M.** (1990) Dolomitization front geometry, fluid flow patterns, and the origin of massive dolomite: The Triassic Latemar buildup, Northern Italy. *American Journal of Science*, **290**, 741-796.

**Yang, Z., Zhong, D., Whitaker, F., Lu, Z., Zhang, S., Tang, Z., Liu, R. and Li, Z.** (2020) Syn-sedimentary hydrothermal dolomites in a lacustrine rift basin: Petrographic and geochemical evidence from the lower Cretaceous Erlan Basin, Northern China. *Sedimentology*, **67**, 305-329.

## FIGURE CAPTIONS

**Fig. 1.** Regional geological framework of the study area. **(A)** Map of the Dolomite Mountains in the south-eastern Alps (modified from Hardebol *et al.*, 2015). **(B)** A cross-section in the south-eastern Alps including the Dolomites based on Doglioni (1987) and modified from Hardebol *et al.*, 2015. **(C)** Distribution of sedimentary and igneous rocks covering the Latemar and Monte Agnello carbonate buildups near Predazzo in northern Italy. The study areas are marked by black boxes: 1 = contact aureole; 2 = Latemar slope; 3 = Latemar interior. Modified from Carmichael *et al.* (2008).

**Fig. 2.** **(A)** Stratigraphic chart of the Dolomite Mountains, including ranges for study areas ‘B’ and ‘C’ (modified from Jacquemyn, 2013; Jacquemyn *et al.*, 2014). See Fig. 1 for study area locations. **(B)** Dyke-perpendicular cross-section across the Latemar buildup including relation to the Predazzo Intrusion, located about 2 to 3 km south-east. The south-east Latemar slope is excluded from this area. UTF = Upper Tepee Facies, UCF = Upper Cyclic Facies, MTF = Middle Tepee Facies, LCF = Lower Cyclic Facies, LTF = Lower Tepee Facies, LPF = Lower Platform Facies. Array 1 (white line) covers the metamorphosed Contrin Formation at the Predazzo Intrusion contact aureole. Array 2 covers the Latemar slope, which consists of Lower Platform Facies and Contrin Formation. Array 3 covers the partly dolomitized Latemar interior, which consists of Lower Cyclic Facies, Lower Tepee Facies and the upper part of the Lower Platform Facies. Modified from Preto *et al.* (2011) and Jacquemyn (2013). **(C)** Geological schematic of Canzoccoli quarry at the contact with the Predazzo Intrusion. Modified from Ferry *et al.* (2002). **(D)** to **(F)** Conceptual schematics of the Predazzo Intrusion petrologic evolution modified from Casetta *et al.* (2018a). **(D)** The first intrusive pulse consists of shoshonitic silica saturated rocks. The position of the Canzoccoli quarry at the contact aureole is marked with a red rectangle. **(E)** The second pulse is represented by the intrusion of a granitic/syenogranitic unit that was dated as  $t_2 = 237$  Ma by Mundil *et al.* (1996). **(F)** The final pulse crops out in the eastern part of the complex and consists of shoshonitic silica undersaturated rocks. Note: The Predazzo Intrusion does not sit directly below the Latemar mountain. Sciliar Formation carbonates in **(D)** to **(F)** comprise the hardly accessible and largely eroded direct vicinity of the intrusion. See text for SiSa, GU and SiUSa.

**Fig. 3.** Overview of dolostone occurrences at the Latemar isolated platform (A) to (E) and the contact with the Predazzo Intrusion (F) to (G). Dolostone occurrences are marked by dashed lines. (A) to (C) Latemar interior (array 3 in Fig. 2B). Hydrothermal dolostones occur as patches with sharp contacts to host limestone and dykes (A). The width in the centre is about 500 m. Hydrothermal dolostones often occur as facies bound (B) or as isolated bodies with sharp and often brittle centimetre to decimetre thick transition zones (C). (D) and (E) Latemar slope (array 2 in Fig. 2B). (D) Dolostone body morphologies appear similar to the Latemar interior but contain different dolomite cements such as cell dolomite displayed in (E). (F) and (G) Contact metamorphosed Contrin Formation dolostones at the Predazzo Intrusion (array 1 in Fig. 2B) were largely dedolomitized (F), but some dolomite marble (G) with visible later metamorphic and tectonic overprint was preserved. Dolostone – dolomite marble in (F) – bodies are indicated by dashed lines.

**Fig. 4.** Transmitted light images (left) placed against cathodoluminescence properties (right) of different phases in early diagenetic Contrin Formation dolostones from the base of the Latemar buildup (A) and (B) and partly dedolomitized Contrin Formation dolomite marbles from the contact metamorphic aureole of the Predazzo Intrusion in the Canzoccoli quarry. (A) and (B) Contrin Formation dolostone. Note pervasively recrystallized, patchy luminescent Cdol 1 matrix with *dasycladacean* algae. Note pores occluded by darker red, zoned Cdol 2. (C) and (D) Contrin Formation Dol marble 1 with sharp contact to calcitic Dedol marble 2. Note non-luminescent forsterite and clinohumite in the marble matrix. (E) and (F) LMC 1 vein in Dedol marble 2 and lizardite (Mg-serpentine). Note elongated Dol marble 3 crystals cut by tiny LMC 2 veins. (G) and (H) Calcitic Dedol marble 1 with brucite and non-luminescent to pink / bright yellow luminescent spinel.

**Fig. 5.** Microprobe element maps of the contact metamorphosed Contrin Formation near the Predazzo Intrusion. (A) to (D) Sharp contact from dolomite marble 1 (right) to dedolomite marble 2 (left). Note the generally low strontium content that is mainly accumulated in calcitic Dedol marble 2. (E) to (H) Dedol marble 1 containing about 30 vol.% brucite. Note magnesium mobilization along grain boundaries and tiny fissures. The strontium content is generally low and

mainly accumulated in calcitic Dedol marble 1. Br = brucite, Fo = forsterite. (A) and (E) Calcium map. (B) and (F) Magnesium map. (C) and (G) Silicon map. (D) and (H) Strontium map.

**Fig. 6.** Scanning electron microscope images from the Contrin Formation at the contact metamorphic aureole of the Predazzo Intrusion. (A) Dol marble 1 matrix with spherical-shaped magnesium silicates. (B) Close-up of (A). Note the spherical forsterite grains which are in transition to clinohumite. (C) Dedol marble 1 fabric with brucite. Note platy crystal habitus of brucite. (D) LMC 1 vein with elongated Dol marble 3 grains and spinel crystals.

**Fig. 7.** Transmitted light images (left) placed against cathodoluminescence properties (right) of different paragenetic phases in dolomitized limestone facies of the Latemar buildup. (A) and (B) Latemar slope. Sharp contact between oolitic ironstone and Dol 1. Note dolomitized ironstone which was cemented by Qz 1 in a later diagenetic stage. Pores are occluded by Dol 2 cement. (C) and (D) Latemar slope. Dol 2 cement overgrows Dol 1. Note finely layered zonation and partly dedolomitization and replacement by Fe-oxides. (E) and (F) Latemar interior. Two generations of the volumetrically most significant replacement dolomite Dol 3. An inclusion-rich, patchy luminescent older phase is overgrown by less inclusion-rich dolomite cement. (G) and (H) Latemar interior. Partly dolomitized Lower Tepee Facies limestone. Note limestone matrix and early marine dog tooth cements overgrown by replacement Dol 3. Open pores are partly occluded by blocky LMC 1.

**Fig. 8.** Fluid inclusion salinity *versus* homogenization temperature ( $T_h$ ) uncorrected plot for phase-specific fluid inclusions from the contact aureole, Latemar slope and interior. Dolomitization temperature ranges from former studies: (1) dolomite fluid inclusion homogenization temperatures by Wilson *et al.* (1990); (2) clumped isotope temperatures by Ferry *et al.* (2011); and (3) dolomite fluid inclusion homogenization temperatures by Jacquemyn (2013).

**Fig. 9.** Simplified temporal evolution of subsequent events affecting the Contrin Formation (not to scale) and Sciliar Formation carbonates in the present study. Temporal uncertainties are denoted

by a question mark ‘?’’. For abbreviations see Table 2, Table 3 and Fig. 2. Dolomitization of Contrin Formation limestones commenced in the Anisian and was followed by Sciliar Formation deposition and faulting of the Contrin Formation in the Anisian and Ladinian. Emplacement of three intrusive bodies of the Predazzo Intrusion occurred between 232 Ma and 238 Ma in the Late Ladinian. Contact metamorphic induced processes and dolomitization of the Latemar roughly took place simultaneously, with an unknown time gap between the onset of contact metamorphism and the emplacement of dykes. The metamorphic succession of the contact aureole is characterized by decreasing temperature and the dolomitizing sequence of the Sciliar Formation limestones by decreasing Fe-content. Timings are compiled from Ferry *et al.* (2002) and Jacquemyn *et al.* (2014) and complemented by interpretations in those studies.

**Fig. 10.** Complete successions of metamorphic and diagenetic phases with typical cathodoluminescence colours related to their diagenetic and tectonic environment of precipitation or formation. **(A)** Contact metamorphic succession of the Contrin Formation dolostones. Non-luminescent phases are marked in black. **(B)** The paragenetic succession of the Sciliar Limestones. The remaining pore space is marked in black.

**Fig. 11.** Metamorphic pathway for contact metamorphosed Contrin Formation dolostones at Canzoccoli quarry. Pressure and temperature data from Ferry *et al.* (2002).

**Fig. 12.** A sequence illustrating decreasing temperature with increasing distance to the Predazzo Intrusion and displaying rock types representing the three target areas and some of their characterizing metamorphic and diagenetic features. **(A)** and **(D)** Dolomite marble from the Contact aureole. Note foliation of magnesium silicates cut by LMC 1. **(B)** and **(E)** ‘Cell dolomite’ dolostone from the Latemar slope. Besides massive replacement dolostone, this type is only present in this area. Note high Dol 2 cement content in Dol 1 matrix dolostone and fluid traces. **(C)** and **(F)** The gradual transition from Lower Teepee Facies limestone to Dol 3 replacive dolostone. Note Dol 3 vein increase towards the dolostone and vugs occluded by marine cements, Dol 3 and LMC 1 (Latemar).

**Fig. 13.** Two examples of preservation in Contrin Formation dolostone. Transmitted light images (left) placed against redrawn features (right). The field of view is 2.5 x 2.5 cm. **(A)** Fabric preserving dolomitization. Fine-grained, early diagenetic dolostone with well-preserved *dasycladacean* algae and pore-filling (saddle) dolomite cement. **(B)** Fabric destructive dolomitization. Medium-grained to coarse-grained, largely recrystallized Contrin dolostone from the Latemar slope with poorly preserved *dasycladacean* algae.

**Fig. 14.** Cross-plot of  $\delta^{18}\text{O}$  and  $\delta^{13}\text{C}$  data for dolomite and calcite phases from the contact aureole. **(A)** The isotopic composition of Middle/Late Triassic marine calcite is indicated in the solid purple and dashed purple boxes (from Korte *et al.*, 2005; Grossman, 2012; Saltzman & Thomas, 2012; Veizer & Prokoph, 2015). The range of seawater associated with early diagenetic Middle/Late Triassic dolostones is indicated in the light green box (from Geske *et al.*, 2012; Chatalov, 2018; Rieder *et al.*, 2019). Data from previous studies (intrusion: Ferry *et al.*, 2002; Latemar: Jacquemyn *et al.*, 2014) is marked in dark green (dolomite) and blue (calcite) boxes. The annotated trends indicate a shift in  $\delta^{13}\text{C}$  of about -2‰ from Dol marble 1 towards Dedol marble 2. **(B)** Data from **(A)** is set in the context of available pore space, mineralogical processes, metamorphic temperatures and fluid flow.

**Fig. 15.** Cross-plot of the isotopic composition ( $\delta^{18}\text{O}_{\text{VSMOW}}$ ) of the formation fluid calculated from  $\delta^{18}\text{O}_{\text{VPDB}}$  values of the investigated marbles from the Predazzo Intrusion contact aureole by considering oxygen isotope equilibration based on Sheppard & Schwarcz (1970) and Friedman & O'Neil (1977) for dolomite and calcite, respectively. The distinct formation temperature ranges (50°C, 100°C, 200°C, 300°C, 500°C and 650°C) are exemplary for the metamorphic temperature range at the Predazzo Intrusion contact aureole obtained from Ferry *et al.* (2002) and potential late retrograde diagenesis. Note that the oxygen isotope fractionation between both dolomite and calcite, and the fluid is reduced at elevated temperature, thus at 600°C, the  $\delta^{18}\text{O}_{\text{carbonate-H}_2\text{O}}$  value is only about +1‰. The oxygen isotope composition of basaltic fluids and primary magmatic H<sub>2</sub>O is derived from Harmon & Hoefs (1995), Giggenbach (1992) and Vho *et al.* (2019). The isotopic composition of contact aureole marbles is indicated below the x-axis in green (Dol marbles) and blue (Dedol marbles).

**Fig. 16.** Oxygen-isotope composition *versus* strontium-isotope ratios of dolomite and calcite phases compared to Middle/Late Triassic unaltered marine calcites from Korte *et al.* (2003) and ranges of former studies by Wilson *et al.* (1990), Blendinger (1997, 2011) and Jacquemyn *et al.* (2014). Except for some calcites and less radiogenic dolomites (0.7074), all Latemar samples fit in the Middle/Late Triassic range and agree with former studies. Some marbles from the contact aureole display Triassic values, while the majority are more radiogenic (up to 0.7100). This trend is counterintuitive as the intrusion displays values from 0.7036 to 0.7064 (shoshonitic units, Sloman, 1989; Marrocchino *et al.*, 2009; Jacquemyn *et al.*, 2014; Casetta *et al.*, 2018b) and 0.6000 to 0.6200 (Jacquemyn *et al.*, 2014). No marbles were analyzed at the Latemar slope/interior.

**Fig. 17.** Cross-plots of  $\delta^{18}\text{O}$  and  $\delta^{13}\text{C}$  data for all analyzed dolomite and calcite phases from (A) Latemar slope and (B) Latemar interior. The isotopic composition of Middle/Late Triassic marine calcite is indicated by the solid purple and dashed purple boxes (from Korte *et al.*, 2005; Grossman, 2012; Saltzman & Thomas, 2012; Veizer & Prokoph, 2015). Data from Jacquemyn *et al.* (2014) is marked in dark green (dolomite) and blue (calcite) boxes. The annotated trends indicate a shift in  $\delta^{13}\text{C}$  of about -2‰ from Dol 1 towards Dol 3 and 4 in (A) and a shift in  $\delta^{13}\text{C}$  of about -1‰ from Dol 1 towards Dol 3 and 4 in (B).

### Table captions

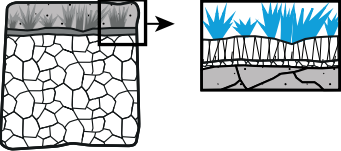
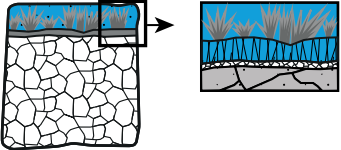
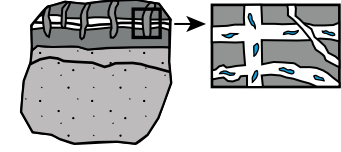
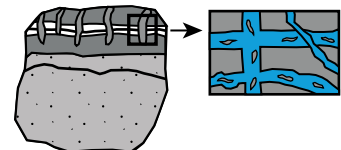
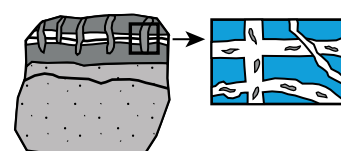
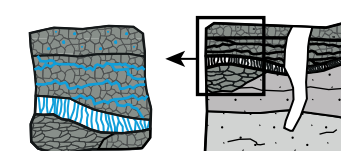
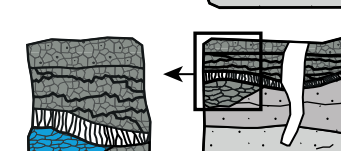
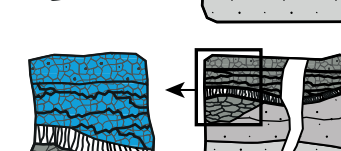
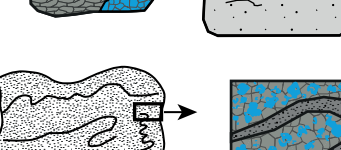
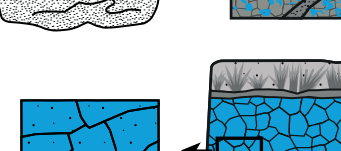
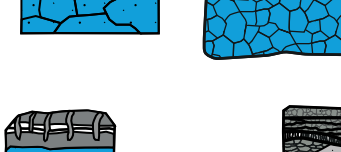
**Table 1.** Summary of a selected set of important studies of the Latemar carbonate buildup in the past decades. Studies are grouped by their main focus, topics and research fields. Many more studies, especially with regional geological focus, are not included in this table.

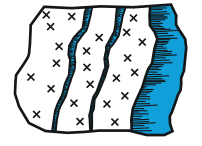
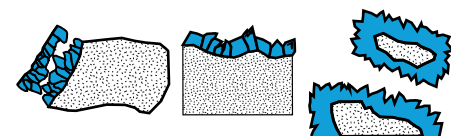
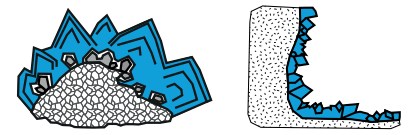
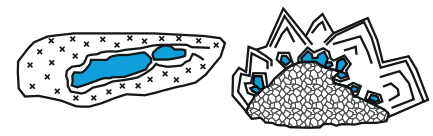
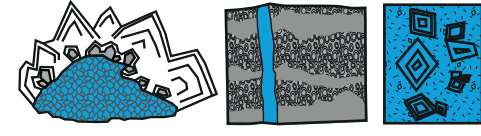
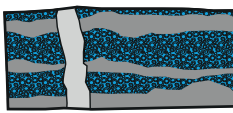
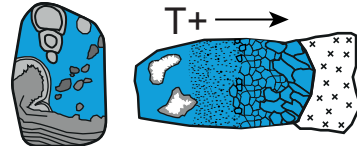
**Table 2.** Paragenetic sequence (starting with precursor limestone and ending with HMC 1) of the Latemar slope and interior along with phase-specific petrography, characteristic features, crystal size, volumetric significance, luminescence, and their carbon-isotope, oxygen-isotope and strontium-isotope composition. Additional geochemical data for individual samples and groups are provided in Appendix S1. Blue refers to the mineral or cement phase.

**Table 3.** Complete succession (starting with Contrin Dol and ending with AC 1) of the contact metamorphic aureole near the Predazzo Intrusion along with phase-specific petrography, characteristic features, crystal size, volumetric significance, luminescence, and their carbon-isotope, oxygen-isotope and strontium-isotope composition. Additional geochemical data for individual samples and groups are provided in Appendix S1. Blue refers to the mineral or cement phase.

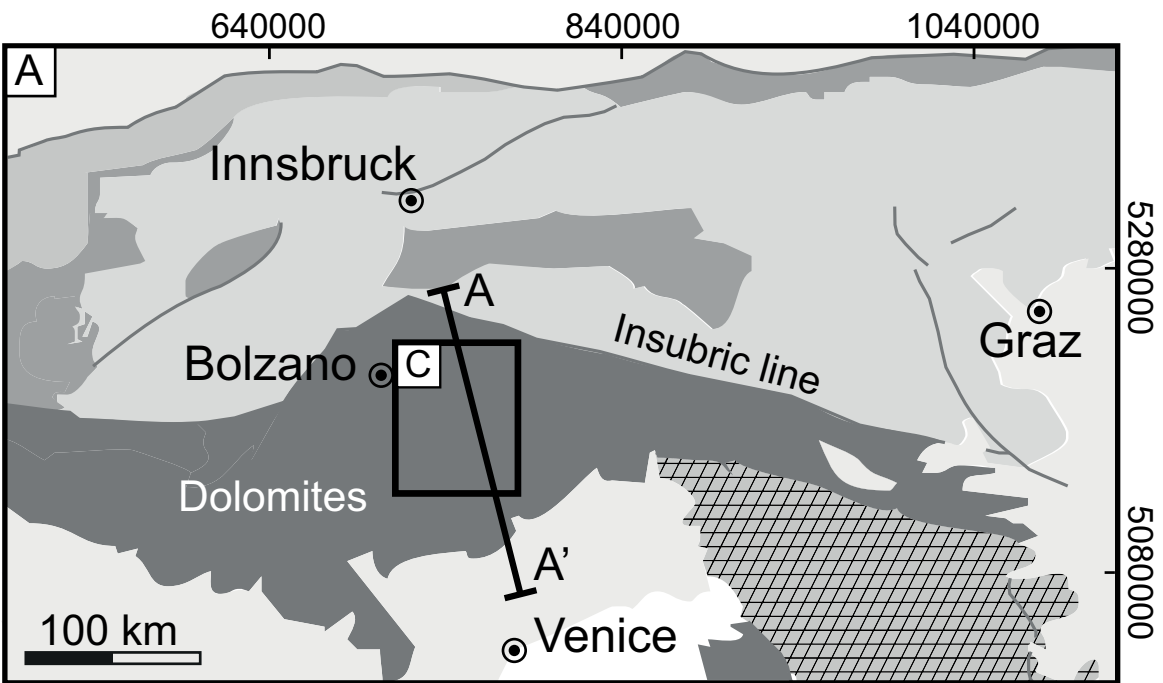
**Table 4.** Mean values of fluid inclusion data from the contact aureole, Latemar slope and Latemar interior. Temperatures are given in °C.

	Authors	Topic	Research field	
Latemar interior and margin	Wilson <i>et al.</i> (1990)	Dolomitization / diagenesis	Sedimentology / Geochemistry	
	Schubel <i>et al.</i> (2005)	Dolomitization	Sedimentology / Crystallography	
	Schubel & Veblen (2005)	Dolomitization / diagenesis	Sedimentology	
	Goldhammer <i>et al.</i> (1987)	Orbital cyclicity	Sedimentology	
	Goldhammer & Harris (1989)	Orbital cyclicity	Sedimentology / Palaeoclimatology	
	Hinnov & Goldhammer (1991)	Orbital cyclicity	Sedimentology / Palaeoclimatology	
	Preto <i>et al.</i> (2001)	Orbital cyclicity	Sedimentology / Palaeoclimatology	
	Brack & Rieber (1993)	Biostratigraphic and chronostratigraphic	Sedimentology	
	Kent <i>et al.</i> (2004)	Biostratigraphic and chronostratigraphic	Sedimentology	
	Zühlke <i>et al.</i> (2003)	Biostratigraphic and chronostratigraphic	Sedimentology	
	Christ <i>et al.</i> (2012)	Cycle tops	Sedimentology / Geochemistry	
	Goldhammer <i>et al.</i> (1993)	Facies relationships	Sedimentology	
	Egenhoff <i>et al.</i> (1999)	Facies relationships	Sedimentology	
	Harris (1993)	Reef facies characterization	Sedimentology	
	Seeling <i>et al.</i> (2005)	Sedimentation / cementation	Sedimentology	
	Marangon <i>et al.</i> (2011)	Platform growth	Sedimentology	
	Franceschi <i>et al.</i> (2016)	Carbonate production	Sedimentology / Num. modeling	
	Nemeth & Budai (2009)	Volcanism	Sedimentology / Volcanology	
	Latemar interior and/or slope	Carmichael <i>et al.</i> (2008)	Dolomitization / diagenesis	Sedimentology / Geochemistry
		Carmichael & Ferry (2008)	Dolomitization	Geochemistry
Ferry <i>et al.</i> (2011)		Dolomitization temperature	Geochemistry	
Jacquemyn <i>et al.</i> (2014)		Dolomitization / diagenesis	Sedimentology / Geochemistry	
Jacquemyn <i>et al.</i> (2015)		Dolomitization	Reservoir modeling	
Blomme <i>et al.</i> (2017)		Dolomitization	Sedimentology / Num. modeling	
Riva & Stefani (2003)		Intraplatform collapse		
Emmerich <i>et al.</i> (2005)		Facies	Sedimentology / Palaeontology	
Preto <i>et al.</i> (2011)		Platform growth geometry	Reservoir analogue	
Preto <i>et al.</i> (2019)		Facies zonation	Sedimentology / Geochemistry	
Franceschi <i>et al.</i> (2020)		Microbial mound drowning	Sedimentology	
Boro <i>et al.</i> (2013)		Fracture development	Reservoir analogue	
Hardebol <i>et al.</i> (2015)	Fracture characterization	Reservoir analogue		
Bigi <i>et al.</i> (2015)	Fracture modeling	Reservoir analogue		
Intrusion or aureole	Castellarin <i>et al.</i> (1982)	Petrological evolution	Petrology	
	Lucchini <i>et al.</i> (1982)	Petrological evolution	Petrology	
	Sloman (1989)	Petrological evolution	Petrology	
	Visona (1997)	Petrological evolution	Petrology	
	Ferry <i>et al.</i> (2002)	Metamorphic fluid flow	Metamorphic petrology	
	Marrocchino <i>et al.</i> (2009)	Tectono-magmatic significance	Petrology	
	Casetta <i>et al.</i> (2018a)	Petrological evolution	Petrology	
	Casetta <i>et al.</i> (2018b)	Physics and chemistry	Petrology	

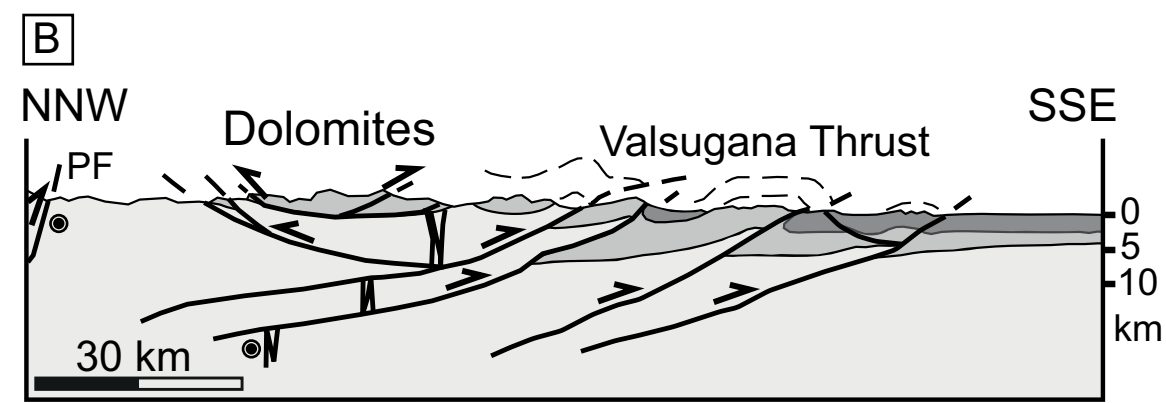
Phase	Petrography	Characteristic features	Crystal size	Volumetric significance	Luminescence	$\delta^{13}\text{C}$ (‰) min./max./mean	$\delta^{18}\text{O}$ (‰) min./max./mean	$^{87}\text{Sr}/^{86}\text{Sr}$ ( $\pm 2\sigma$ ) min. max.
AC 1		Form tubular veins/precipitates on top of older marble phases, fibrous needles	Micro- to macro-crystalline	Low	Non-luminescent to dark blue	-0.3/1.0/0.3	-13.9/-9.2/-10.5	No data
Dol 1 / Dedol 1		Form tubular veins/precipitates on top of older marble phases, partially include curved dolomite crystal faces	Crypto- to macro-crystalline	Low	Dark blue, dark to bright magenta, blue to bright blue			No data
Dol marble 3		Elongated crystals, only known in LMC 1 CC veins.	Micro- to macro-crystalline	Very low	Dark red to intense red		No data	
LMC 1/2 CC		Blocky white calcite, dynamically recrystallized microfabric, LMC 1 CC is perpendicular or parallel to foliation of older phases	Micro- to macro-crystalline	Low	Dark orange to bright orange	-0.5/1.6/0.5	-7.1/-4.5/-5.8	0.709116 (4) 0.710011 (6)
Phyllo-silicates (undiff.)		Decimetre-thick veins associated with LMC 1 CC	Crypto- to microcrystalline	Low	Non-luminescent		Not applicable	
Mg-silicates		Overgrow older phases, form veins/striations	Crypto- to macro-crystalline	High	Non-luminescent, pink-orange, bright yellow		Not applicable	
Dol marble 2		Elongated crystals, overgrow Dedol 2 matrix	Micro- to macrocrystalline	Moderate	Dark red to intense red	0.1/1.1/0.6	-3.2/-1.2/-2.6	0.708853 (5) 0.709508 (5)
Dedol marble 2		Grey calcite crystals, dynamically recrystallized microfabrics, moderate to very high magnesium silicate content, foliated	Micro- to macro-crystalline	High	Bright red to bright orange	-0.7/1.7/0.3	-5.4/-3.3/-4.6	0.708319 (5) 0.709556 (7)
Brucite		Foliated clear crystals, common in Dedol 1 and 2	Micro- to macro-crystalline	Moderate	Non-luminescent		Not applicable	
Dedol marble 1		White blocky calcite crystals, iron poor, annealed to twinned and dynamically recrystallized microfabrics, very few magnesium silicates	Micro- to macro-crystalline up to 15 mm	Very high	Dark red, magenta red to orange	-0.2/1.7/1.0	-8.2/-2.8/-5.8	0.707832 (5) 0.707942 (5)
Dol marble 1		Grey Contrin dolomite marble, semi-annealed microfabric	Microcrystalline	Moderate	Dark red	0.7/2.4/2.0	-3.3/-1.0/-2.0	0.707658 (5) 0.708929 (5)
Contrin Dol		Pervasively recrystallized dolostone typically overgrown by dol cements	Meso- to macro-crystalline	High at Latemar slope	Dark red to bright red	3.2/3.3/3.2	-2.9/-2.8/-2.9	0.707755 (5) 0.707755 (5)

Phase	Petrography	Characteristic features	Crystal size	Volumetric significance	Luminescence	$\delta^{13}\text{C}$ (‰) min./max./mean	$\delta^{18}\text{O}$ (‰) min./max./mean	$^{87}\text{Sr}/^{86}\text{Sr}$ ( $\pm 2 \sigma$ ) min. max.
HMC 1		Forms botryoidal shaped fibrous aggregates	Microcrystalline	Very low	Non-luminescent to dark red		No data	
LMC 3		Zoned blocky crystals, pore- and cavity infill, iron poor	Micro- to macro-crystalline	Very low	Yellow and non-luminescent		No data	
LMC 2		Fibrous to blocky crystals, only known from veins in dikes	Cryptocrystalline	Very low	Bright orange	1.2/1.5/1.4	-5.1/4.1/-4.7	0.706666 (5) 0.706694 (6)
LMC 1		Zoned blocky crystals, pore- and cavity infill, iron poor	Micro- to macro-crystalline up to 50 mm	Low	Red, orange to bright yellow	1.6/2.0/1.8	-12.3/-11.2/-11.9	0.708470 (6) 0.708530 (5)
Fe-oxides		Replacement of desintegrated dolomite cement zones	Cryptocrystalline	Low to moderate	Bright yellow		Not applicable	
Dol 4		Curved crystal faces, sweeping extinction, iron poor, common in cell dolomite, "mega cavities" and rarely veins, patchy luminescence	Macrocrystalline up to 10 mm	Low to moderate	Bright red to orange	2.0/2.5/2.3	-9.0/-3.8/-6.4	0.707595 (5) 0.707916 (5)
Dol 3		Moderately iron rich hydrothermal replacement dolomite, euhedral to anhedral, partly patchy luminescence	Micro- to macrocrystalline	High	Intense red to orange	2.1/2.9/2.4	-9.8/-1.5/-4.0	0.707599 (5) 0.707906 (5)
Dol 2		Iron rich hydrothermal dolomite, typically occurs as cavity infill, common in cell dolomite, sweeping extinction, curved crystal faces	Micro- to macro-crystalline	Low to moderate	Non-luminescent to bright red	2.3/3.9/3.0	-4.9/-2.1/-3.6	0.707636 (6) 0.707776 (5)
Qz 1/2		Cavity infill in dikes or anhedral to euhedral crystals grown on dolomite	Macrocrystalline	Very low	Non-luminescent to intrinsic		Not applicable	
Dol 1		Iron rich hydrothermal replacement dolomite, euhedral to anhedral close to dikes, partly patchy luminescence	Micro- to macro-crystalline	Moderate	Non-luminescent to orange	2.2/4.9/3.3	-6.7/-0.8/-2.8	0.707424 (6) 0.708031 (5)
Oolitic ironstone		Heavily silicified or dolomitized, only known from the slope	Microcrystalline	Low to moderate	Intrinsic (Qz) to red (Dol)	3.3/5.0/4.3	-3.3/-1.6/-2.2	0.707742 (5) 0.707806 (5)
Limestone		Dominantly algal limestone with marine cements, locally recrystallized close to dikes	Micro- to macro-crystalline	Very high	Non-luminescent to bright red	1.9/3.9/2.4	-7.8/-2.2/-5.1	0.707637 (5) 0.708589 (5)

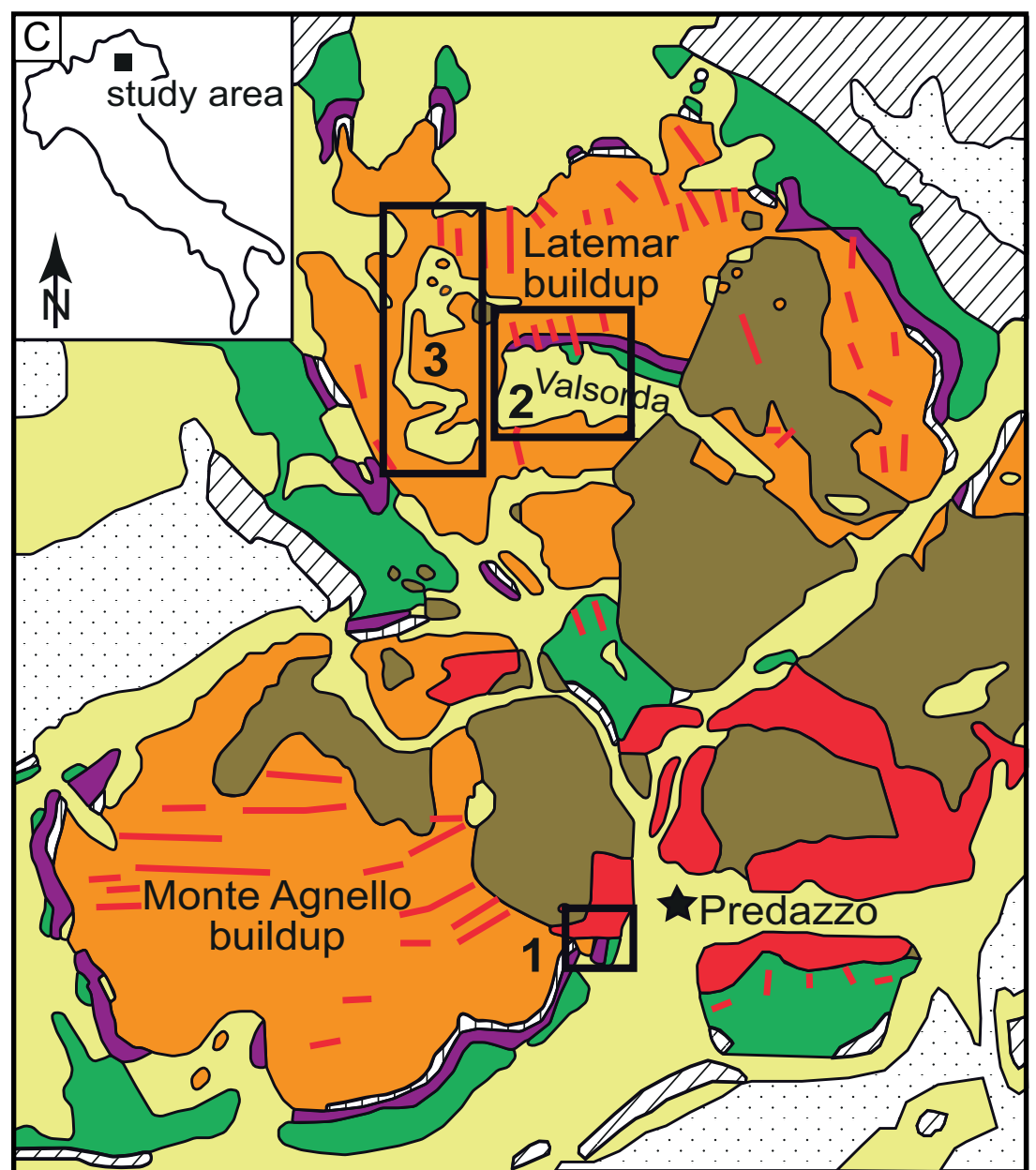
Number of inclusions	Host	FIA	Area	T <sub>m</sub> (l)	T <sub>h</sub> hh corrected	T <sub>h</sub>	Salinity	NaCl wt. %	CaCl <sub>2</sub> wt. %
6	Dedol marble 2	isoDedol2_1	Intrusion contact	-17.8	-21.6	215	20.7	19.5	1.2
3	Contrin dolomite	pContrindol-1/2	Latemar slope	-23.6	-24.8	193	28.7	20.5	8.2
3	Dol 2 slope	isoDol2	Latemar slope	-11.7	-21.2	282	15.7	15.6	0.1
5	LMC 1 Latemar	pDol2A-1	Latemar slope	-0.7	-21.2	191	1.1	1.1	0.0
5	Dol 2 interior	pDol2A-1	Latemar interior	-21.8	-5.2	59	25.9	23.9	2.0



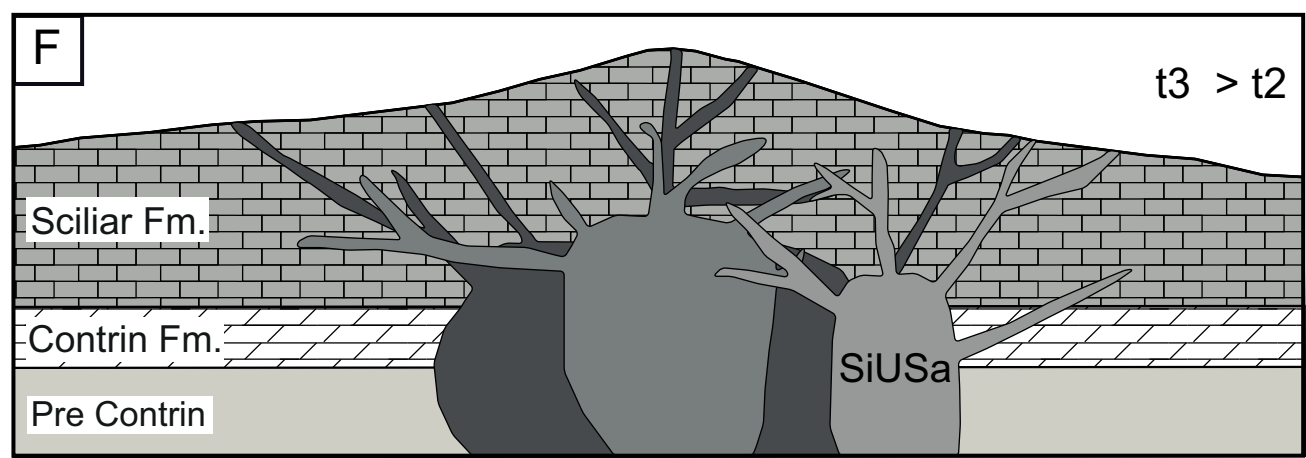
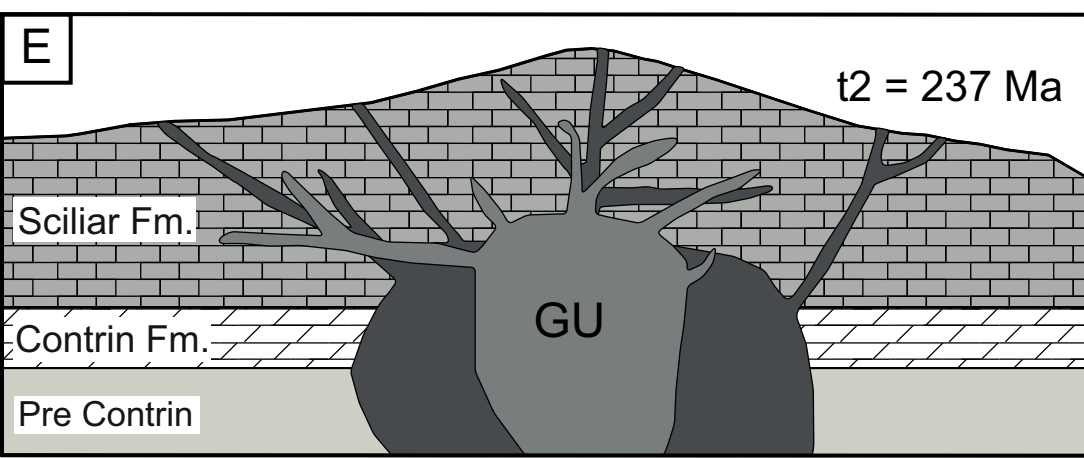
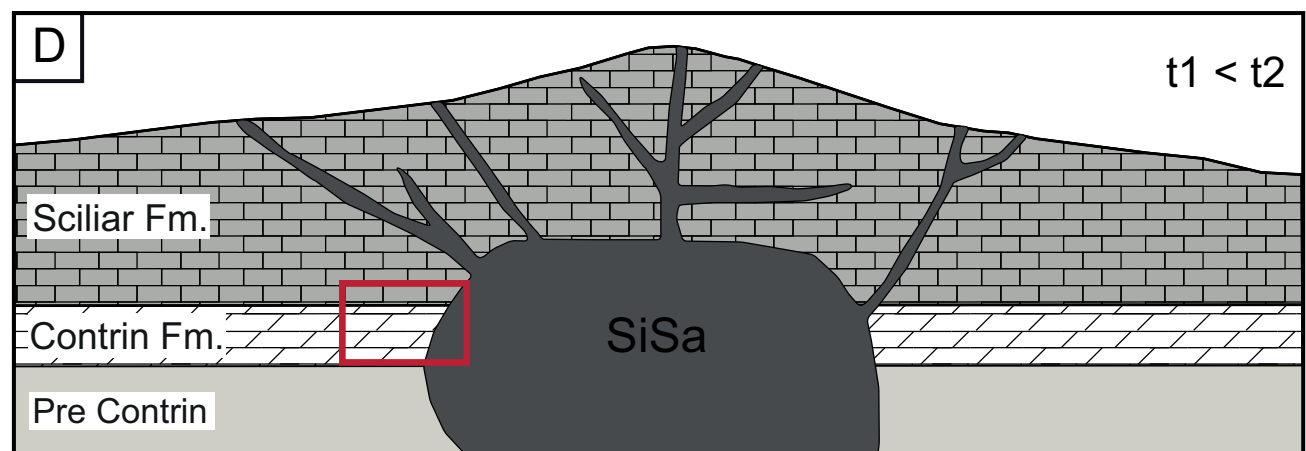
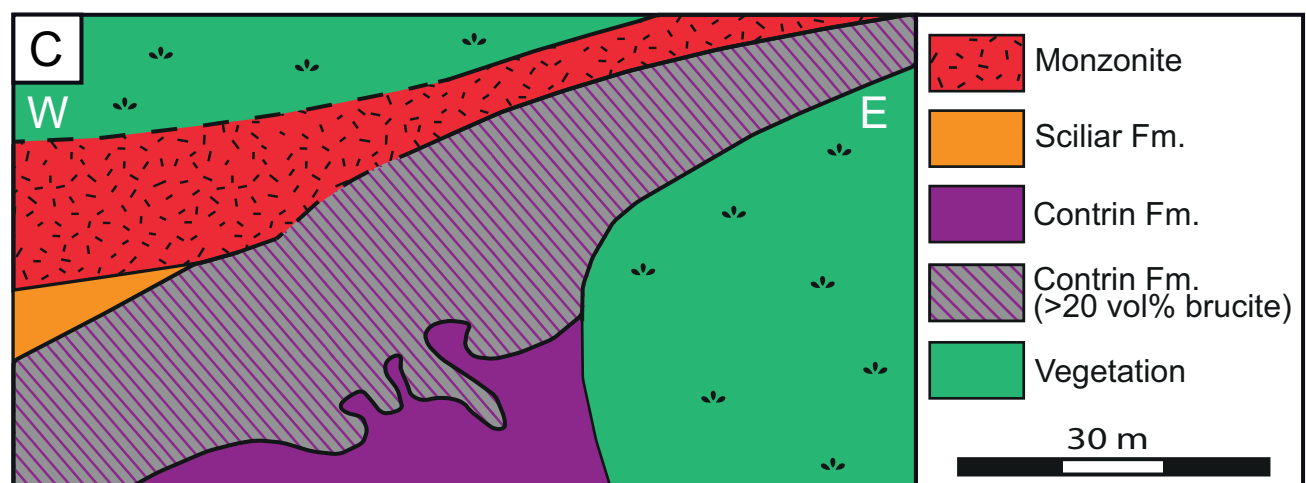
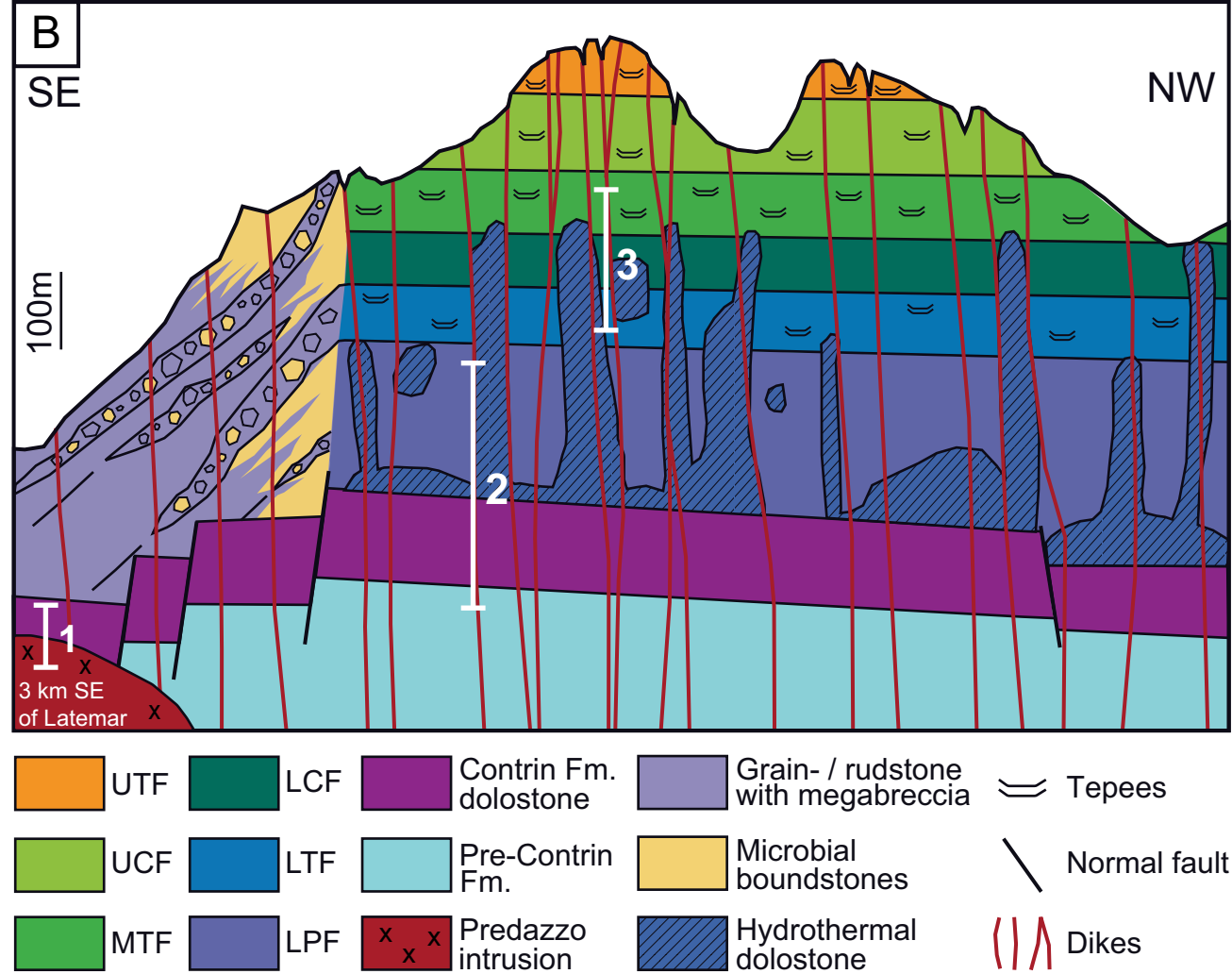
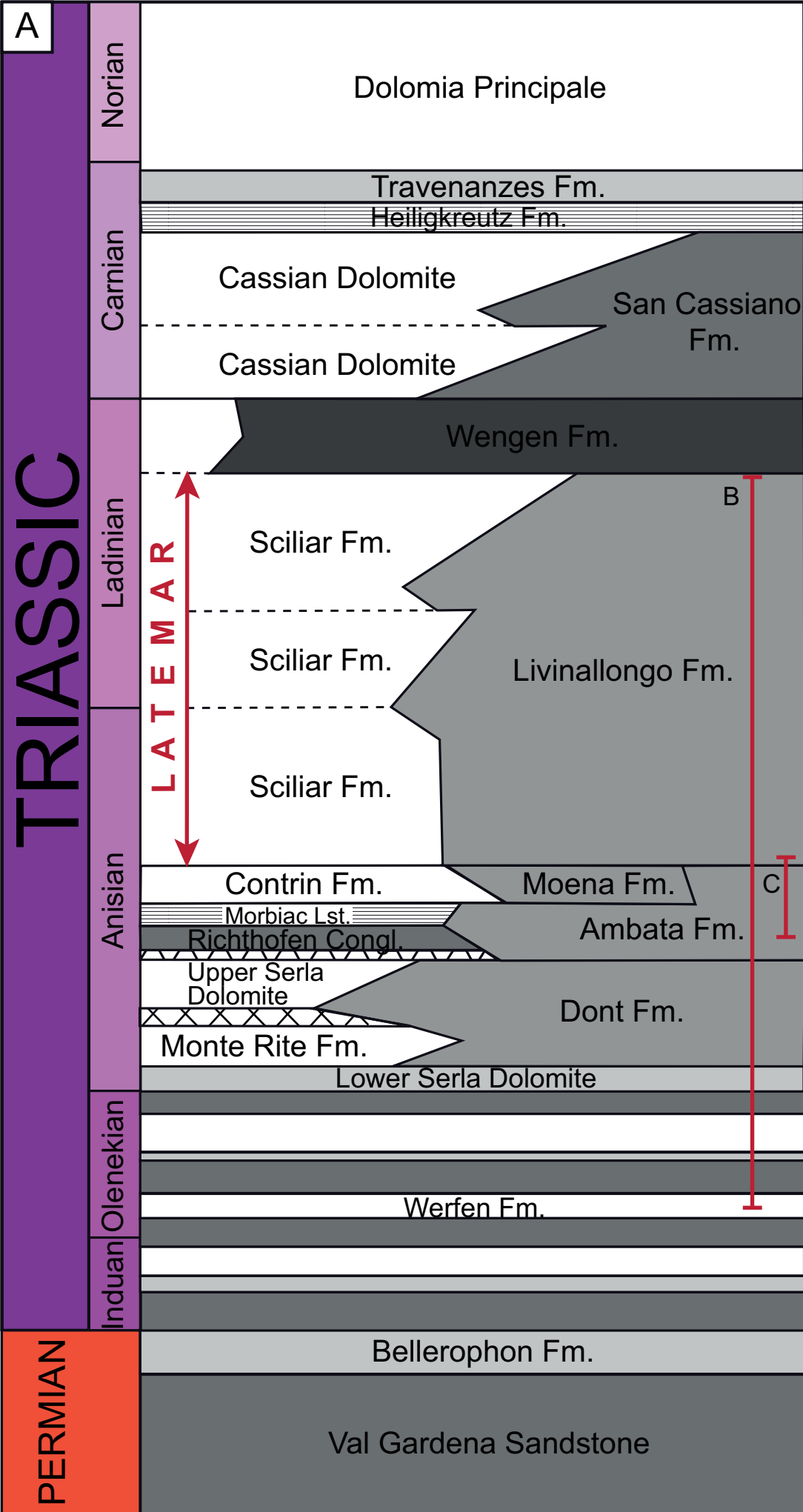
- |           |               |          |
|-----------|---------------|----------|
| Recent    | Austroalpine  | Helvetic |
| Dinarides | Southern Alps | Penninic |



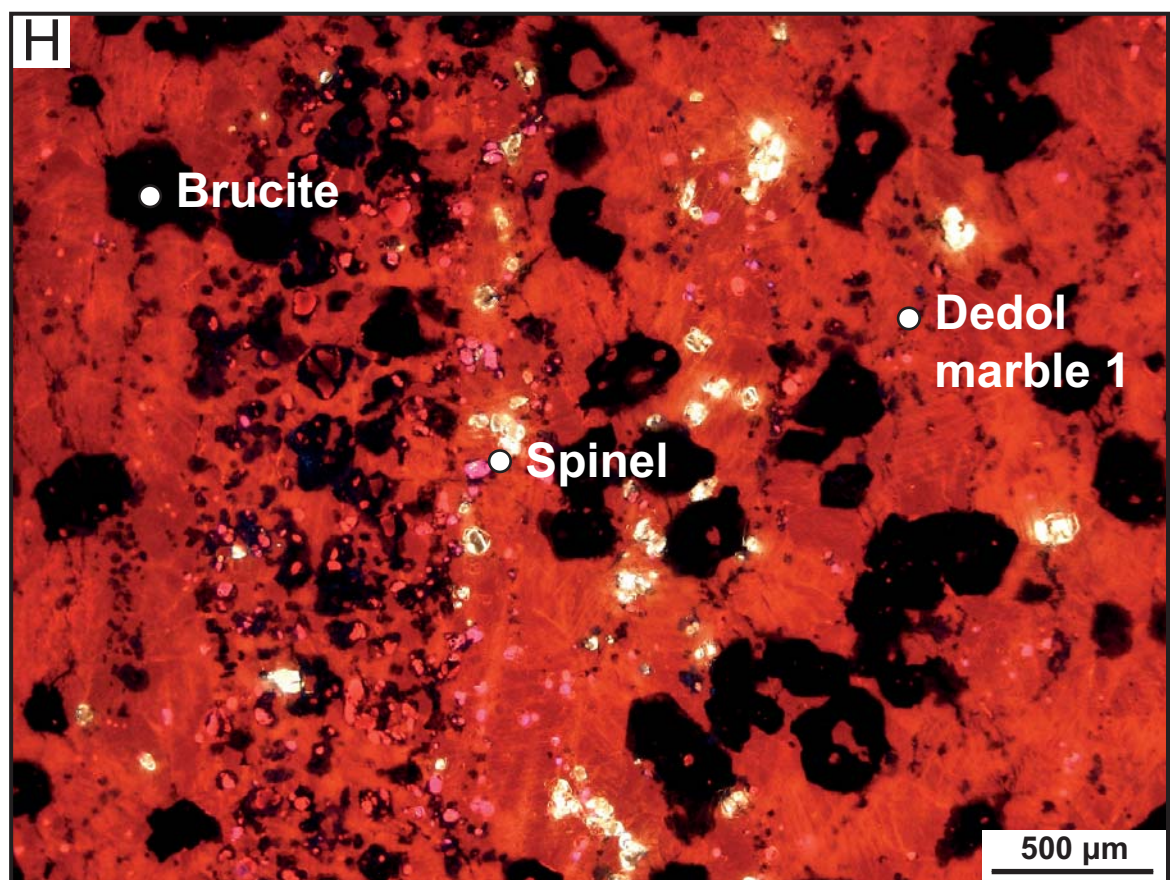
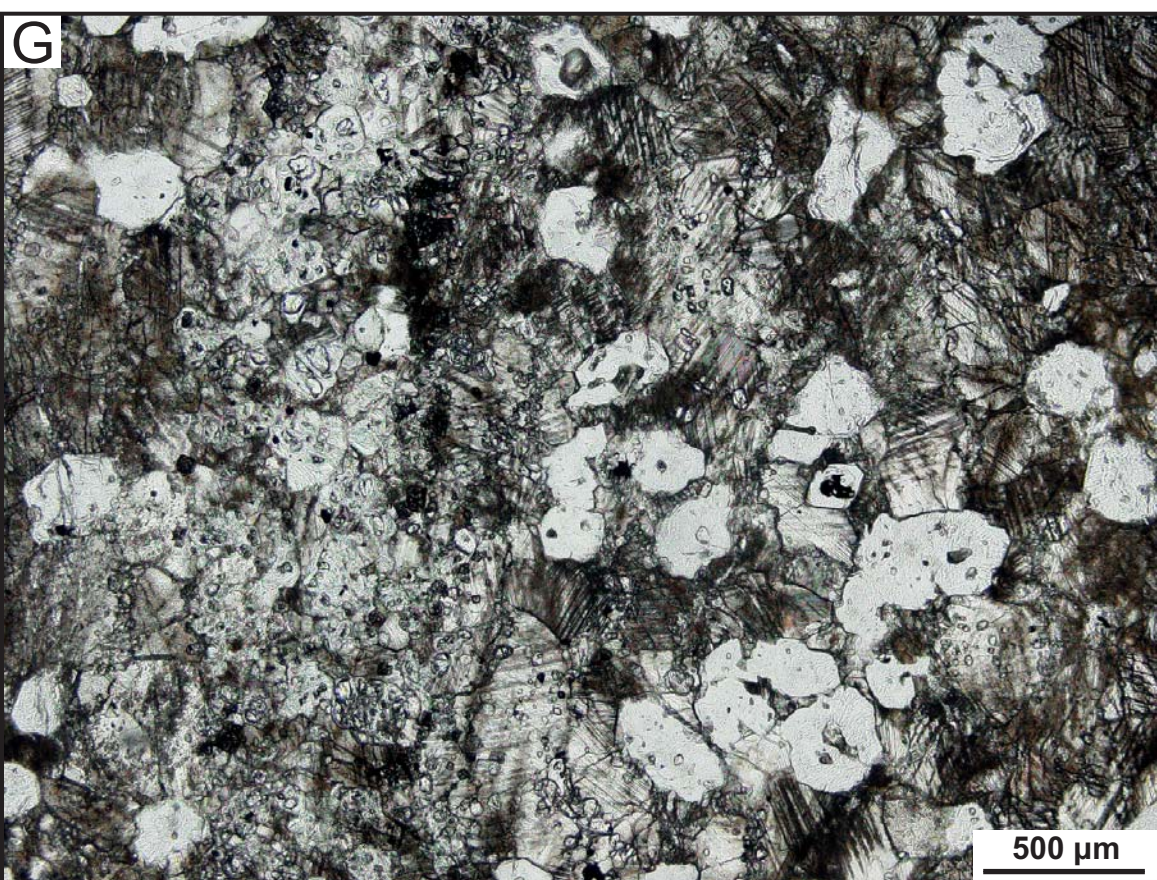
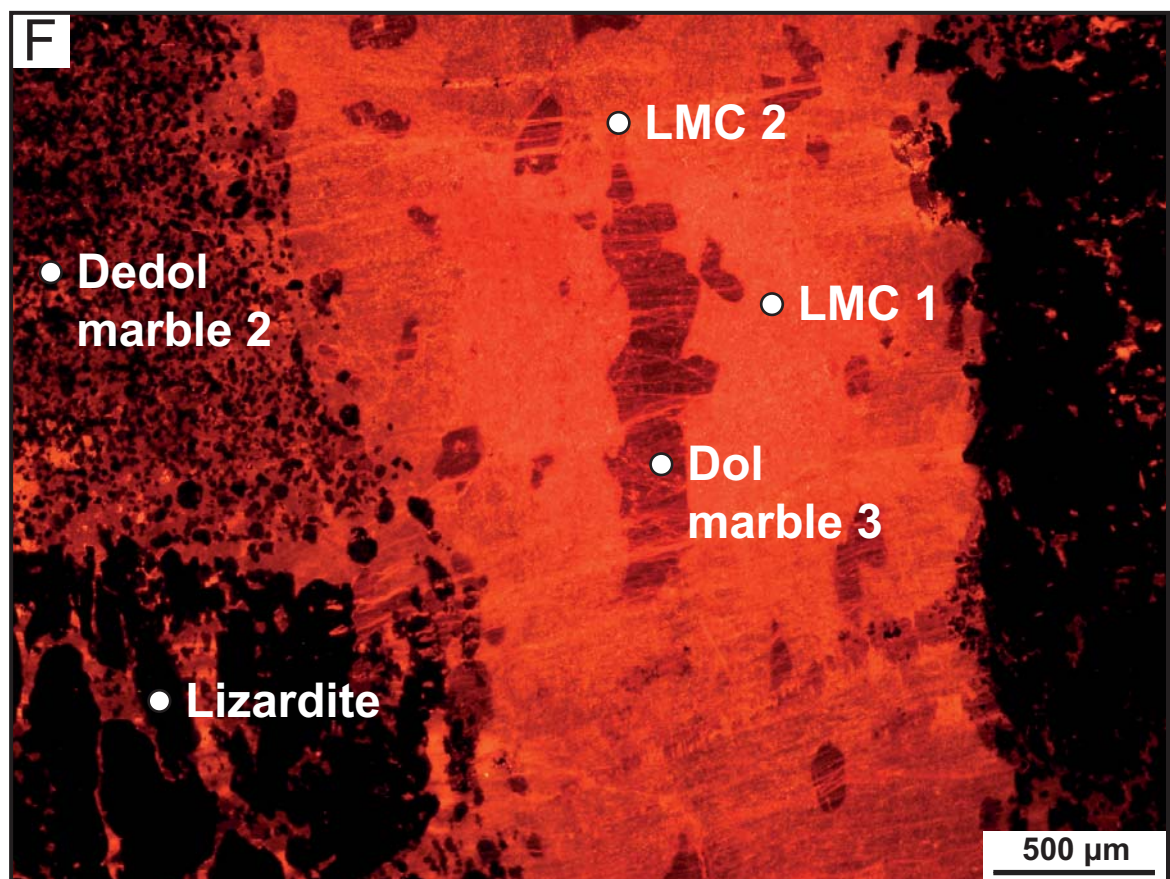
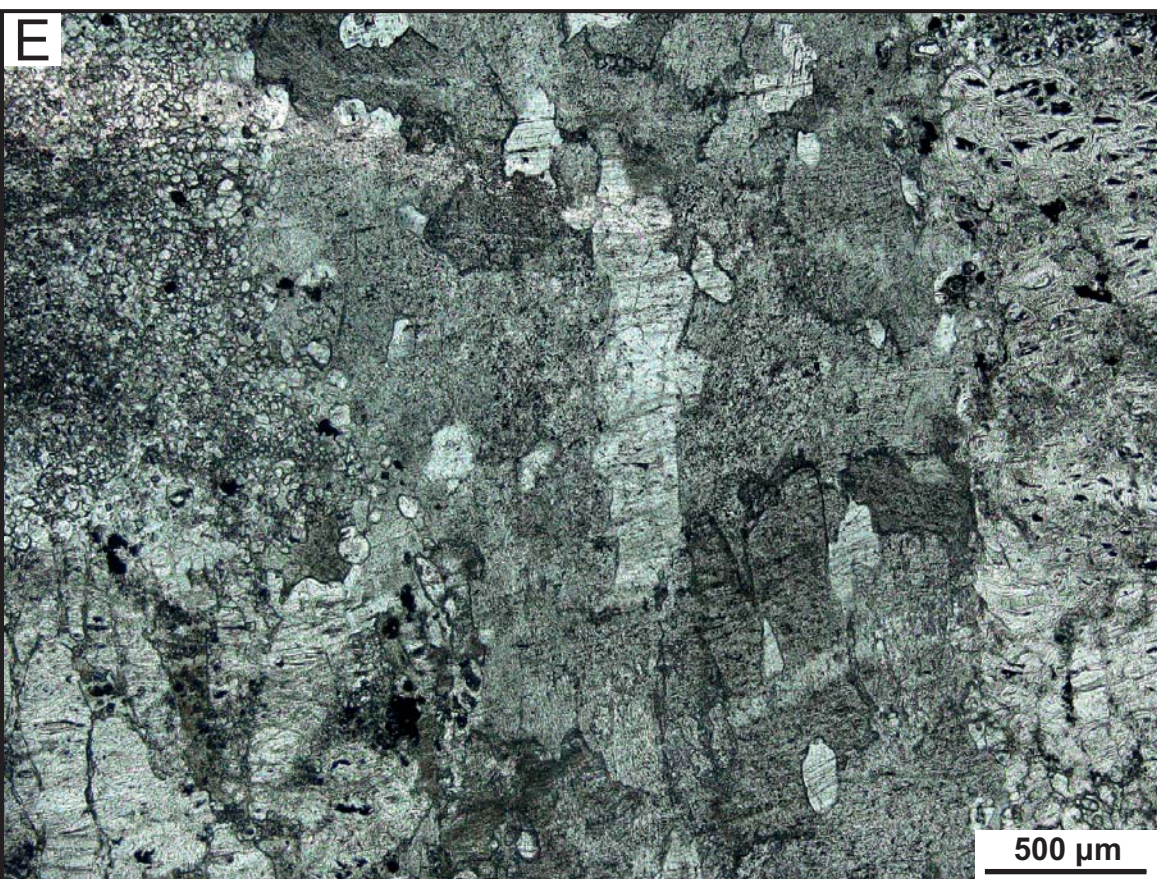
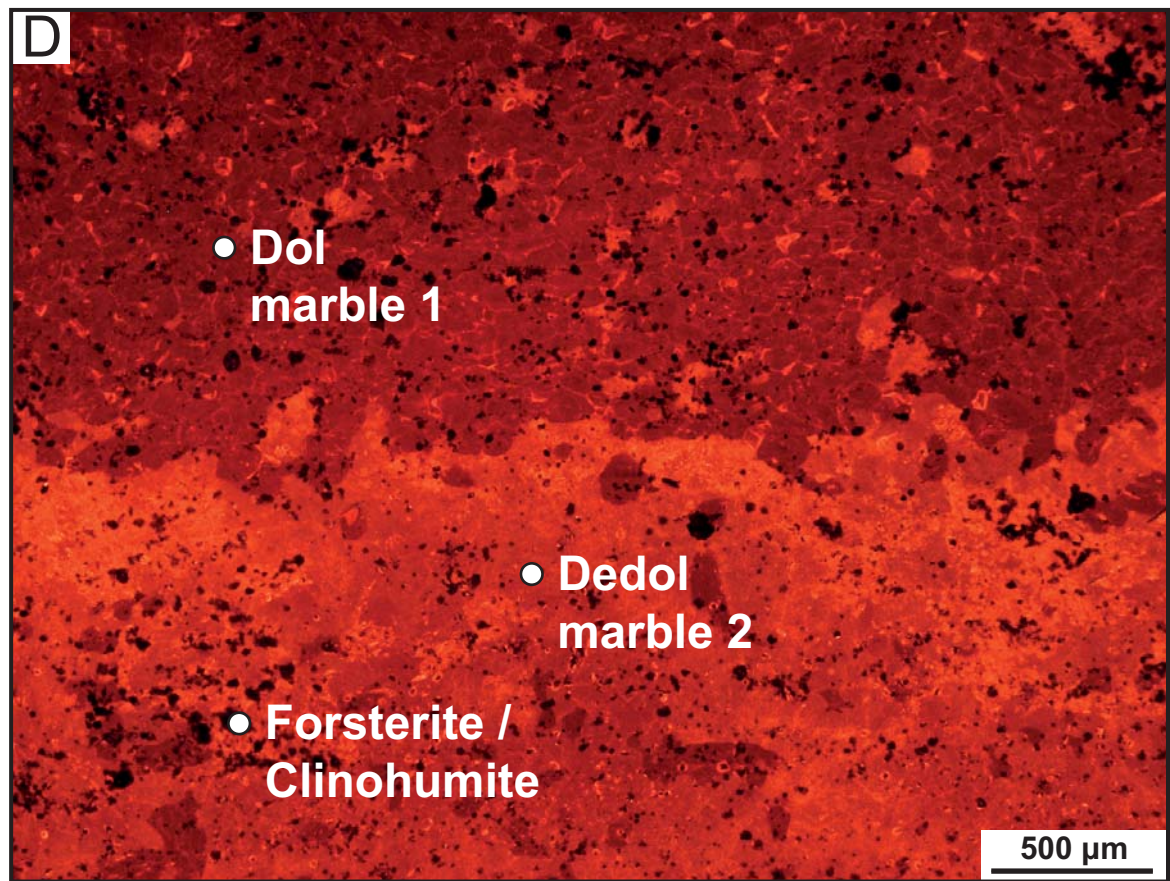
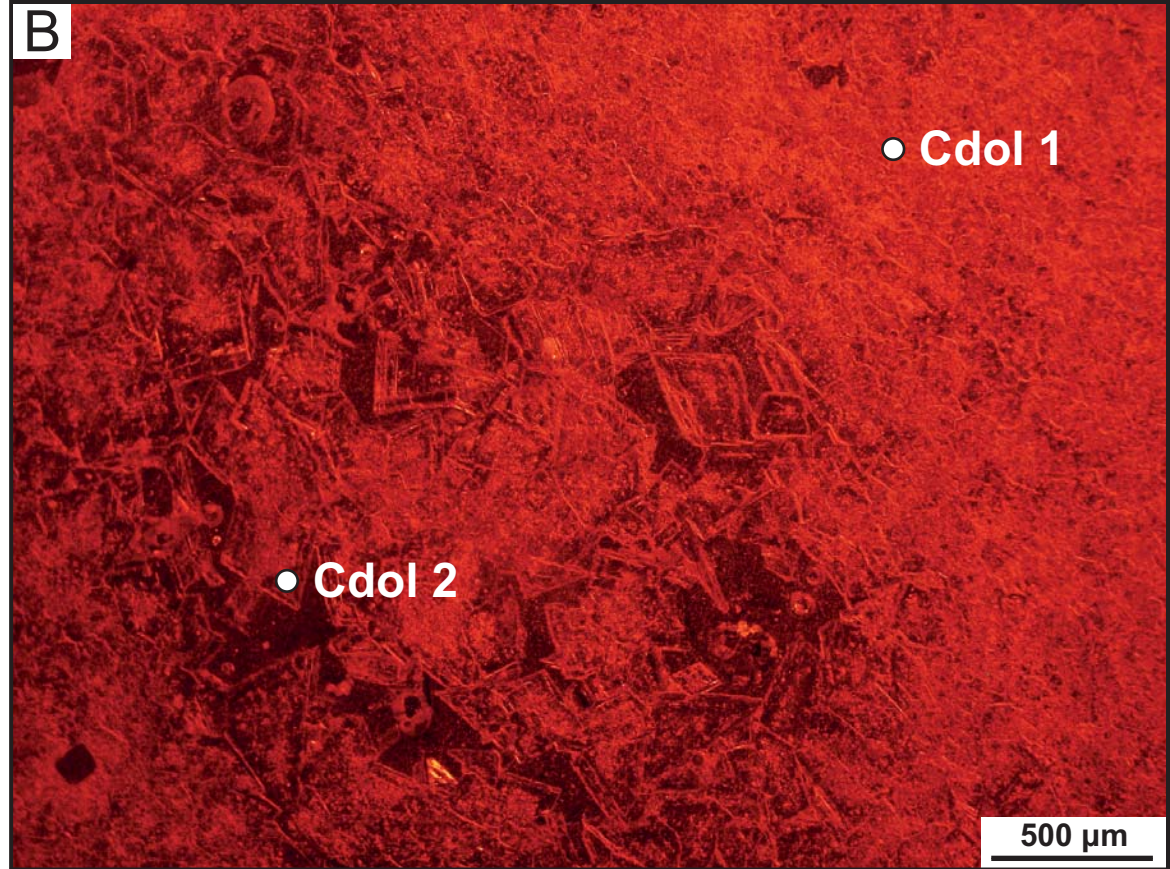
- |                    |                  |
|--------------------|------------------|
| Palaeogene-Neogene | Permian-Mesozoic |
| Basement           |                  |

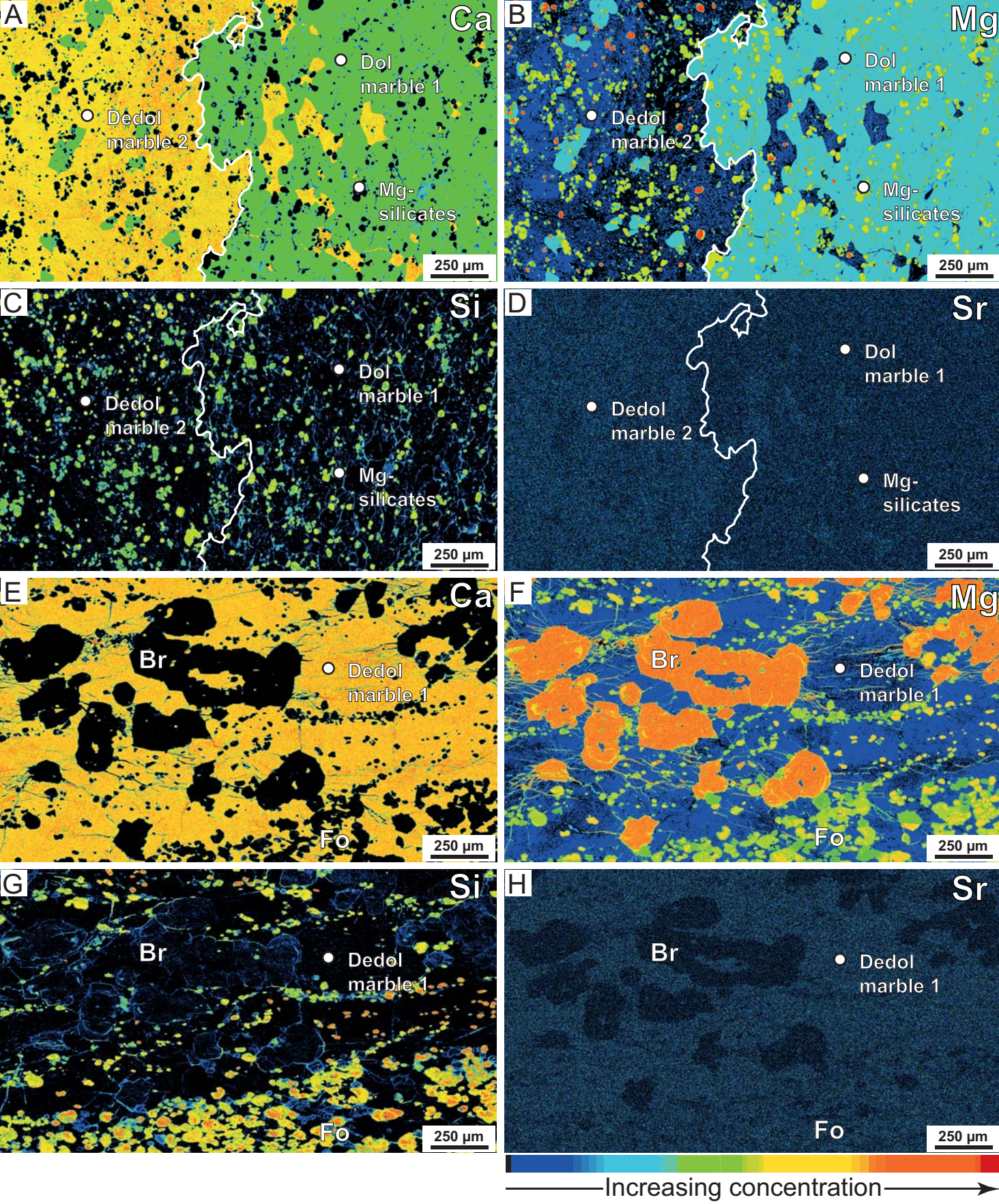


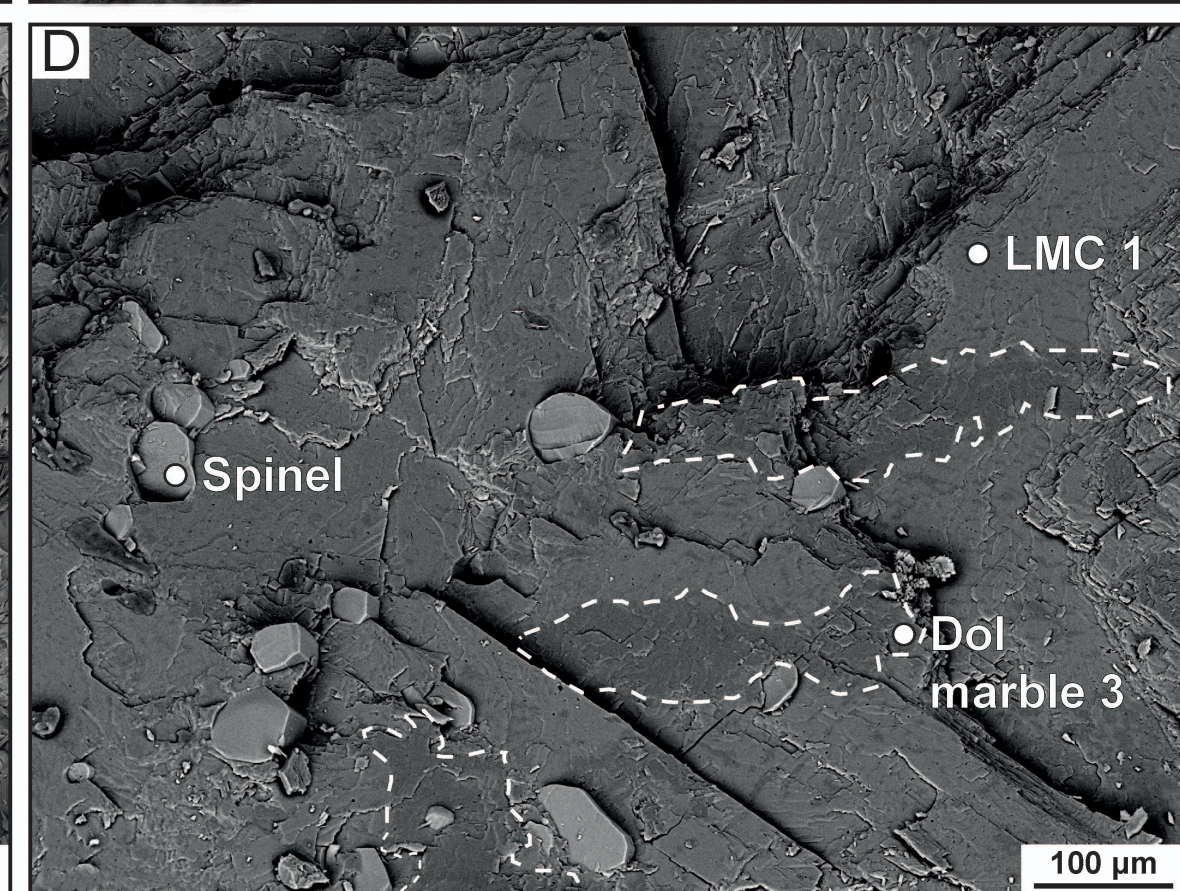
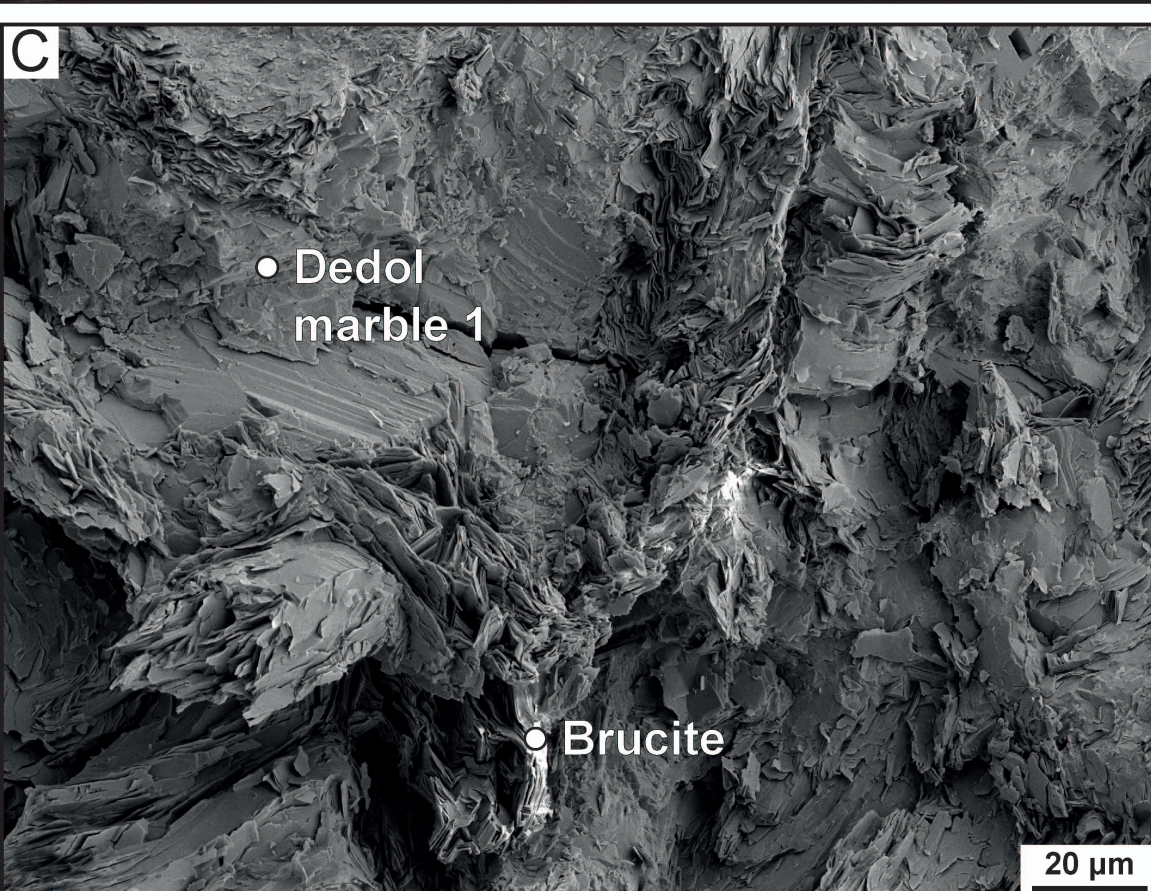
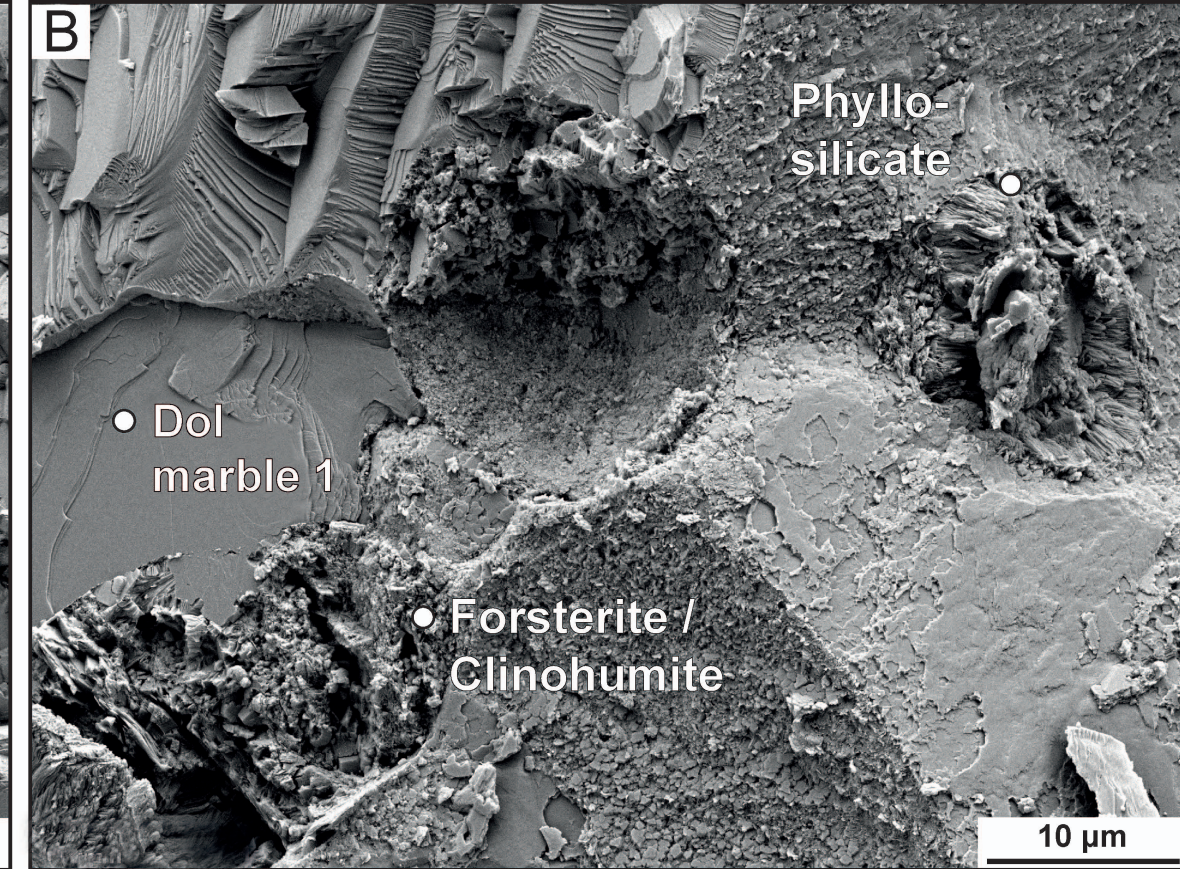
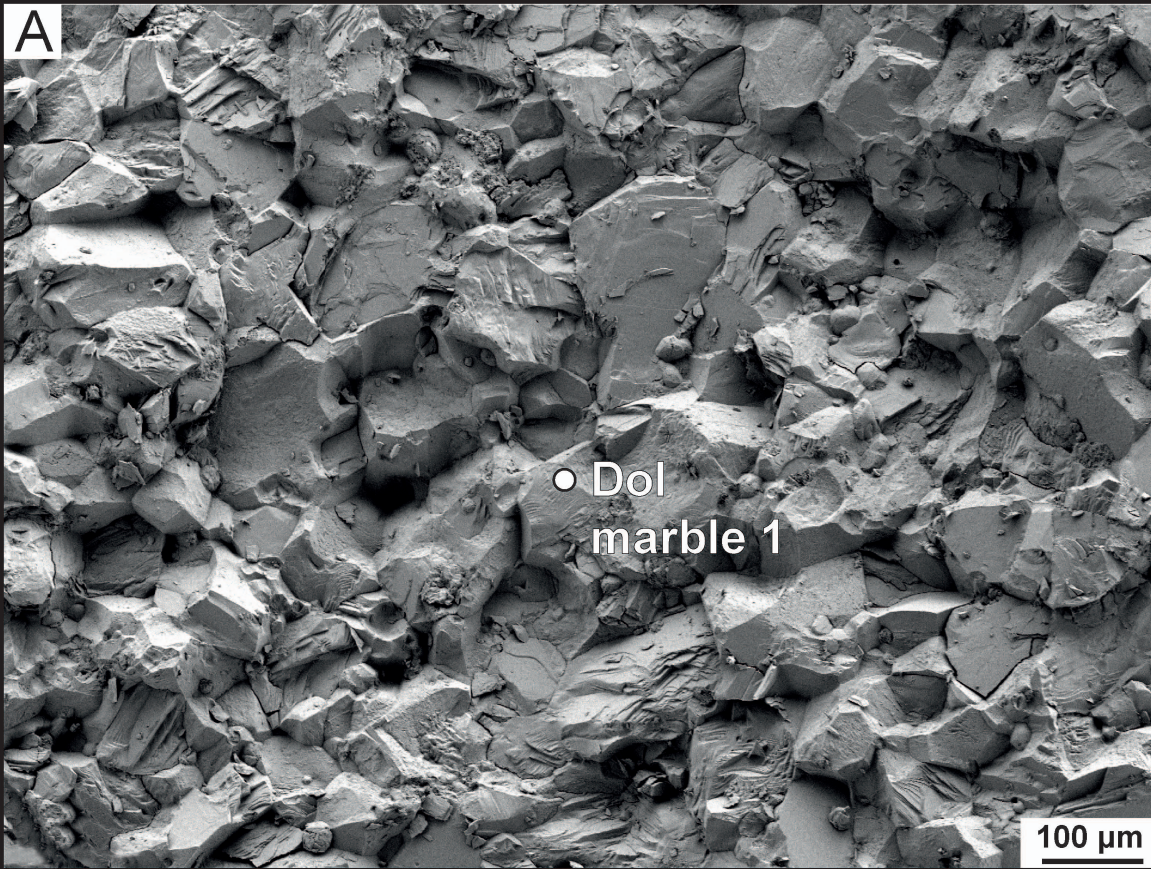
- |                        |                                    |
|------------------------|------------------------------------|
| Sciliar limestones     | Plutonic rocks of Predazzo complex |
| Livinallongo Formation | Triassic volcanics/volcaniclastics |
| Contrin Formation      | Triassic dike                      |
| Werfen Formation       | Quaternary sediments               |
| Bellerophon Formation  | Study area                         |
| Permian volcanics      | 4 km                               |

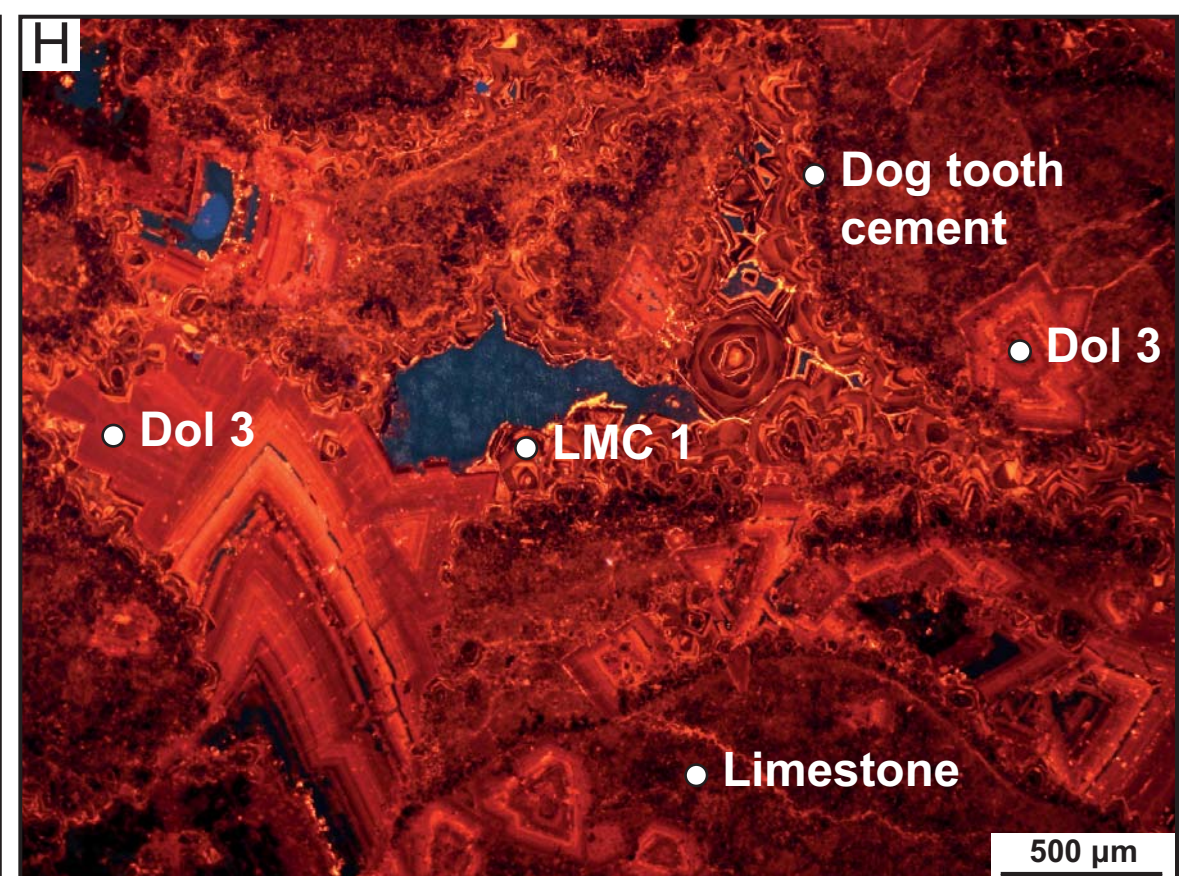
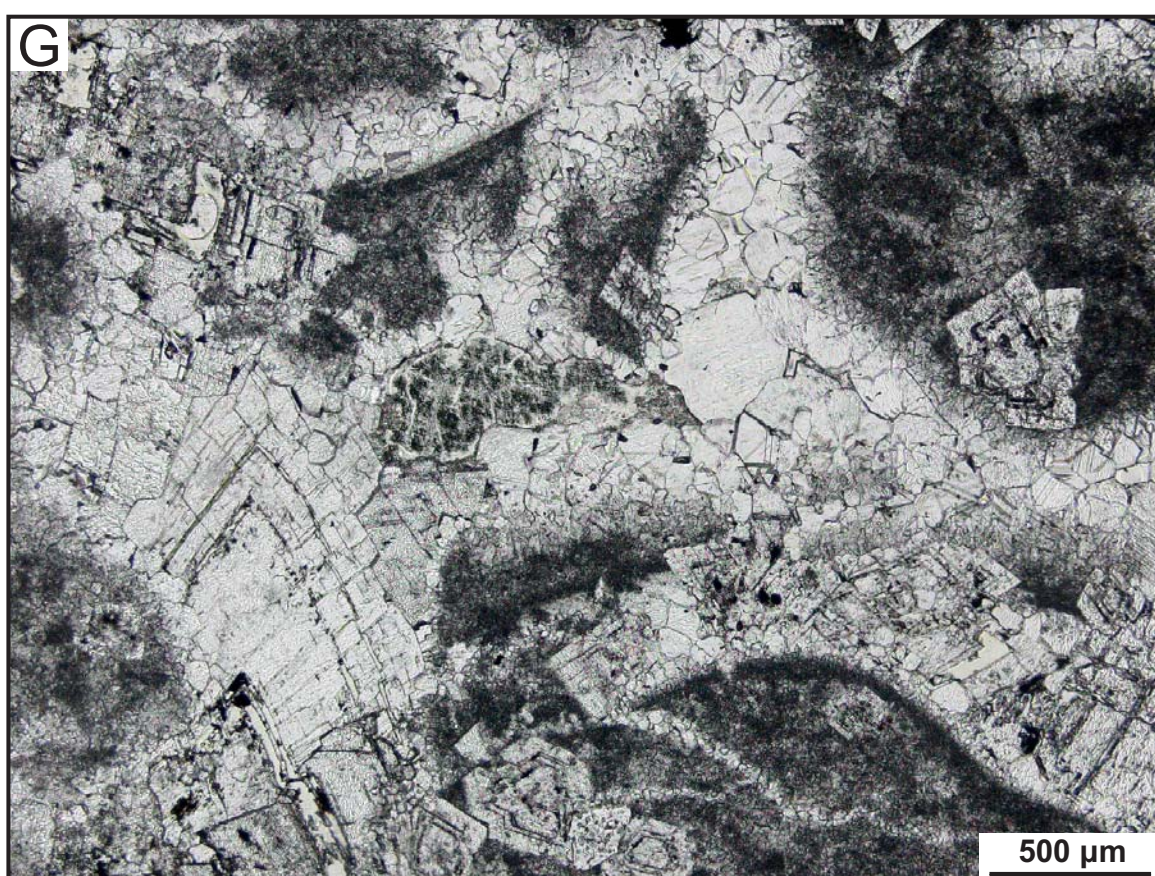
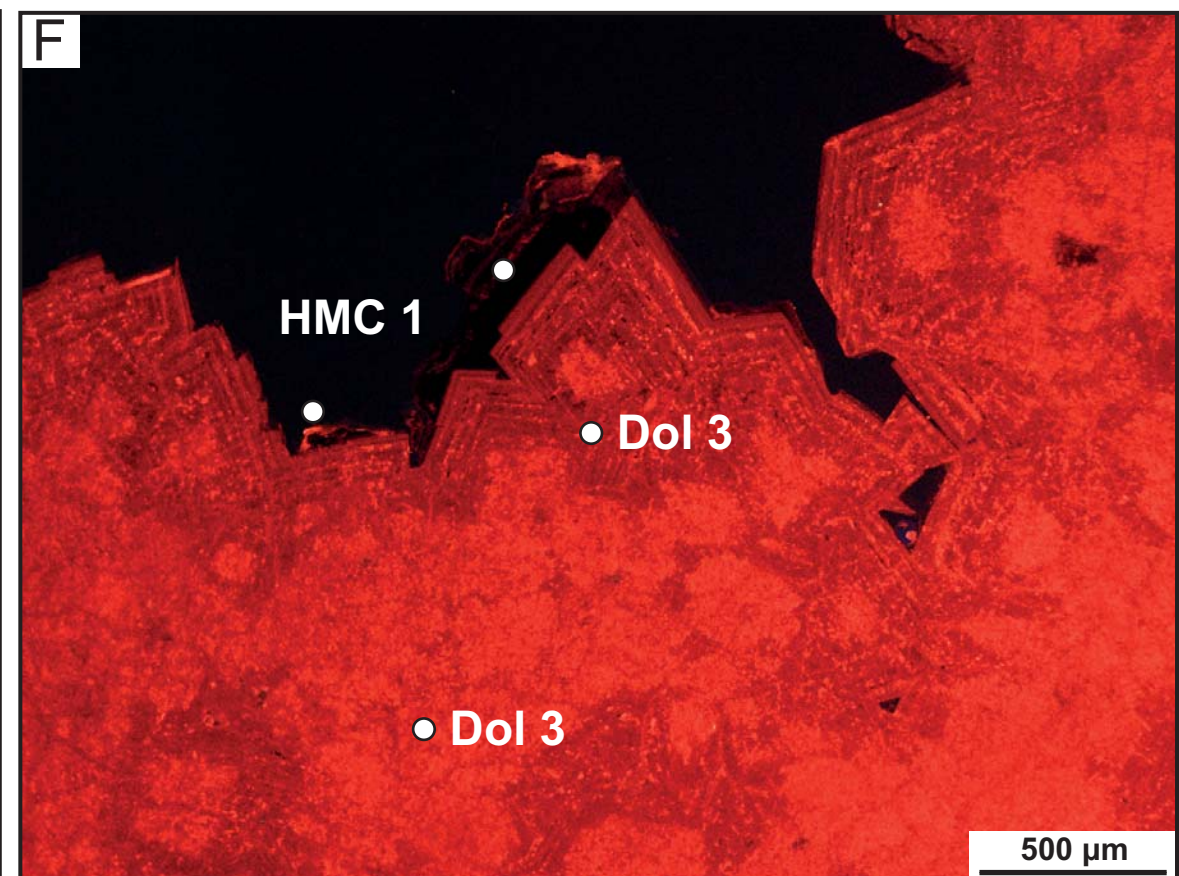
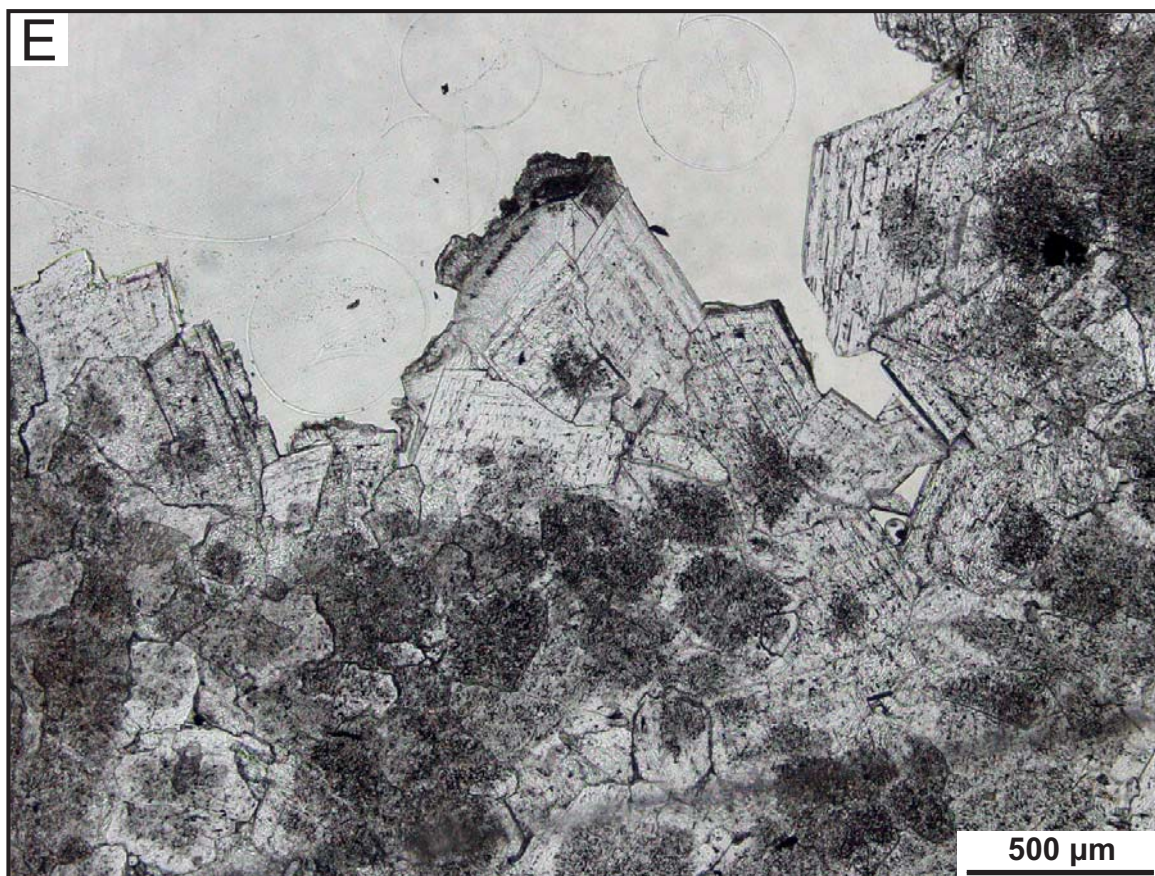
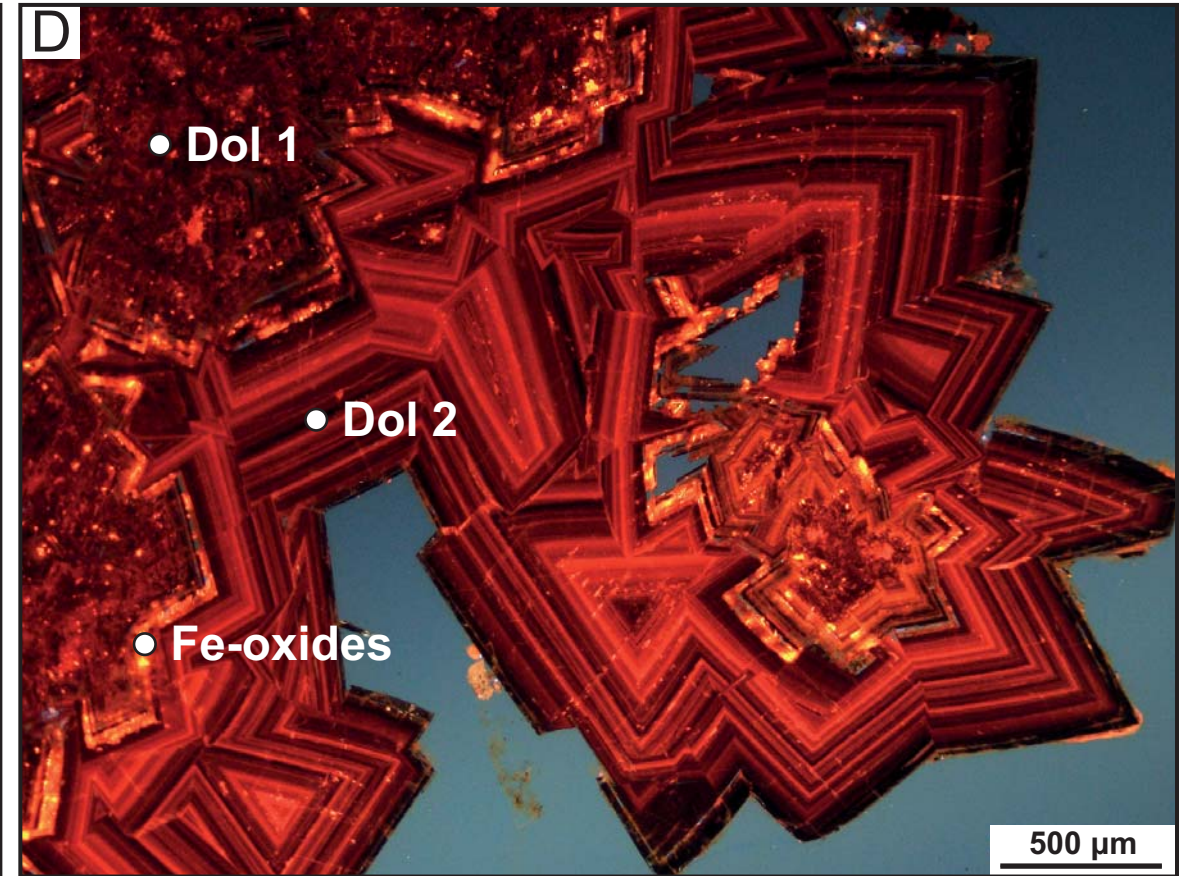
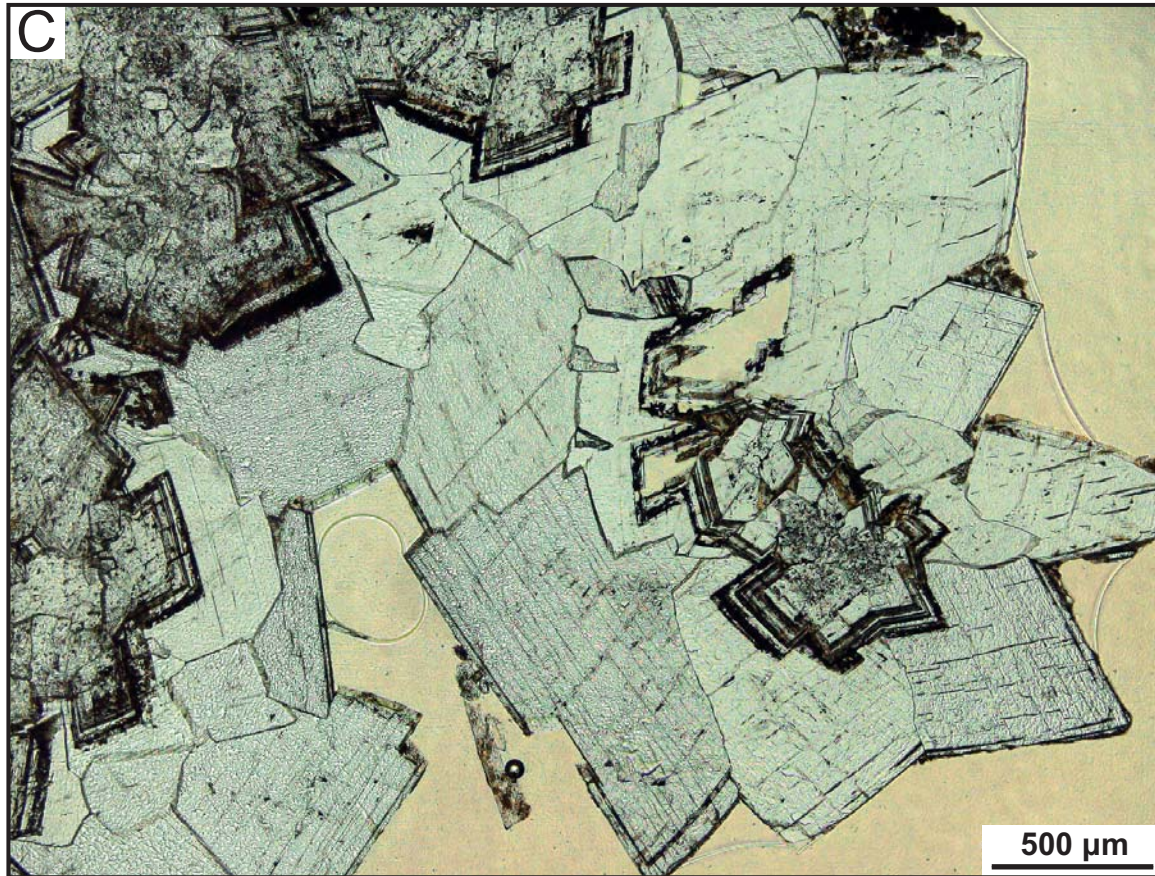
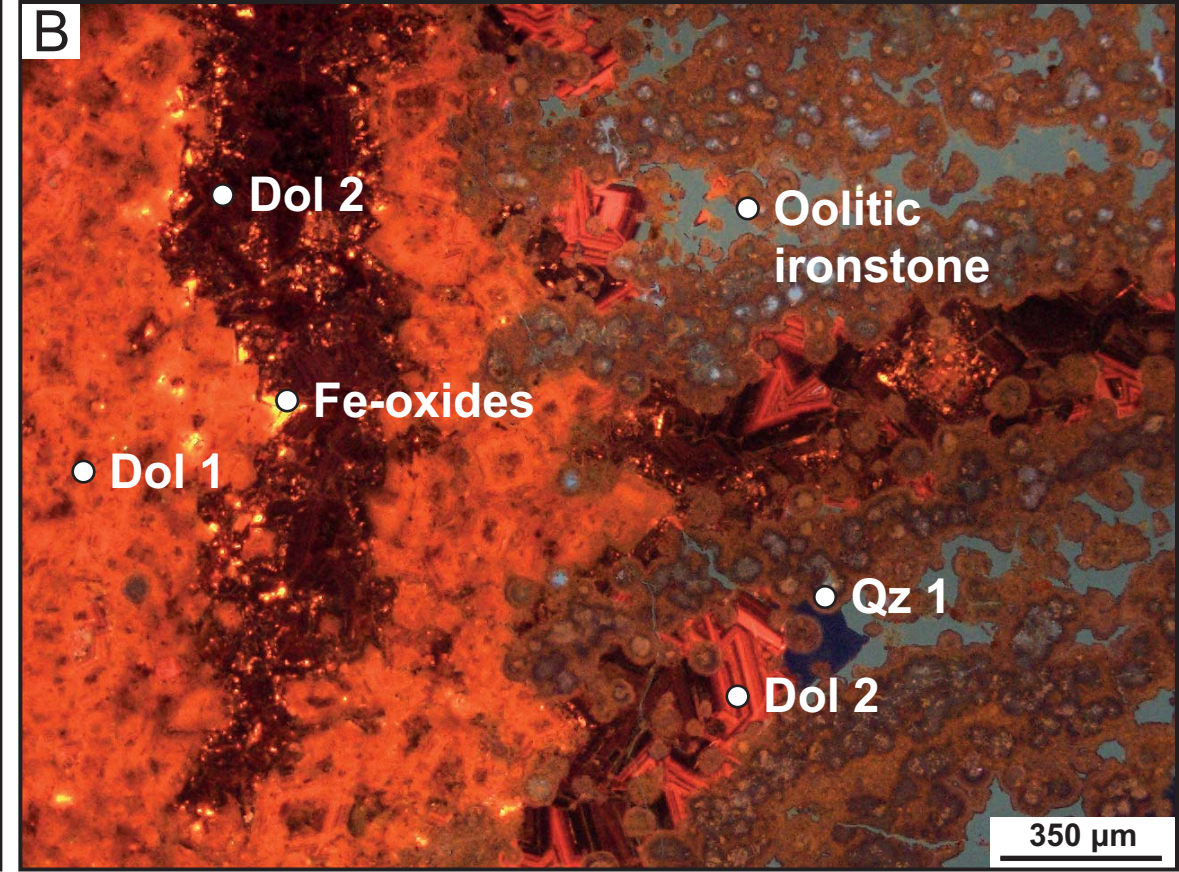
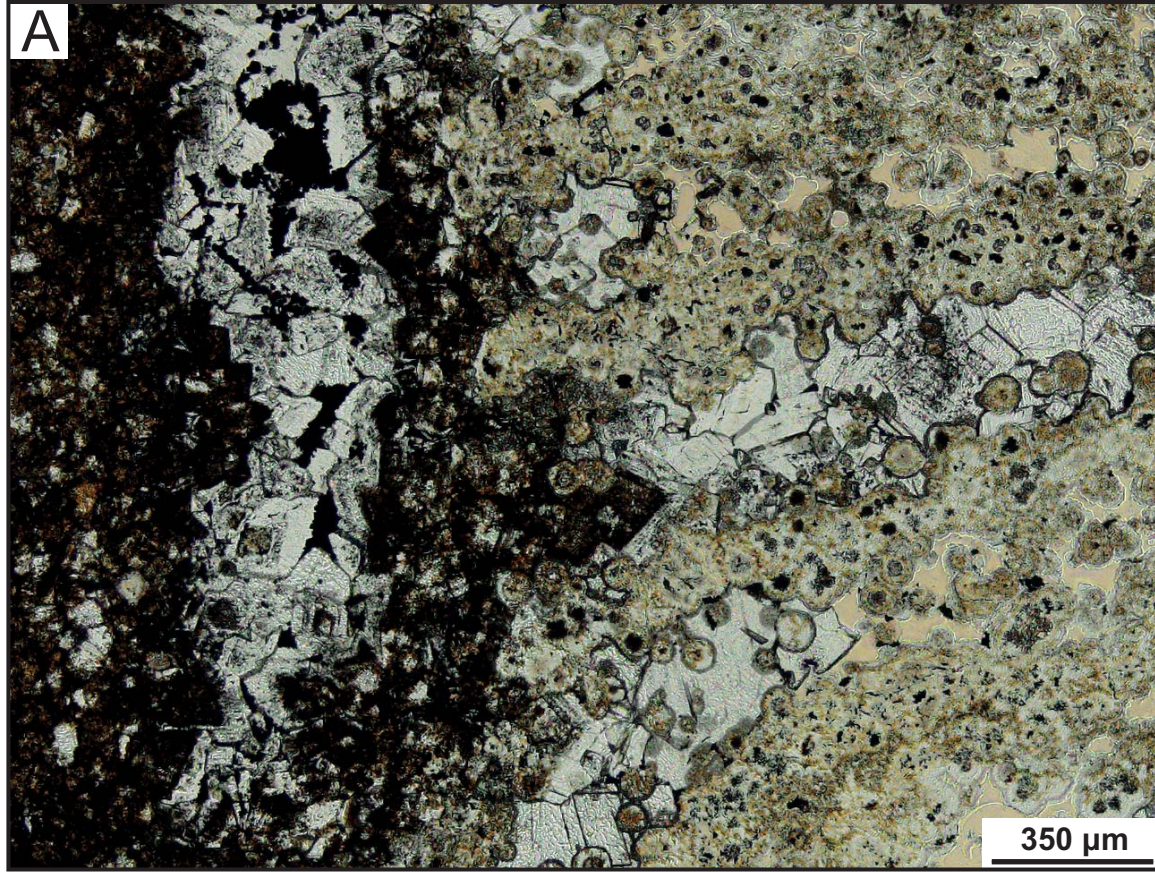


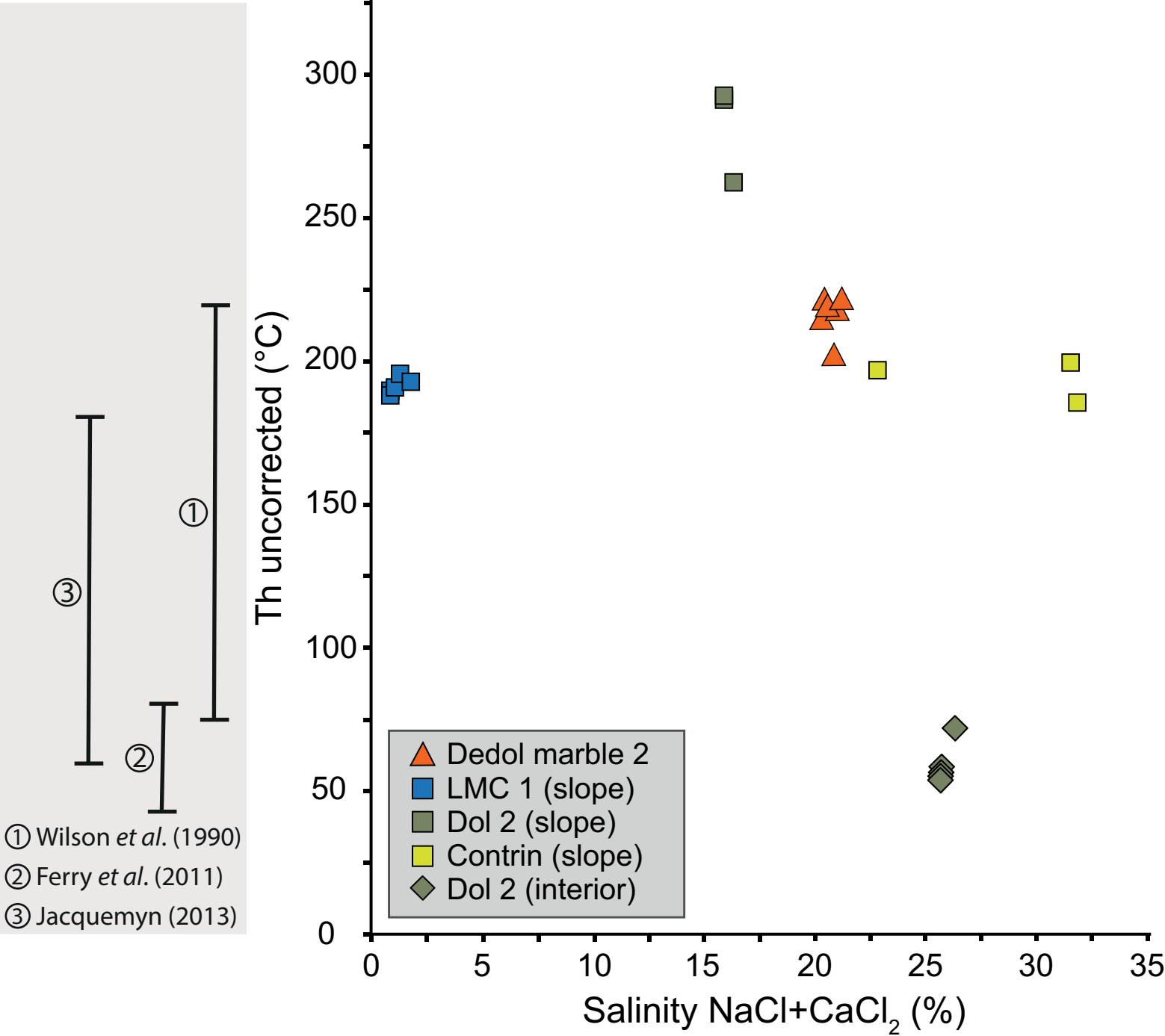


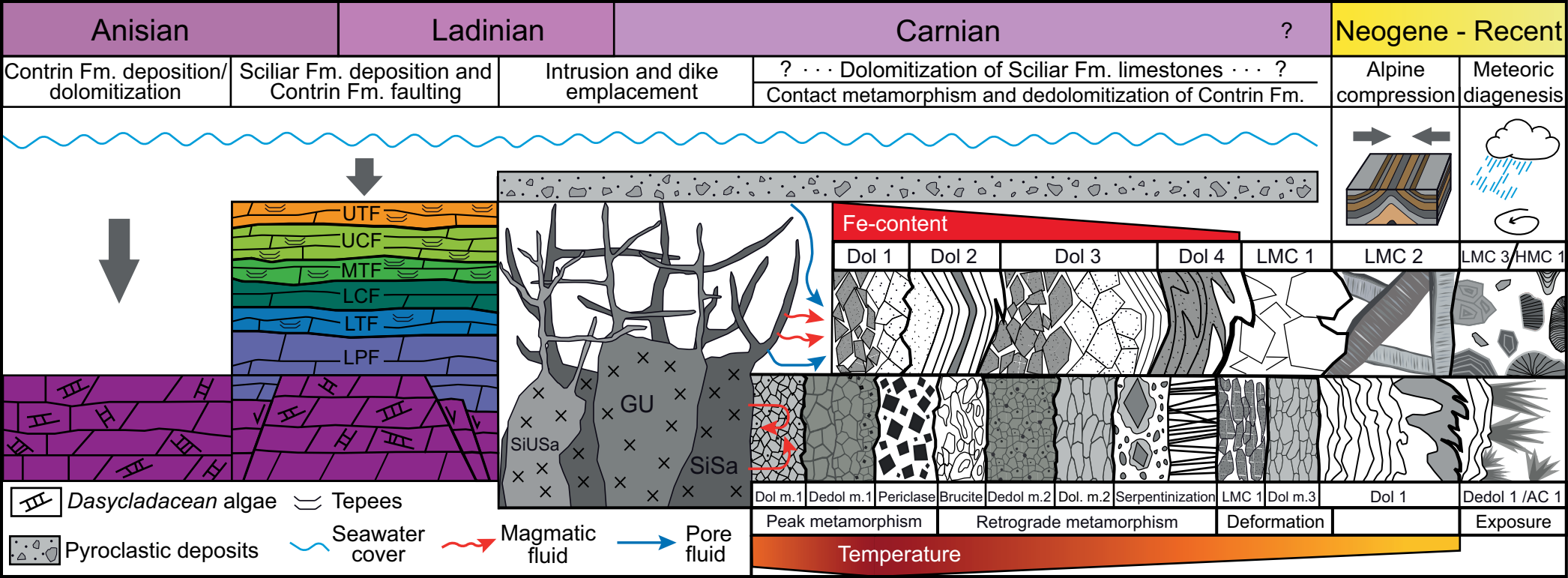




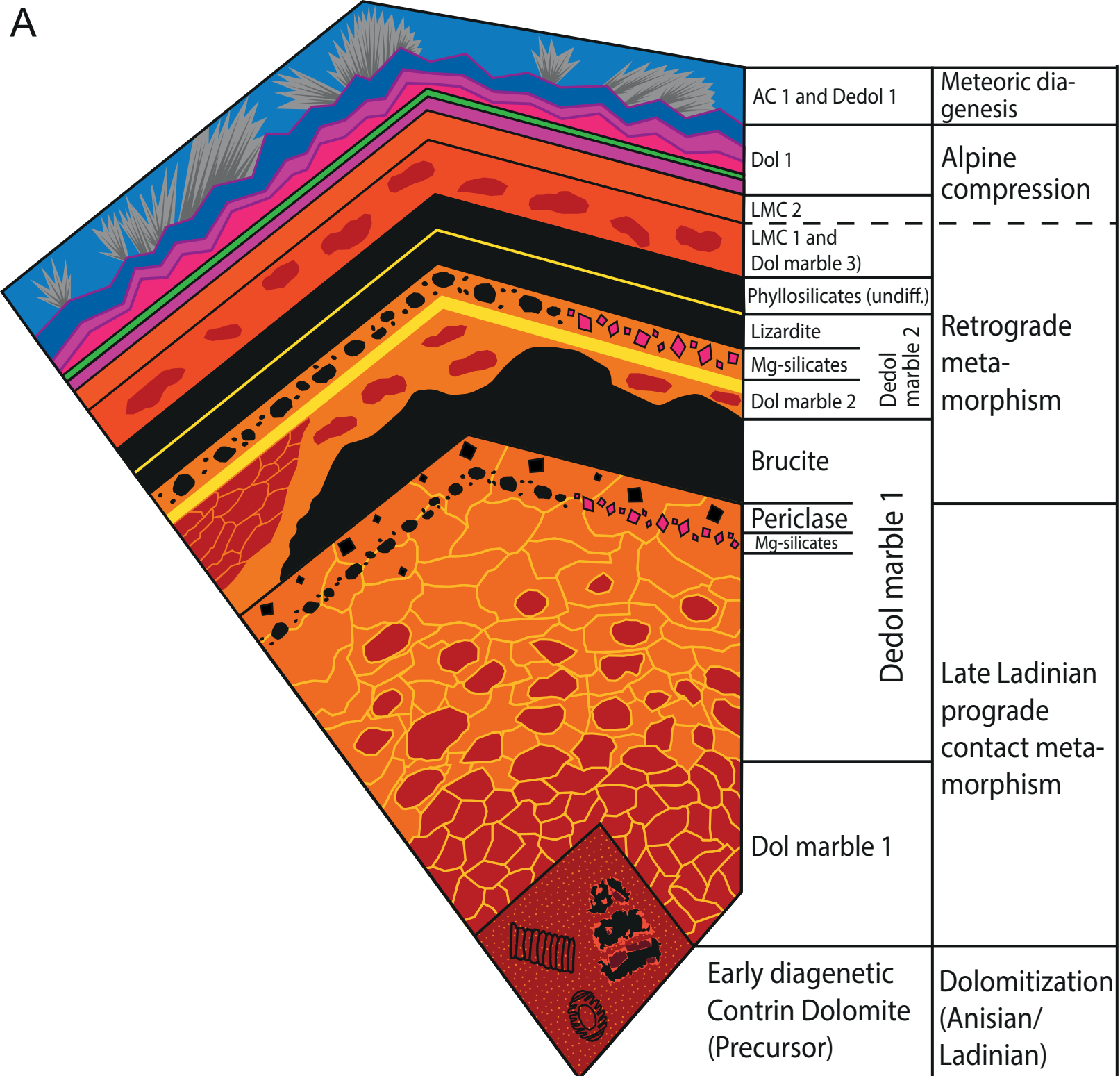




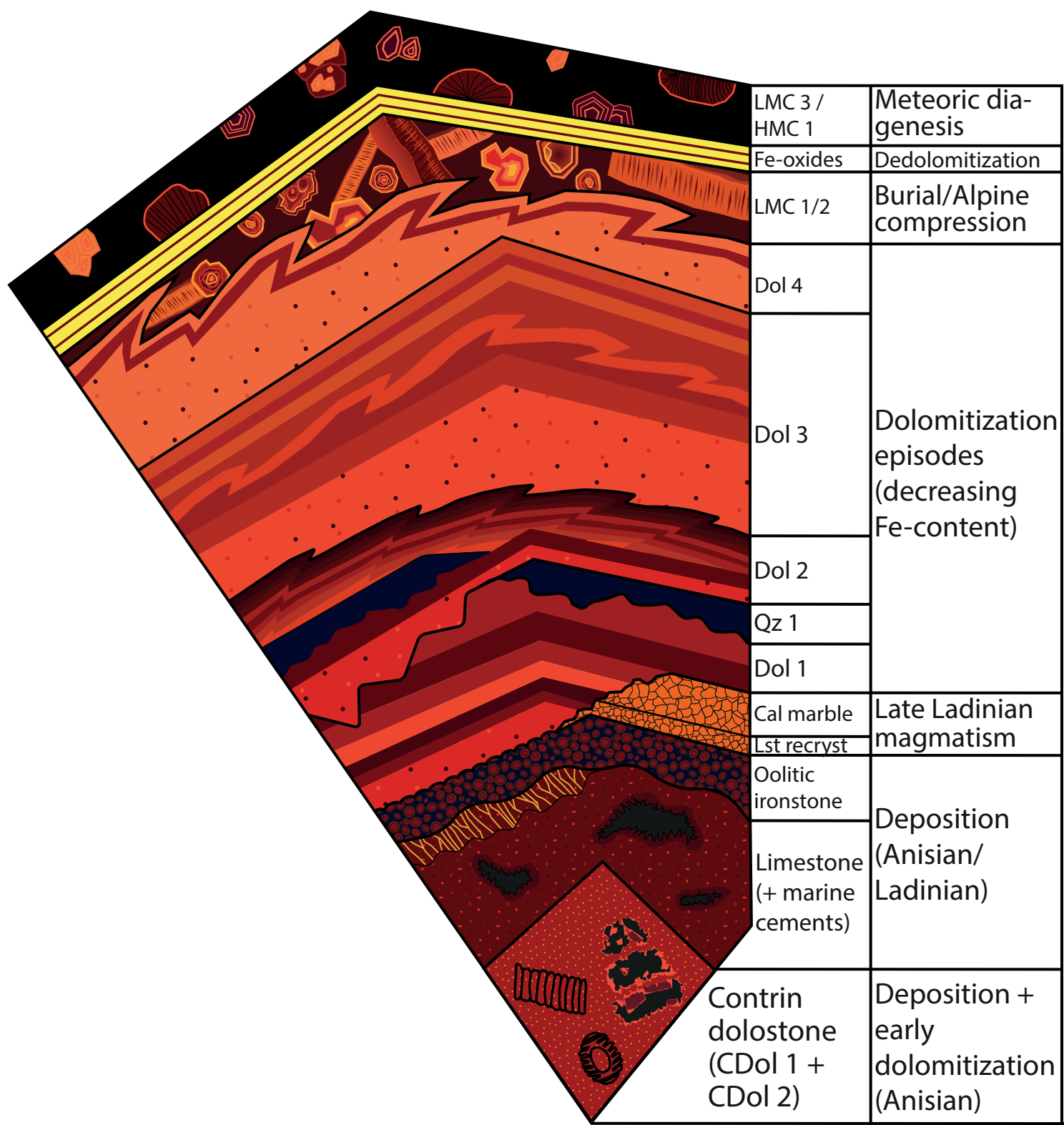


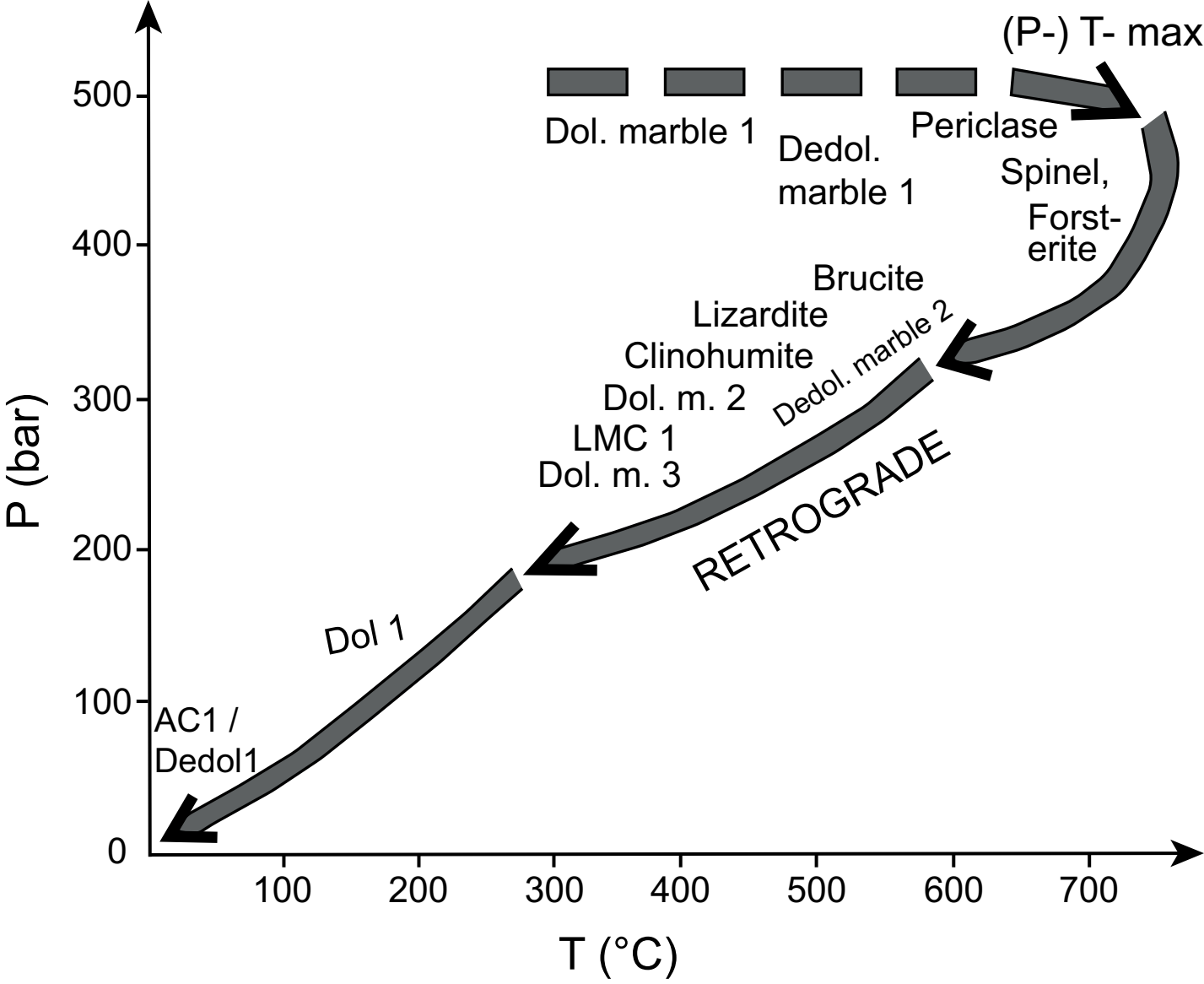


A



B





# Decreasing temperature with increasing distance from Predazzo Intrusion

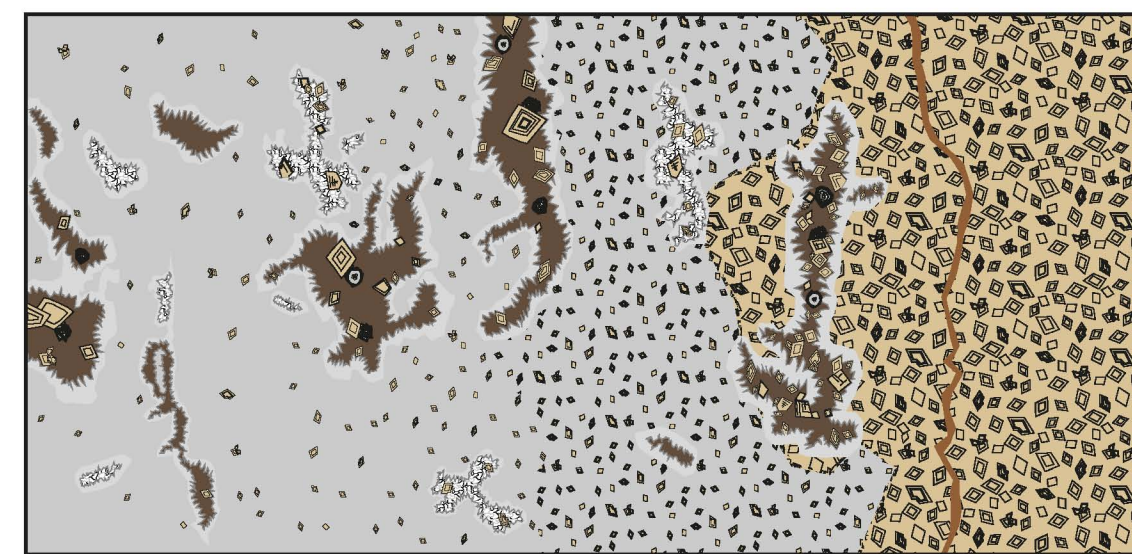
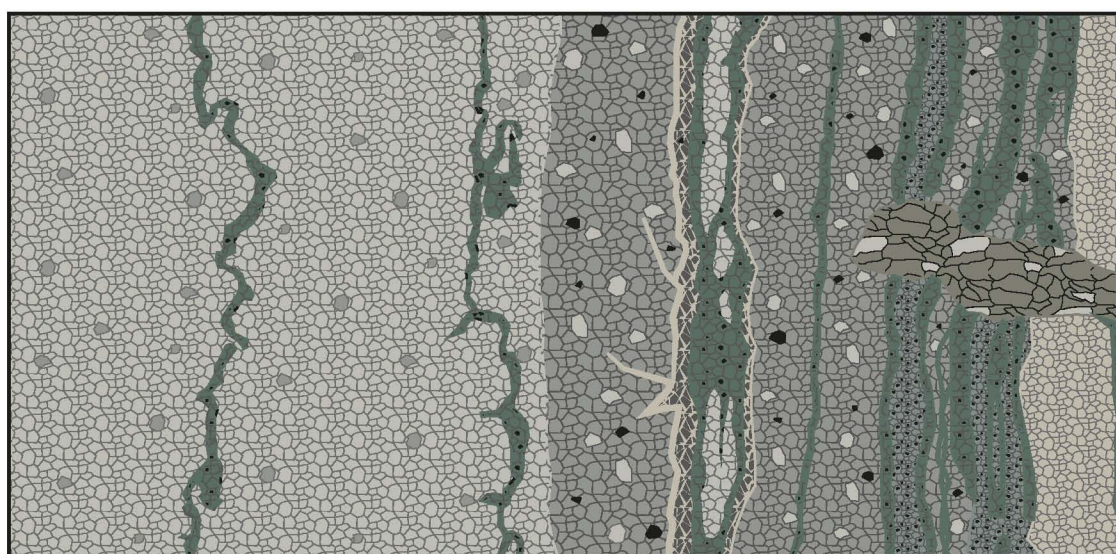
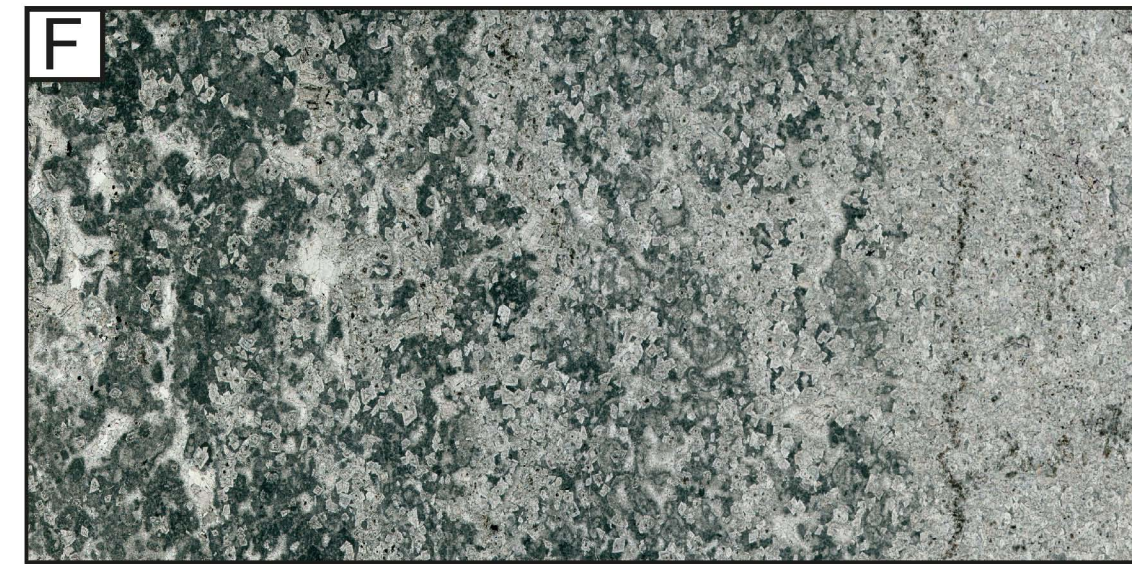
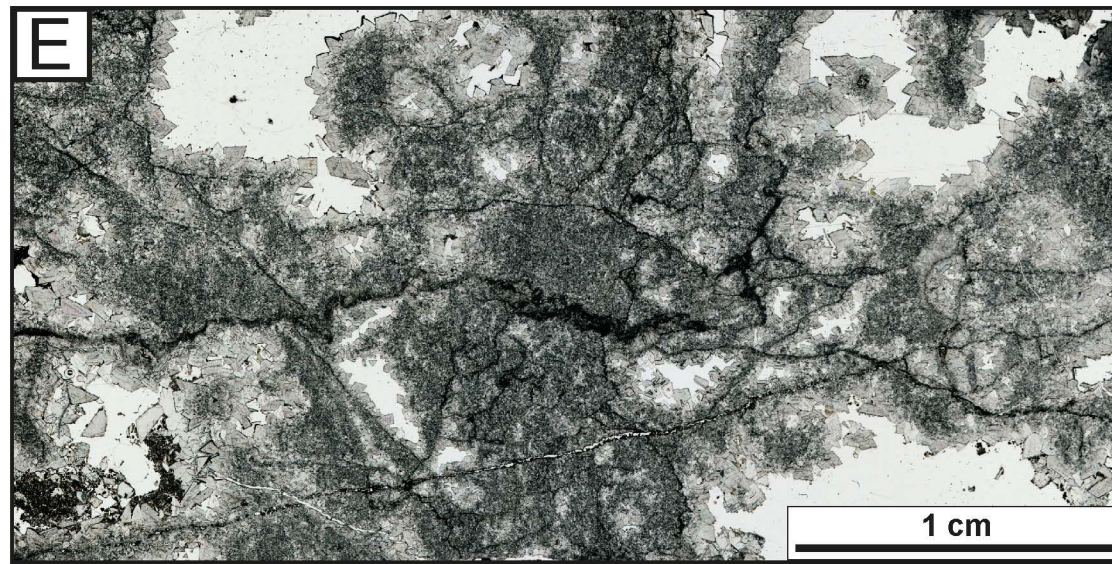
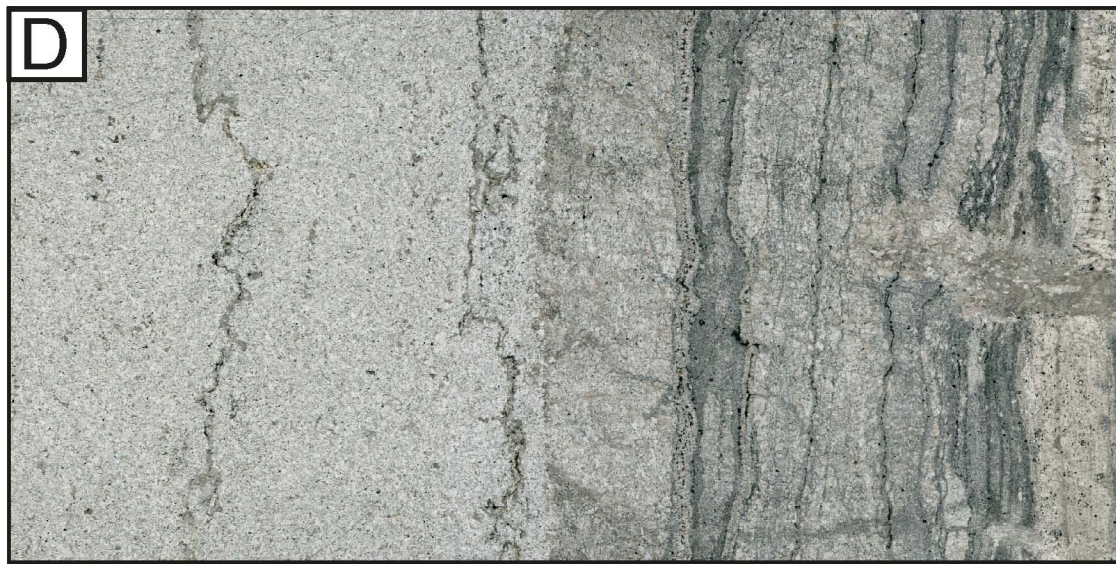
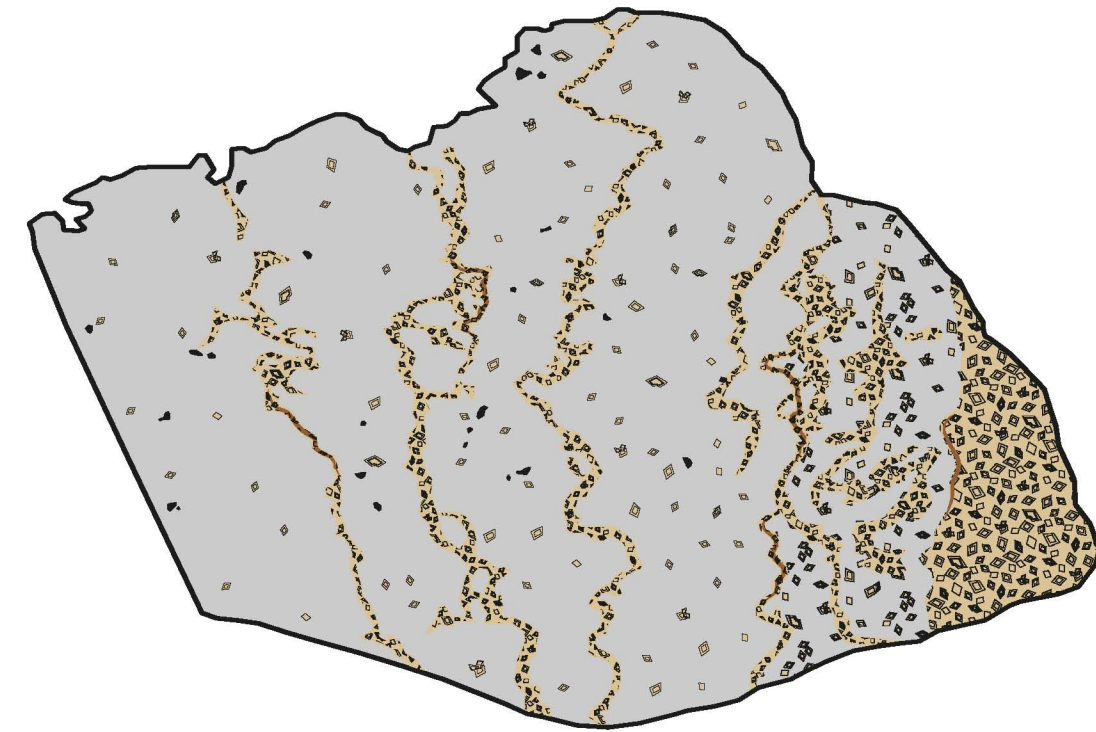
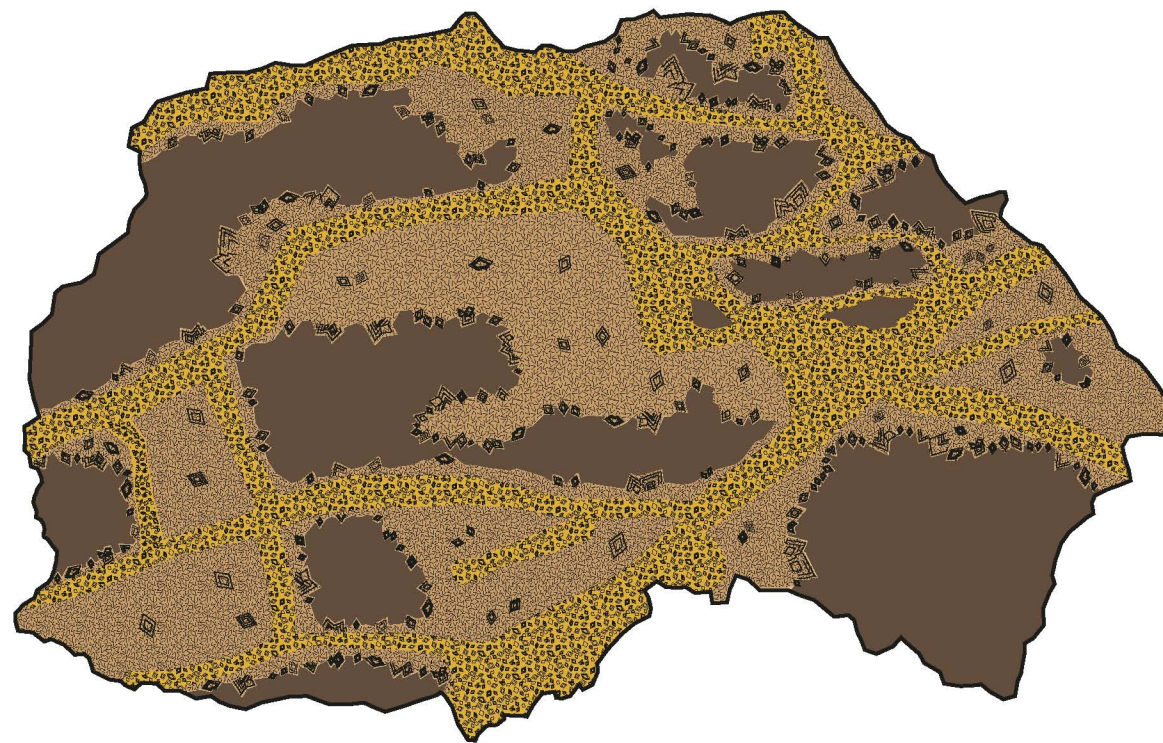
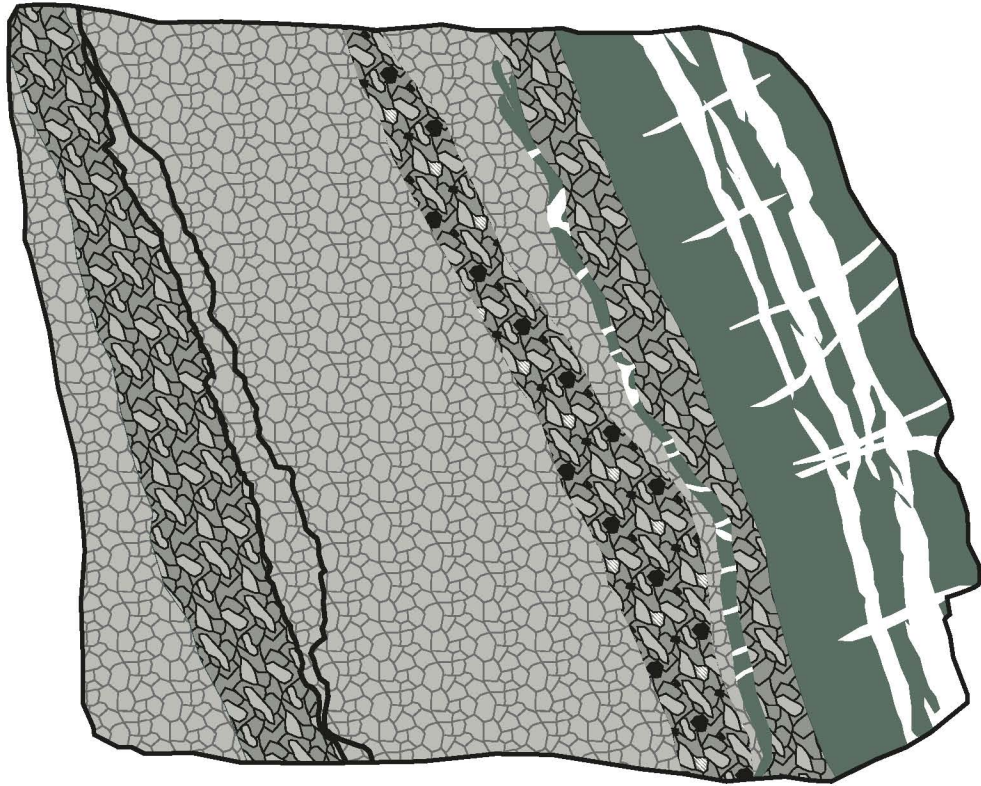


High T

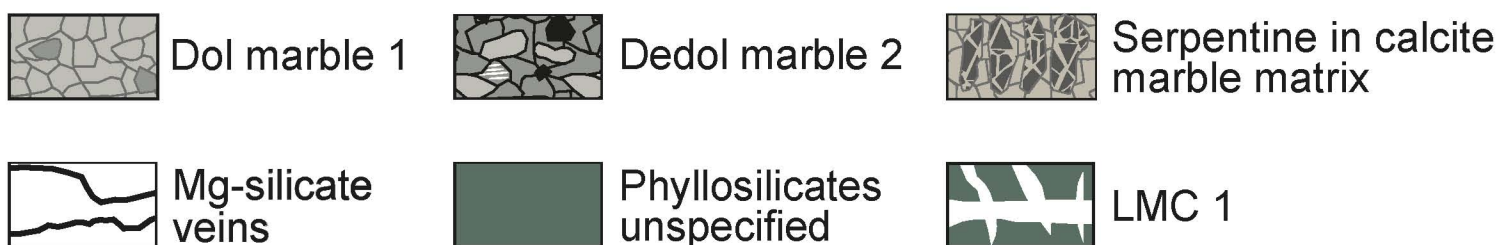
Low T



5 cm



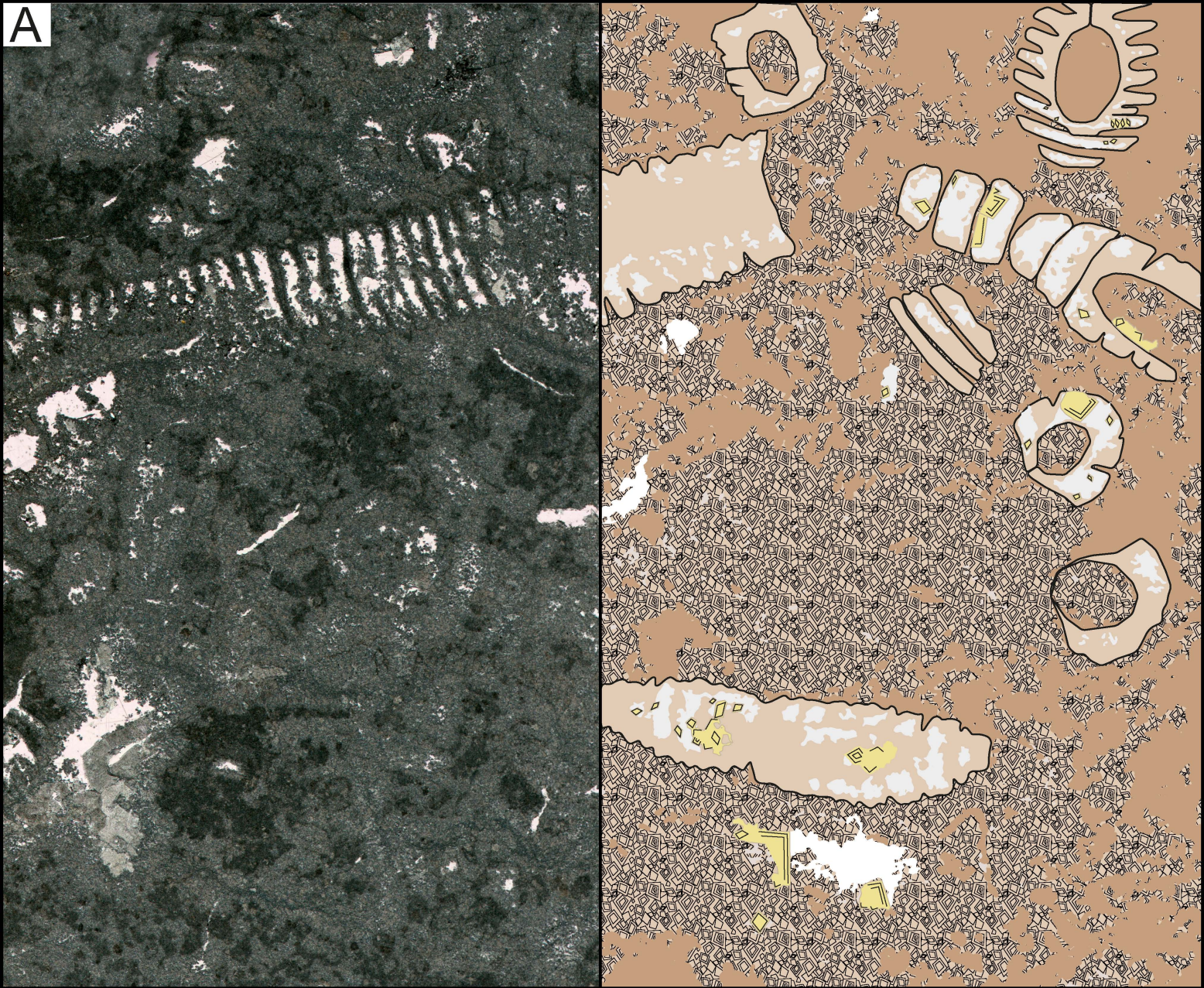
## Metamorphic features



## Diagenetic features

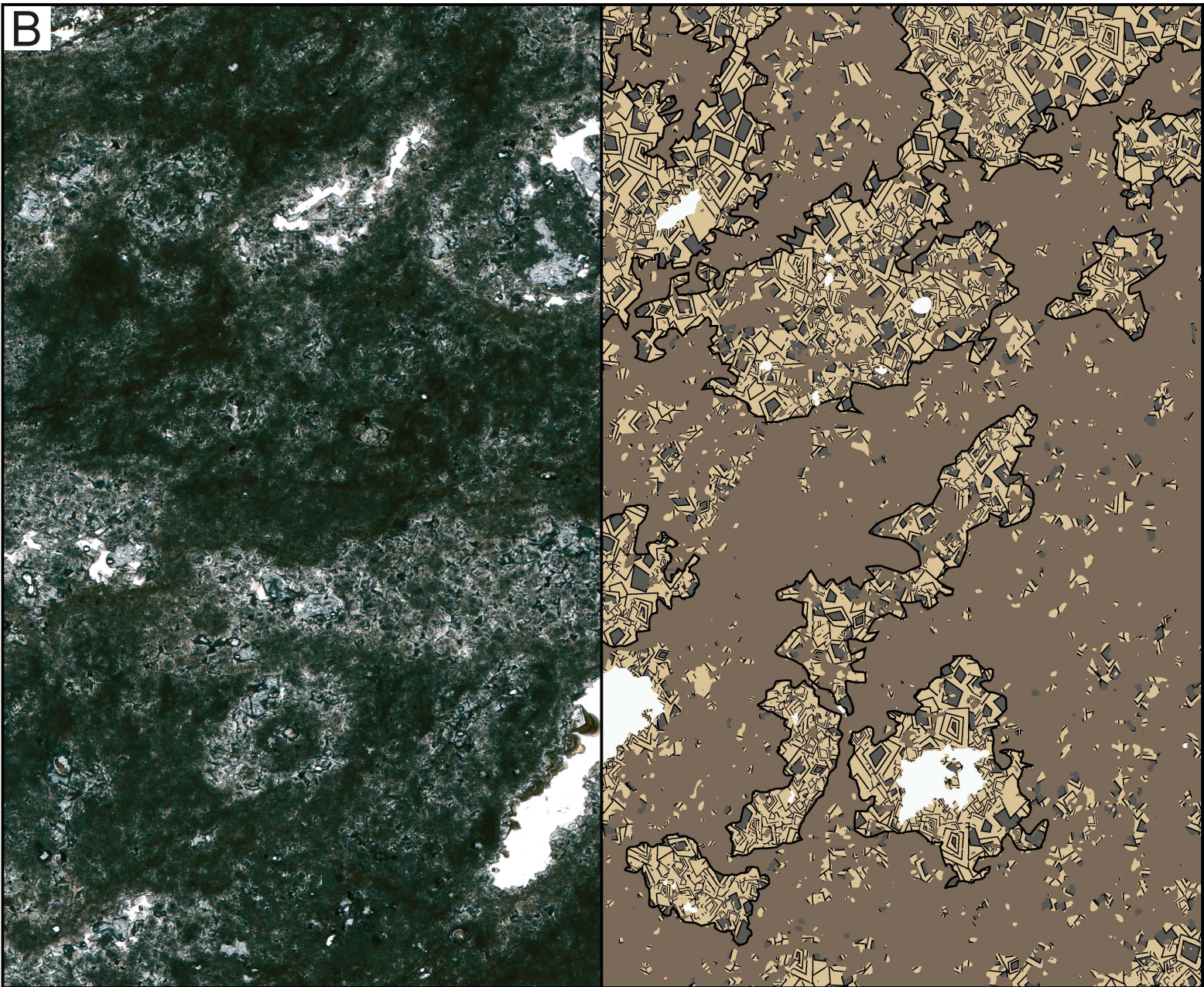


A



Fine grained CDol 1
  Fine grained CDol 2
  Coarse grained CDol 3
  *Dasycladaceae* green algae

B



Coarse grained CDol 1
  Coarse grained CDol 2
  Pervasively recrystallized *Dasycladaceae*

